



โครงการการเรียนการสอนเพื่อเสริมประสบการณ์

โครงสร้างภายในสามมิติของแอ่งทรุดตัว
จากแบบจำลองทางกายภาพย่อส่วน

โดย

นายธนกฤต ตั้งคำเจริญ
เลขประจำตัวนิสิต 5732727023

โครงการนี้เป็นส่วนหนึ่งของการศึกษาระดับปริญญาตรี
ภาควิชาธรณีวิทยา คณะวิทยาศาสตร์ จุฬาลงกรณ์มหาวิทยาลัย

ปีการศึกษา 2560

บทคัดย่อและแฟ้มข้อมูลฉบับเต็มของโครงการทางวิชาการที่ได้บริการในคลังปัญญาจุฬาฯ (CUIR)

เป็นแฟ้มข้อมูลของนิสิตเจ้าของโครงการทางวิชาการที่ส่งผ่านทางคณะที่สังกัด

The abstract and full text of senior projects in Chulalongkorn University Intellectual Repository(CUIR)

are the senior project authors' files submitted through the faculty.

3D INTERNAL STRUCTURE OF RIFT BASINS
FROM SCALED PHYSICAL MODELS

Mr. Thanakit Tangkamcharoen

A Project Submitted in Partial Fulfillment of the Requirements
for the Degree of Bachelor of Science Program in Geology
Department of Geology, Faculty of Science, Chulalongkorn University
Academic Year 2017

โครงสร้างภายในสามมิติของแองทรีดตัว
จากแบบจำลองทางกายภาพย่อส่วน

นายธนกฤต ตั้งคำเจริญ

โครงการนี้เป็นส่วนหนึ่งของการศึกษาตามหลักสูตรวิทยาศาสตร์บัณฑิต
ภาควิชาธรณีวิทยา คณะวิทยาศาสตร์ จุฬาลงกรณ์มหาวิทยาลัย
ปีการศึกษา 2560

Project Title	3D INTERNAL STRUCTURE OF RIFT BASINS FROM SCALED PHYSICAL MODEL
By	Mr. Thanakit Tangcomejaroen
Field of Study	Geology
Project Advisor	Sukonmeth Jitmahantakul, Ph.D.

Submitted date.....

Approval date.....

.....

Project Advisor
(Sukonmeth Jitmahantakul, Ph.D.)

ธนภฤต ตั้งคำเจริญ: โครงสร้างภายในสามมิติของแอ่งทรุดตัวจากแบบจำลองทางกายภาพย่อส่วน.
(3D INTERNAL STRUCTURE OF RIFT BASINS FROM SCALED PHYSICAL MODELS) อ.ที่ปรึกษาโครงการหลัก: อาจารย์ ดร.สุคนธ์เมธ จิตรมหันตกุล, 108 หน้า

รูปทรงเรขาคณิตสามมิติและโครงสร้างภายในของแอ่งทรุดตัวถูกควบคุมโดยทิศทางของแรงยึดและโครงสร้างเก่าที่วางตัวข้างใต้แอ่งทรุดตัว ดังนั้นการศึกษาเกี่ยวกับพื้นผิวรอยเลื่อนสามมิติภายในแอ่งทรุดตัวจะช่วยให้เข้าใจวิวัฒนาการที่เกิดขึ้นภายในแอ่งทรุดตัวและโครงสร้างเก่าที่เป็นตัวควบคุมรูปทรงเรขาคณิตของแอ่งทรุดตัว โดยการศึกษานี้ได้ทำการสร้างแบบจำลองดิจิทัลสามมิติจากชุดภาพตัดขวางของแบบจำลองทางกายภาพย่อส่วน (แบบจำลองทรุดตัวแบบตั้งฉากและแบบจำลองทรุดตัวแบบเฉียง) ของแอ่งทรุดตัว และได้ทำการเปรียบเทียบโครงสร้างภายในของทั้งสองแบบจำลอง ซึ่งเทคนิคใหม่สำหรับการสร้างแบบจำลองรอยเลื่อนสามมิตินี้ได้ถูกพัฒนาจากการใช้การผสมผสานของซอฟต์แวร์เปลี่ยนภาพถ่ายเป็นข้อมูลไหวสะเทือน (Kogeo®) ซอฟต์แวร์แปลความข้อมูลไหวสะเทือน (OpenTect® และ Petrel 2014) และซอฟต์แวร์วิเคราะห์โครงสร้าง (Move™) แบบจำลองทรุดตัวแบบตั้งฉากและแบบเฉียงถูกแสดงลักษณะโดยรอยย่อยย่อยบริเวณขอบแอ่งทรุดตัวที่มีการวางตัวขนานกับโครงสร้างเก่าข้างใต้แอ่งทรุดตัว ในขณะที่รอยเลื่อนภายในแอ่งทรุดตัวนั้นมีการวางตัวที่เกือบตั้งฉากถึงตั้งฉากกับทิศทางของแรงยึด มุมเทของรอยเลื่อนทั้งสองแบบมีการลดลงตามระดับความลึก การเคลื่อนตัวของรอยเลื่อนในแบบจำลองทรุดตัวแบบเฉียงมักมีการเคลื่อนตัวที่มากกว่าแบบจำลองทรุดตัวแบบตั้งฉาก ซึ่งการเคลื่อนตัวสูงสุดที่ถูกรับในรอยเลื่อนภายในแอ่งทรุดตัวนั้นทำให้เกิดศูนย์สะสมของแอ่งในทั้งสองแบบจำลอง การเชื่อมตัวของรอยเลื่อนนั้นสามารถถูกพบในแบบจำลองทรุดตัวแบบเฉียงได้ง่ายกว่าแบบจำลองทรุดตัวแบบตั้งฉาก โดยผลลัพธ์ทั้งหมดนี้จะถูกนำไปเปรียบเทียบกับระบบรอยเลื่อนในตัวอย่างของแอ่งทรุดตัวธรรมชาติ และสามารถถูกนำไปประยุกต์ใช้กับระบบปิโตรเลียมเกี่ยวกับลักษณะการกักเก็บแบบรอยเลื่อน และเส้นทางการเคลื่อนที่ของไฮโดรคาร์บอนได้อีกด้วย

ภาควิชา.....ธรณีวิทยา.....ลายมือชื่อนิสิต.....

สาขาวิชา.....ธรณีวิทยา.....ลายมือชื่อ อ.ที่ปรึกษาหลัก.....

ปีการศึกษา.....2560.....

5732727023: MAJOR GEOLOGY

KEYWORDS: RIFT BASIN / FAULT DISPLACEMENT / FAULT LINKAGE

THANAKIT TANGKAMCHAROEN: 3D INTERNAL STRUCTURE OF RIFT
BASINS FROM SCALED PHYSICAL MODELS. ADVISOR: SUKONMETH
JITMAHANTAKUL, Ph.D., 108 pp.

Three-dimensional (3D) geometries and internal structures of rift basins were controlled by extension direction and pre-existing structure beneath the rift basin. The study about 3D fault surfaces in the rift basins will help to understand the evolution occurring into the rift basins and the pre-existing structure controlling the geometry of rift basins. This study constructed the 3D digital models from a series of cross-section images of the scaled physical models (orthogonal rift model and oblique rift model) of the rift basins and compared the internal structure of both models. A new technique for 3D fault model construction was developed from using the combination of image-seismic conversion software (Kogeo®), seismic interpretation software (OpendTect®, Petrel 2014) and structural analysis software (Move™). The orthogonal and oblique rift model are characterized by segmented rift-border faults having orientation to be parallel to the pre-existing structure beneath the rift basin, whereas intra-rift faults having the orientation to be sub-perpendicular to perpendicular to the extension direction. Dip angles of both fault sets decrease with depth. Fault displacements in the oblique rift model are generally higher than that in the orthogonal rift model. Maximum displacement is found in the intra-rift faults forming the basin depocenter in both models. Fault linkages can be easily observed in the oblique rift model than the orthogonal rift model. The results were compared with the fault systems in the examples of natural rift basins and can be used to apply to petroleum system about fault trap and migration pathways of hydrocarbon.

Department:Geology.....Student's Signature.....

Field of Study:Geology.....Advisor's Signature.....

Academic Year:2017.....

Acknowledgements

I would like to express my appreciation to my advisor Dr. Sukonmeth Jitmahantakul for his support, suggestions, and valuable ideas during this work.

I have furthermore to thank the entire department of geology staff for supporting everything during study here.

I am very grateful to the Dynamics Research Group of the Royal Holloway University of London for giving me the great opportunities for providing the model section images from scaled physical models.

Especially, I would like to thank our senior project team, Khanitpong Aiemsintorn, Narudee Saikrasin and Rungkarn Thammasanya and my classmates for their friendship, and encouragement. It has been a great experience knowing all of you.

Finally, my deepest gratitude goes to my family who always stays with me in a good and bad time.

List of Contents

Abstract in Thai	iv
Abstract in English	v
Acknowledgements	vi
List of Contents	vii
List of Figures	ix
Chapter 1 Introduction	
1.1 Introduction	1
1.2 Objectives	1
Chapter 2 Geological Background	
2.1 Rift and passive margin evolution	2
2.2 Scaled physical models	7
Chapter 3 Methodology	
3.1 Literature reviews and software training	10
3.2 Data transformation	10
3.3 Horizon interpretation and 3D fault surface generation	13
3.4 Fault Analysis	46
Chapter 4 Results	
4.1 Introduction	53
4.2 Orthogonal rift model (NRS004-90)	54
4.2.1 Fault systems	54
4.2.2 Fault analysis	58
4.3 Oblique rift model (NRS005-60)	73
4.3.1 Fault systems	73
4.3.2 Fault analysis	77
Chapter 5 Discussions	
5.1 Comparison between orthogonal and oblique rift model	90
5.1.1 Fault systems	90
5.1.2 Dip angle of faults	90

5.1.3 Dip azimuth of faults	90
5.1.4 Fault analysis	91
5.2 Comparisons with natural examples of rift systems	92
5.2.1 Orthogonal rift	92
5.2.2 Oblique rifts	92
5.3 Apply to petroleum system	93
Chapter 6 Conclusions	100
References	101
Appendix	108

List of Figures

Figure 2.1	Main structure styles of continental extension as a function of the increasing extensional strain	3
Figure 2.2	Schematic evolution of a segmented rift system with volcanics	6
Figure 3.1	A workflow of methodology creating 3D internal structure of rift basins from scaled physical models	9
Figure 3.2	Resizing images of scaled physical models: NRS004-90 (orthogonal rift model) and NRS005-60 (oblique rift model)	10
Figure 3.3	A model section image (JPEG file) and a seismic data (SEG-Y file) of section 26 from NRS004-90	11
Figure 3.4	The procedure of selecting the “matching colorbar” and choosing the “load colorbar” for setting the color of SEG-Y file	12
Figure 3.5	The procedure of setting the parameters of “SEG-Y/SU data export parameter” and “floating point export”	12
Figure 3.6	The procedure of setting the parameters of “Create New Survey” in OpendTect®	13
Figure 3.7	The procedure of setting the parameters in “Extract Survey Setup from SEG-Y file” for importing the SEG-Y file into OpendTect®	15
Figure 3.8	The procedure of setting the parameters in “SEG-Y byte location scanning setting”	15
Figure 3.9	The procedure of setting the parameters in “Edit Survey Parameter”	16
Figure 3.10	The procedure of defining the value for locating the section of SEG-Y file to OpendTech®	16
Figure 3.11	The map visualization, north visualization and the oblique visualization of 2D horizon lines from NRS004-90 and NRS005-60 in OpendTect®	17

Figure 3.12	The procedure of setting the parameters in “Export 2D Horizon”	18
Figure 3.13	The procedure of setting the parameters in “ASCII Import Options”	19
Figure 3.14	The procedure of setting the parameters in “Coordinate System”	20
Figure 3.15	The model section images of NRS004-90 and NRS005-60 that were used in the procedure of the digitizing horizons and faults	21
Figure 3.16	The 2D cross-section image (sec 11) of NRS004-90 that was digitized the horizon of syn-rift 1	22
Figure 3.17	The procedure of setting the parameters in “Create Surface” of syn-rift 1	23
Figure 3.18	Horizon lines and a horizon surface of syn-rift 1 created from the horizon lines of syn-rift 1	24
Figure 3.19	Setting stratigraphy of NRS004-90 that was defined from amounts of horizons	25
Figure 3.20	The procedure of setting the parameters in “Color Map”	26
Figure 3.21	The surface map of syn-rift 1 from NRS004-90 that wasn’t changed the color map and was changed the color map	27
Figure 3.22	The correction of some surface that has a distortion coming from the creating surface	28
Figure 3.23	The procedure of setting the parameters in “Smooth”	29
Figure 3.24	The horizon surfaces of syn-rift 1 from NRS004-90 before will be adjusted to be a smooth surface and after has been adjusted to be the smooth surface already	30
Figure 3.25	The procedure of setting the parameters in “Create Surface” to create the surface from the fault lines	32

Figure 3.26	The fault lines of WFault01 (west dipping fault) that were digitized from the horizon surfaces and the model sections in NRS004-90	33
Figure 3.27	Creating fault surface from fault lines of WFault01 in NRS004-90	34
Figure 3.28	The method using the relationship between the Petrel and Move™ to cut off the dip angle and the dip azimuth of the horizon surfaces	35
Figure 3.29	In UX mode, the Move Link button will be visible in the Home	36
Figure 3.30	Using the Classic user interface, it appears as a tool Button appended to the File Group the File Group	36
Figure 3.31	Move Link for Petrel tab before connect Petrel with the TCP Server	36
Figure 3.32	Move Link for Petrel tab after connected Petrel with the TCP Server	37
Figure 3.33	The location of “Move Link for Petrel” on the “Modules” tab	37
Figure 3.34	Move Link for Petrel tab before connect Move™ with Petrel	37
Figure 3.35	Move Link for Petrel tab after connected Move™ with Petrel	37
Figure 3.36	The destination folder within the appropriate tree	38
Figure 3.37	The objects in the Petrel project that were appeared in Move™	38
Figure 3.38	The procedure of setting the parameters in “Make/edit surface” of syn-rift 2	41
Figure 3.39	The procedure of setting the parameters in “Color” of syn-rift 2	41
Figure 3.40	The Procedure of cutting off dip azimuth from a horizon surface of pre-rift 6 in NRS004-90	42
Figure 3.41	The Procedure of cutting off dip angle from a horizon surface of pre-rift 6 in NRS004-90	43

Figure 3.42	The procedure of setting the parameters in “Make/edit surface” of EFault 03	45
Figure 3.43	The objects from Petrel that would like to transfer from Petrel to Move™	45
Figure 3.44	The procedure of the surface geometry analysis that created the dipping of surface in NRS004-90	47
Figure 3.45	The procedure of the surface geometry analysis that trimmed the dipping surface in NRS004-90 for using in the fault analysis	48
Figure 3.46	A map visualization and an oblique visualization of faults map of orthogonal rift model	50
Figure 3.47	Fault throw profiles of EFault01 in orthogonal rift model	51
Figure 3.48	Fault scaling of faults in orthogonal rift model	52
Figure 4.1	The map visualization of elevation maps from orthogonal rift model that consists of pre-rift 1 to pre-rift 7 and syn-rift 1 to syn-rift 2	55
Figure 4.2	The dip azimuth map of pre-rift 7 from orthogonal rift model that present the west dipping faults and the east dipping faults occurring in the rift basin	56
Figure 4.3	The rose diagrams of pre-rift 2 to pre-rift 7 from orthogonal rift model	57
Figure 4.4	The map visualization and 3D oblique visualization of pre-rift 6 surface from orthogonal rift model	61
Figure 4.5	Dipping fault profile and dip azimuth fault profile, NRS004-90 EFault 01	62
Figure 4.6	Displacement profile and fault offset, NRS004-90 EFault 01	63
Figure 4.7	Dipping fault profile and dip azimuth fault profile, NRS004-90 EFault 02	64
Figure 4.8	Displacement profile and fault offset, NRS004-90 EFault 02	65

Figure 4.9	Dipping fault profile and dip azimuth fault profile, NRS004-90 WFault 01	66
Figure 4.10	Displacement profile and fault offset, NRS004-90 WFault 01	67
Figure 4.11	Dipping fault profile and dip azimuth fault profile, NRS004-90 WFault 02	68
Figure 4.12	Displacement profile and fault offset, NRS004-90 WFault 02	69
Figure 4.13	Dipping fault profile and dip azimuth fault profile, NRS004-90 WFault 03	70
Figure 4.14	Displacement profile and fault offset, NRS004-90 WFault 03	71
Figure 4.15	Fault scaling of orthogonal rift model	72
Figure 4.16	The map visualization of elevation maps from oblique rift model that consists of pre-rift 1 to pre-rift 7 and syn-rift 1 to syn-rift 2	74
Figure 4.17	The dip azimuth map of pre-rift 7 from oblique rift model that present the west dipping faults and the east dipping faults occurring in the rift basin	75
Figure 4.18	The rose diagrams of pre-rift 2 to pre-rift 7 from oblique rift model	76
Figure 4.19	The map visualization and 3D oblique visualization of pre-rift 6 surface from oblique rift model	80
Figure 4.20	Dipping fault profile and dip azimuth fault profile, NRS005-60 EFault 01	81
Figure 4.21	Displacement profile and fault offset, NRS005-60 EFault 01	82
Figure 4.22	Dipping fault profile and dip azimuth fault profile, NRS005-60 EFault 02	83
Figure 4.23	Displacement profile and fault offset, NRS005-60 EFault 02	84
Figure 4.24	Dipping fault profile and dip azimuth fault profile, NRS005-60 WFault 01	85

Figure 4.25	Displacement profile and fault offset, NRS005-60 WFault 01	86
Figure 4.26	Dipping fault profile and dip azimuth fault profile, NRS005-60 WFault 02	87
Figure 4.27	Displacement profile and fault offset, NRS005-60 WFault 02	88
Figure 4.28	Fault scaling of oblique rift model	89
Figure 5.1a	East African rift system, Kenya. Landsat thematic mapper (TM) image of the Gregory rift west of Nairobi, Kenya	94
Figure 5.1b	Line diagram interpretation of the Gregory rift west of Nairobi, Kenya	95
Figure 5.2a	Radar image of the volcanic tablelands, Bishop, California	96
Figure 5.2b	Line diagram interpretation of the volcanic tablelands, Bishop, California	97
Figure 5.3	Oligocene structural and tectonic evolution of Mergui basin	98
Figure 5.4	Early-Miocene structural and tectonic evolution of Mergui basin	99

Chapter 1

Introduction

1.1 Introduction

Three-dimensional (3D) geometries and internal structures of rift basins were controlled by extension direction and pre-existing structure beneath the rift basins (McClay et al., 1995; Morley et al., 2004). The study about 3D fault surfaces in the rift basins will help to understand the evolution occurring into the rift basins and the pre-existing structure controlling the geometry of rift basins.

Data of internal structures in the rift basins from a field survey and 2D & 3D seismic-interpretation, each method has its limitations. Hence, the examination of interpretation usually compares with the scaled physical models of the rift basins such as East African Rift System (Corti, 2012) and Gulf of Aden (d'Acremont et al., 2005).

However, almost of data typically come from the 2D seismic data, which consist of distributional fault mapping and seismic-sections. Although, the 3D modelling from the scaled physical models can be modelled by MRI tool but this tool is very expensive.

Thus, this study will develop the 3D modelling from series of cross-section images of the scaled physical models (orthogonal rift model and oblique rift model) of the rift basins, which were supported by the Dynamics Research Group of the Royal Holloway University of London, and will create the 3D internal structures from both scaled physical models having stretching to be perpendicular and 60 degrees to the pre-existing structure beneath the rift basins. The results of these interpretations can be compared the internal structure of the natural rift basins in the Gregory rift in East Africa, the Extended Volcanic Tablelands in Owens Valley, north of Bishop, California (McClay et al., 2002) and the Mergui basin, east of Andaman sea, southern Thailand. Also, these results can be applied to petroleum system about fault trap and migration pathways of hydrocarbon.

1.2 Objectives

- To construct 3D fault models from scaled physical models of rift basins.
- To compare the differences in the internal fault systems between the scaled physical models having stretching to be perpendicular and 60 degrees to the pre-existing structure beneath the rift basins.

Chapter 2

Geological Background

2.1 Rift and passive margin evolution

2.1.1 Overview

Rift systems form boundaries between diverging tectonic plates, where the lithosphere experiences localized extension and thinning. Rift basins are also characterized by vertical movement (e.g. uplift rift flanks and development of lakes or sea basins). Rifts are typically continental extensional basins that have characteristics depending on a number of criteria, e.g. heat flow, strain rate, etc. (Kusznir and Park, 1987). They are genetically related to other basins created in an extensional regime and may either become tectonically inactive and develop into a 'failed' rift (e.g. Central North Sea, Baikal Rift, Sirt Basin) (Ziegler and Cloetingh, 2004), or continue to extend into a 'successful' rift leading to eventual break-up of the continental lithosphere and the production of new oceanic crust (e.g. Southern Red Sea) and the formation of 'passive margin' (e.g. Campos Basin, Gabon and Angolan Shelves, Nigerian and Mississippian Deltas) (Ziegler and Cloetingh, 2004). The timeline of rifting to the development of passive margins and the amount of volcanism (if any) that may occur is varied.

The main structure styles of continental extension develop as a function of the increasing extensional strain (Fig 2.1). Small near-surface extensional strain creates 'Simple Grabens' bounded by faults. These features are considered as minor structural depressions, usually having scales of a few meters to a few km (Olsen and Morgan, 1995). There is no significant lithosphere extension at this stage. Increasing extensional strain during 'Continental Rifting' results in the development of relatively deep, elongate structural depressions associated with which the entire lithosphere has been modified in extension (Olsen and Morgan, 1995). The zone of modification is localized by narrow rifting. In contrast, the greater magnitude of extensional strain in 'Highly Extended Terranes (HET)' is typically associated with the formation of broad, shallow basins. The difference between rifts and HETs is not only the magnitude of extension. Olsen and Morgan (1995) conclude that rifts and HETs represent different modes of extension, but that a continuum of between these modes exists. The products of successful continental separation are 'Passive Continental Margins'.

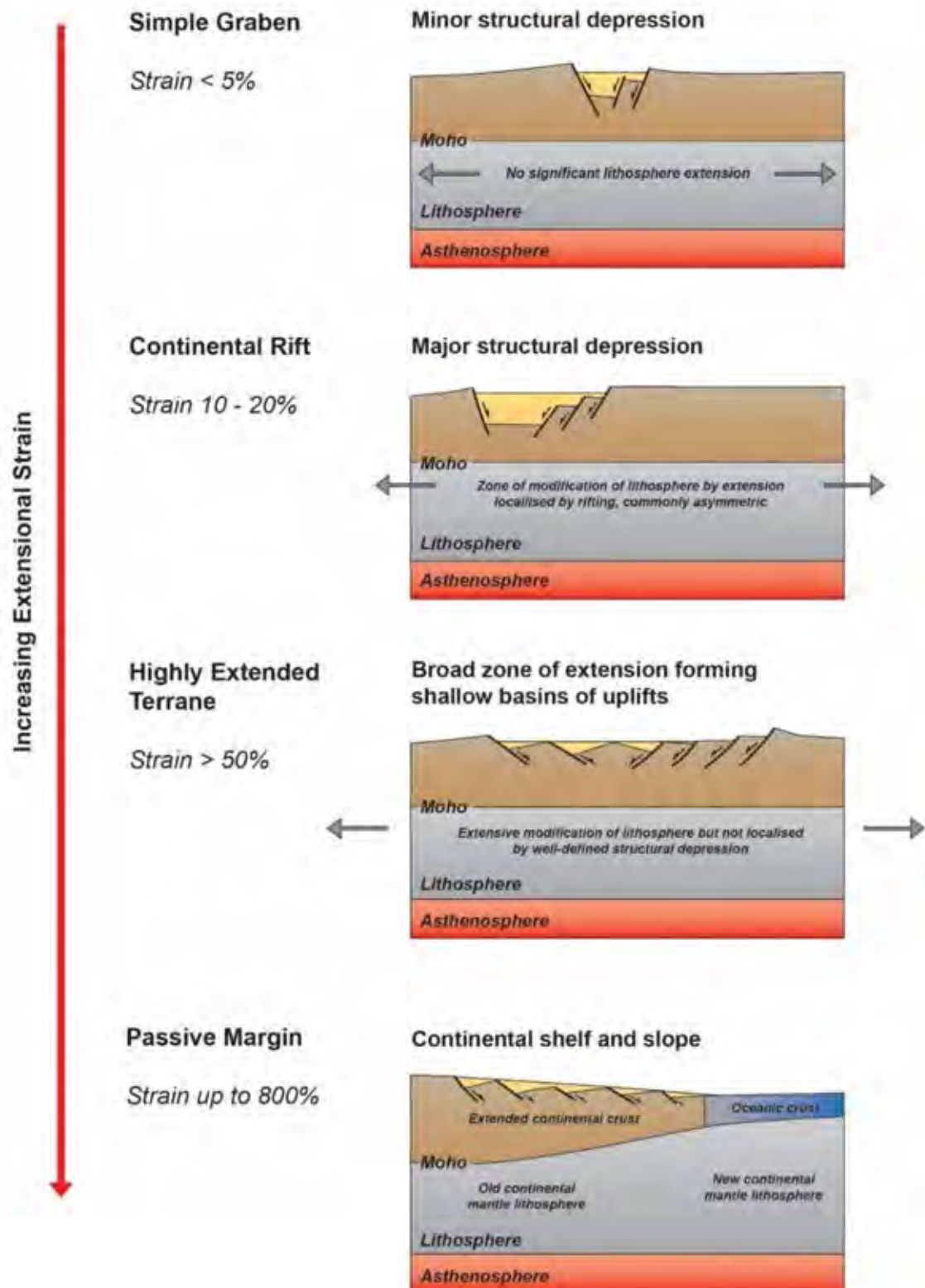


Figure 2.1 Main structure styles of continental extension as a function of the increasing extensional strain (after Olsen and Morgan, 1995).

2.1.2 Influence of pre-existing fabrics on the development of rift basins

Pre-existing structural discontinuities and metamorphic fabrics influence fault segment evolution, the location and architecture of rift basins. For example, on the Northwest Australian margin, pre-existing structures include Precambrian basement fabrics that strongly control the geometries of the Paleozoic and younger Mesozoic rift basins (AGSO, 1994; Pryer et al., 2002). Pre-existing structural fabrics typically create strength anisotropies in the crust that can either facilitate or inhibit deformation. Extension may occur obliquely to the pre-existing structural trends, resulting in oblique rifting. Natural examples of oblique rifting include the North Sea rifts (Faereth et al., 1997); the Gulf of Aden (d'Acremont, et al., 2005); and the main Ethiopian rift (Corti, 2008).

Several authors have used experimental modelling to determine how faults develop with different degrees of oblique extension (e.g. Withjack and Jamison, 1986; Serra and Nelson, 1988; Brun and Tron, 1993; Tron and Brun, 1991; Clifton et al., 2000; Clifton and Sclicsche, 2001; McClay et al., 2004; Corti, 2008). The experiment results show that the geometries of pre-existing fabrics are responsible for changes in fault patterns, for example, switches in fault polarity or locations of accommodation zones that may be due to inheritance from oblique basement faults (McClay et al., 2004) This is supported by field observations of accommodation zones that coincide with basement shear zones (Faulds and Varga, 1998; Ebinger, 1989; Daly et al., 1989; Khalil and McClay, 2001).

2.1.3 Fault evolution in rifts and passive margins

- ***Rift initiation***

Rift initiation is poorly understood due to the fact that extensive stretching, syn- and post-rift magmatism, and post break-up sedimentation usually overprint and bury the record of incipient extension in mature rifts and passive margins. Continental rifts worldwide show consistent patterns that are independent of geodynamic setting, indicating that the thermal and mechanical properties of the lithosphere largely determine the distribution of strain during the early rifting stages (e.g. Bassi 1995, Buck 2004).

During early rifting, faults propagate rapidly forming a broad rift (Meyer et al., 2002) (Fig 2.2a). The margins are characterized by the formation of two large sets of faults, which penetrate through the seismogenic crust (Bosworth, 1985) (Fig 2.2a). Initially only one of these faults will develop into the main rift border fault (Bosworth, 1985) forming half grabens, which may only reach a few 10's of km length depending on the maximum

length of the rift bounding faults. Fault length of the rift bounding faults. Fault length is controlled by the mechanical strength of the lithosphere (Bosworth, 1985).

With continued extension, a full rift develops (Fig 2.2b) as the fault segments link to form continuous structures (Fig 2.2c). Fault segment linkage localizes deformation to large structure, while minor faults become inactive if they do not form part of a linked array and occur within the stress shadows of the larger structures (McLeod et al., 2000; Gawthorpe and Leeder, 2000; Meyer et al., 2002). In addition, once fault density reaches a critical value no new faults will nucleate (Gupta and Scholz, 2000b).

- ***Deformational migration and rift localization***

As rifts develop deformation on faults may progressively migrate basin-ward or localize onto central rift faults (e.g. Gulf of Corinth, Aegean; North Sea rifts, UK; Suez rift, Egypt) (Ebinger et al., 2000; McLeod et al., 2000; Goldsworthy and Jackson, 2001; Meyer et al., 2002; Gawthorpe et al., 2003; Huerta et al., 2007). If the rift has associated volcanism, this too shows a migration of eruptive and dyke activity basin-ward (e.g. Main Ethiopian-Rift) (Hayward and Ebinger, 1996; Ebinger et al., 2000; Keir et al., 2006) (Fig 2.2c). Causes of rift localization have been attributed to changes in the thermal contrasts between crust and mantle (Huerta et al., 2007) and stress changes in the upper crust (Goldsworthy and Jackson, 2001). Gupta et al., (1998) suggested this process of rift localization and the associated rapid subsidence that is typically observed is related to fault segment evolution and linkages. All explanations show positive feedback in which the process of strain localization causes focused on mechanical weakening (Huerta et al., 2007).

- ***Continental break-up and passive margin formation***

Toward the mature stages of rifting, deformation localizes along nascent spreading ridges (d'Acromont et al., 2005) (Fig 2.2d), as dyke injection becomes the dominant process. Examples of continental rifts at the transition stages of sea-floor spreading are the Main Ethiopia Rift (Ebinger and Casey, 2001) and the Woodlark Rift (Papua New-Guinea) (Abers, 2001).

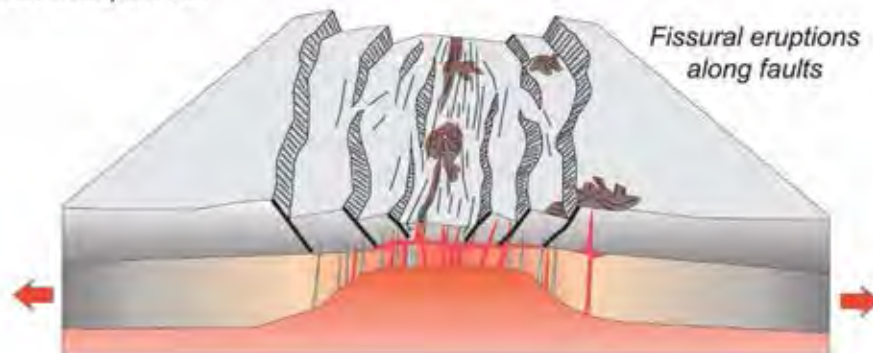
a) Half graben formation ($\beta < 1.2$)
e.g. East African Rift



b) Linkage of half grabens: development into a full rift ($\beta > \sim 1.4$)
e.g. North Sea UK



c) Development of small Intra rift grabens ($\beta \sim 1.6 - 2.0$)
e.g. Main Ethiopian Rift



d) Development of basaltic magmatism and oceanic style rift segmentation ($\beta > \sim 3$)
e.g. Northern Main Ethiopian Rift

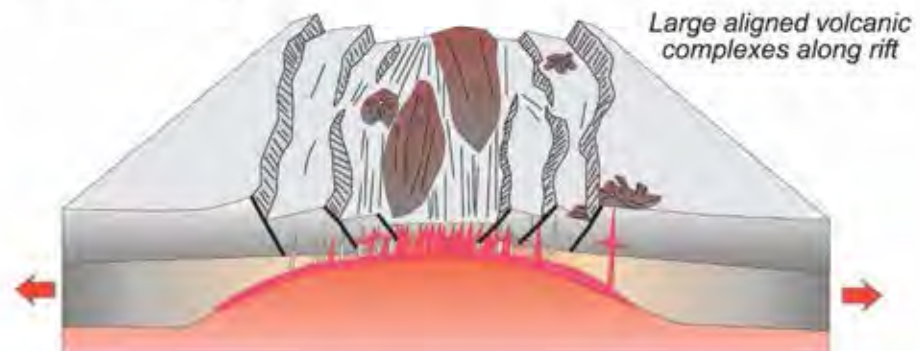


Figure 2.2 Schematic evolution of a segmented rift system with volcanics. B = stretching factor. (Modified after Hayward and Ebinger, 1996).

The final process in rift evolution is continental 'break-up', the formation of a passive margin, and generation of new oceanic lithosphere. The architecture of mid-oceanic ridge systems is strongly controlled by the rate of spreading (e.g. fast spreading East Pacific Rise, versus the slower spreading Ecuador rift) (Carbotte and MacDonald, 1994), and magma supply (MacDonald et al., 1998).

Offset rift basins are basins that are offset from the main locus of breakup (Chenin and Beaumont, 2013). Examples of offset rift basins include the Jeanne s'Arc Basin in the Newfoundland Grand Banks, the Fundy Basin in Nova Scotia, the Newark, Gettysburg, Culpeper, Scottville, Richmond/Taylor and Branchville/Jeburg Basins in the eastern United States (Withjack and Schlische, 2005). With continued extension, the migration of deformation towards the central rift forms confined narrow rift zones. The time period over which this this localization occurs is not fully understood. Some suggest this migration occurs very rapidly (e.g. East African Rift) (Ebinger et al., 2000).

2.2 Scaled physical models

Numerous studies have conducted experimental approaches to understand geological processes using physical models. The first major change in the approach to analogue modelling came when Hubbert (1937) published 'rules' on how to scale models to reflect their geological prototypes (Koyi, 1997). This meant that by selecting appropriately scaled geometries, materials, and kinematics, models could be quantitatively analyzed and compared to natural examples.

In recent years, many results from various types of scaled analogue modelling have been published. Some studies focused on the modelling of specific rift system such as the Afar region (Souriot and Brun, 1992), the North Sea (Brun and Tron, 1993), the Iceland rift system (Clifton and Schlische, 2003), or the Baikal rift (Hus et al., 2006). Others designed their analogue modelling of rift system to determine the effects of weak zones in the lithosphere or the presence of magma in the rift system (Corti et al., 2003; Corti, 2012) and the influences of pre-existing basement fabrics on orthogonal and oblique rifting (e.g. Withjack and Jamison, 1986; McClay and White 1995; Higgin and Harris, 1997; Keep and McClay, 1997; Acocella et al., 1999; Clifton and Schlische, 2001; Schlische et al., 2002; McClay et al., 2002; Michon and Sokoutis, 2005; Bellashen and Daniel, 2005).

A general spatial scaling factor of 10^{-4} to 10^{-5} has been found to be suitable in previous extensional modelling experiments by the Fault Dynamic Research Group (e.g. McClay, 1990; McClay and White, 1995, Dooley, 1994, Whitehouse, 2005).

- ***Geometric similarity***

Geometric similarity means that all lengths in physical models and natural examples (prototypes) are scaled proportionally. For example, the ratio of scaled length is expressed as:

$$L_r = L_m/L_p \quad (\text{Equation 2.1})$$

Where the scaled ratio of length (L_r) is equal to the model length (L_m) divided by the prototype length (L_p)

- ***Stretching factor***

All models were stretched by a total of 6 cm measured parallel to the direction of extension. The beta (β) stretching factor was also calculated for each model (e.g. McKenzie, 1978). Equation 2.2 shows the method applied to the experiments:

$$\beta = L/L_o \quad (\text{Equation 2.2})$$

Where L is the current model length and L_o is the original model length (pre-extension).

Chapter 3

Methodology

The methodology using the combination of geological software: image-seismic conversion software (Kogeo®), seismic interpretation software (OpendTect® and Petrel 2014) and structural analysis software (Move™) to create 3D internal structures of rift basins from scaled physical models, this chapter will explain all of procedures that consists of 6 main procedures following the workflow (Fig 3.1) below:

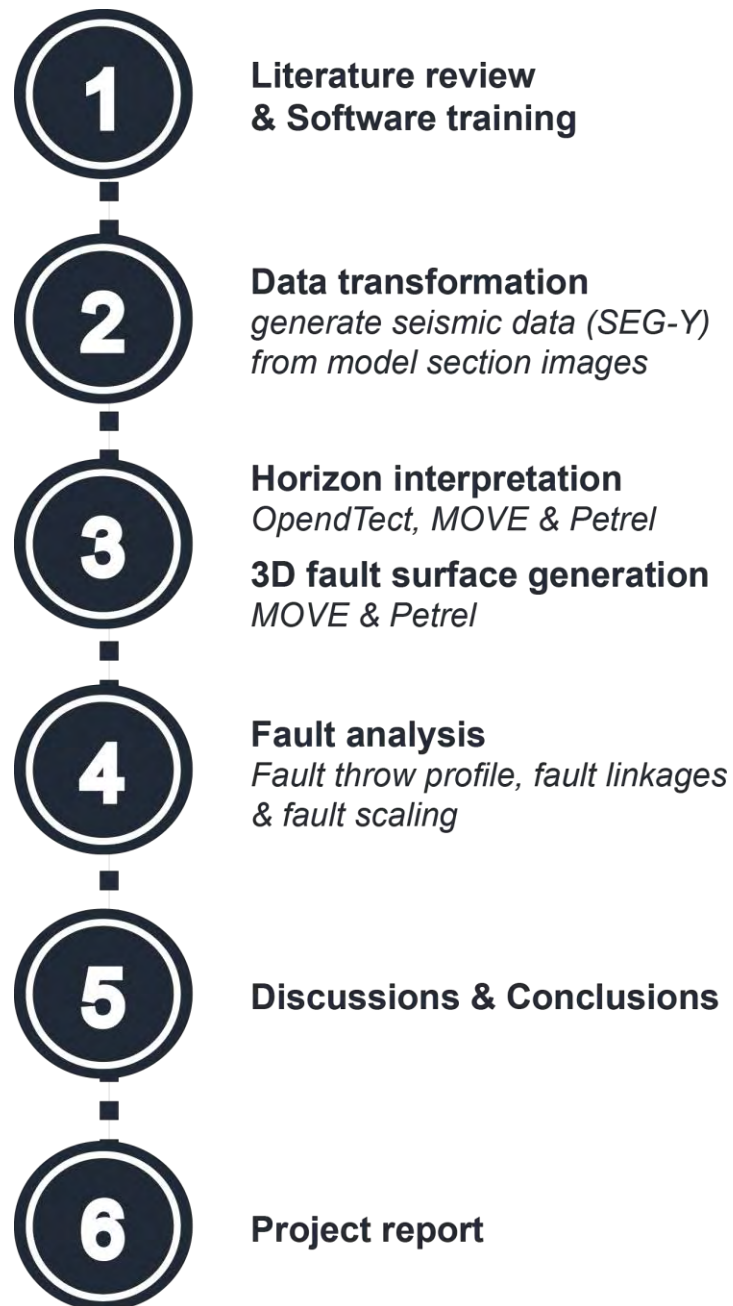


Figure 3.1 A workflow of methodology which were used to creating 3D internal structure of rift basins from scaled physical models.

3.1 Literature reviews and software training

Literature reviews that related the scaled physical models in the rift basin occurring in the present day were studied and gathered such as rift and passive margin evolution and scaled physical models.

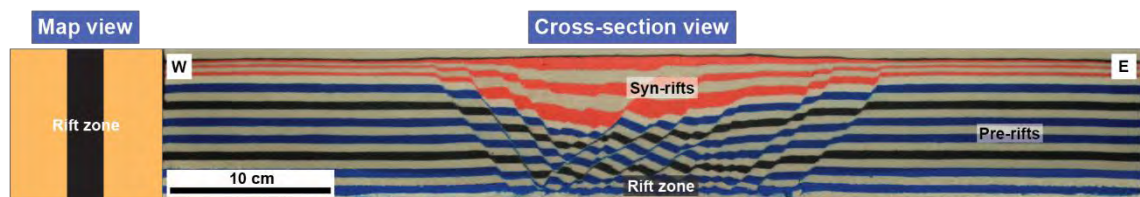
Furthermore, the geological software which are Kogeo®, OpendTech®, Move™ and Petrel 2014 will be studied about procedures and special techniques giving the best quality results for interpretation and analysis.

3.2 Data transformation

3.2.1 Resizing images size of NRS004-90 and NRS005-60 in Photoshop

In Photoshop, image sizes (or pixel dimensions) of model section images from the scaled physical models supported by the Dynamics Research Group of the Royal Holloway University of London will be resized in 6,100 pixels width and 950 pixels high (Fig 3.2a), by comparing 1 pixel to 0.1 millimeter of NRS004-90 (orthogonal rift model) that has extension direction to be perpendicular to the pre-existing structure beneath the rift basin. Moreover, the 108 images of NRS005-60 (oblique rift model) that has the extension direction to be 60 degrees to the pre-existing structure beneath the rift basin will be resized in 7,500 pixels width and 950 pixels high (Fig 3.2b), by comparing 1 pixel to 0.1 millimeter.

a) The Model Section Image (JPEG file) of Section 26 from NS004-90



b) The Model Section Image (JPEG file) of Section 26 from NS005-60

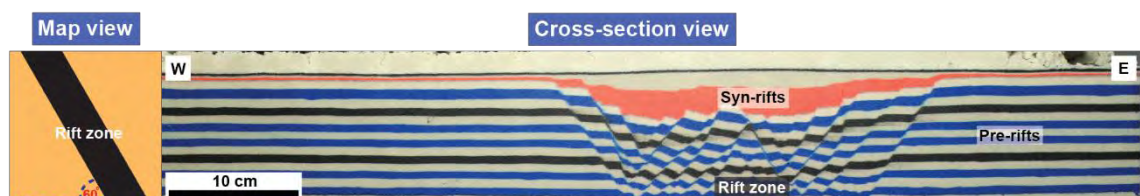


Figure 3.2 Resizing images of scaled physical models: (a) NRS004-90 (orthogonal rift model) and (b) NRS005-60 (oblique rift model). These images show the map view of geometry shape of pre-existing structures and the cross-section view of model section resizing images.

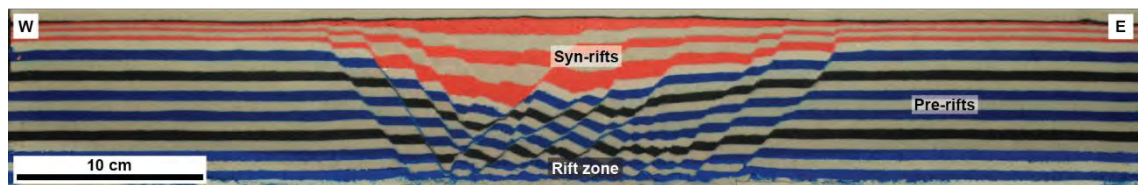
3.2.2 Creating SEG-Y in Kogeo®

In this procedure, the images that have been resized already will be converted from JPEG files to SEG-Y files by Kogeo®, and these SEG-Y files will be used to help the interpretation about 3D internal structures such as 3D horizon surfaces in the next procedures as well.

Procedure

- 1.) Open the “Kogeo®”.
- 2.) Open “Data” and select “Import bitmap data” respectively, after that choose the image from the scaled physical model (NRS004-90 or NRS005-60) that has been resized already.
- 3.) Next, select “matching colorbar” and choose “load colorbar” for adjusting color to be “rainbow2.col” which can be downloaded from “http://www.kogeo.de/index-Dateien/kogeo_download.html”, after that click “OK”, as shown in figure 3.4.
- 4.) In the process of exporting the SEG-Y files, open “Export SEG-Y/SU data” on “Data”, and then set the parameters following figure 3.5.

a) The Model Section Image (JPEG File) of Section 26 from NRS004-90



b) The Seismic Data (SEG-Y File) of Section 26 from NRS004-90



Figure 3.3 (a) A model section image (JPEG file) of section 26 from NRS004-90 that has been resized by Photoshop already. (b) A seismic data of section 26 from NRS004-90 that was converted from JPEG file to SEG-Y file by Kogeo®.

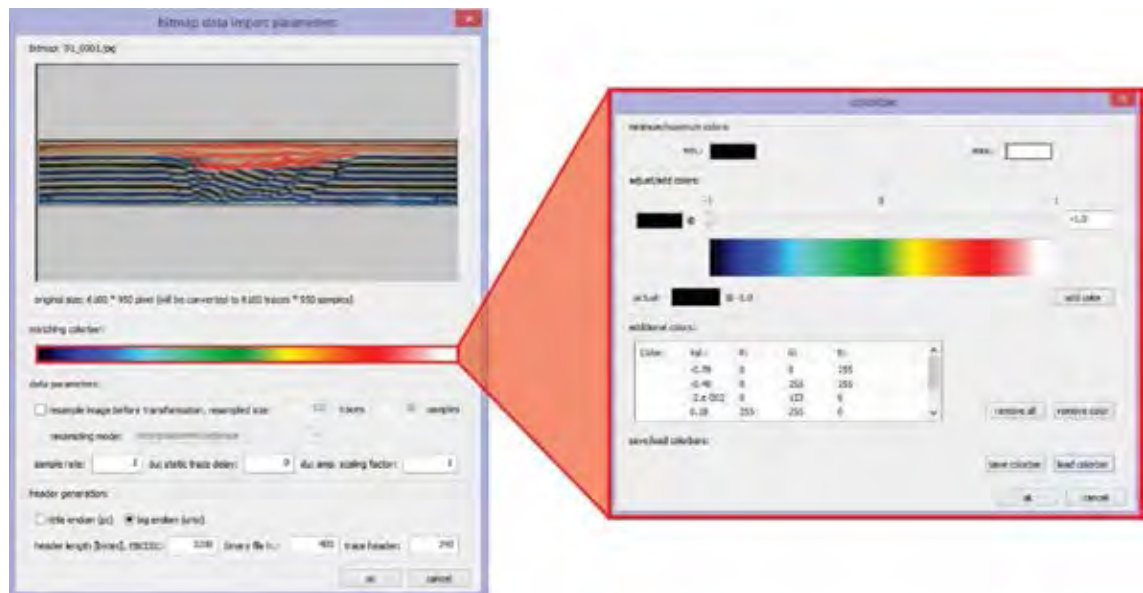


Figure 3.4 The procedure of selecting the “matching colorbar” and choosing the “load colorbar” for setting the color of SEG-Y file.

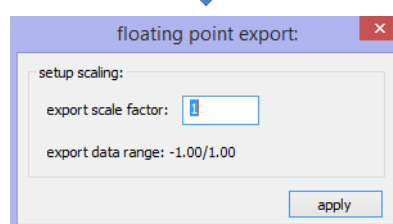
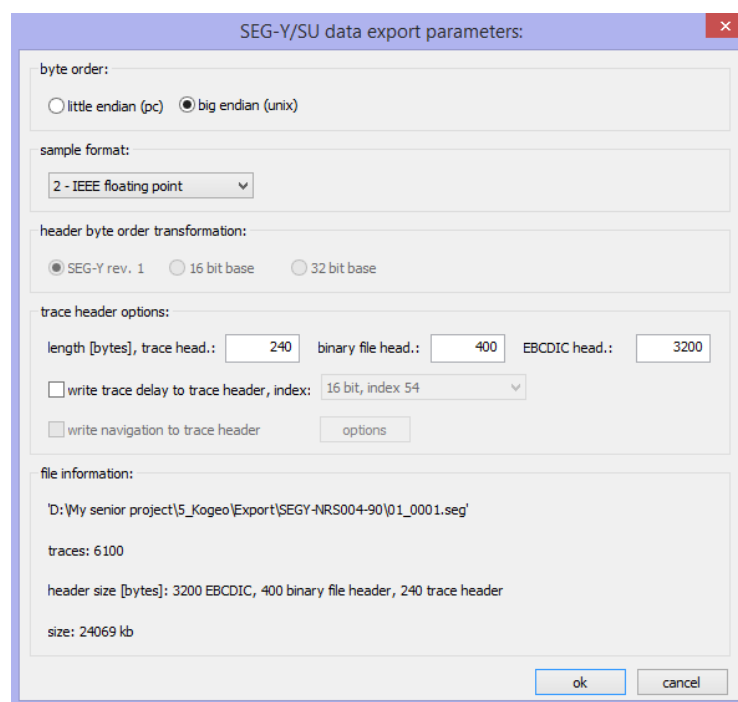


Figure 3.5 The procedure of setting the parameters of “SEG-Y/SU data export parameter” (above) and “floating point export” (below).

3.3 Horizon interpretation and 3D fault surface generation



3.3.1 Horizon interpretation

- **Horizon interpretation (pre-rifts) in OpendTech®**

After the SEG-Y files of both models have been converted already, the horizons of pre-rift will only be interpreted by OpendTech® because a wave phase problem occurring from using the colors of materials in sandbox experiment will affect to tracking the profile sections in this software.

However, if the images have not the problem about the wave phase, all of horizons: pre-rifts, syn-rifts and post-rifts that were SEG-Y files will be interpreted by OpendTech®.

Procedure (importing 2D lines)

- 1.) Open “OpendTech®” and select the “Create New Survey”.
- 2.) Then, create the name that related the model interpreted in this software and set the parameters following figure 3.6 and select “Next”.
- 3.) Select the SEG-Y file that were converted by Kogeo®.
- 4.) In “Extract Survey Setup from SEG-Y”, First, Change the “data type” to “2D Seismic data”. Second, change the “Data format” to “5-IEEE float (32 bits)”. Third, Select “ Setting for byte location scanning” and set the parameters following figure 3.7. Forth, click “ Scan the entire input”. Fifth, change “header of X-coordinate range” to “tracl (byte 1)-trace sequence number within line” and change “header of Y-coordinate range” to “tracl (byte 5)-trace sequence number within reel” which can follow figure 3.8. Finally, select “OK”.

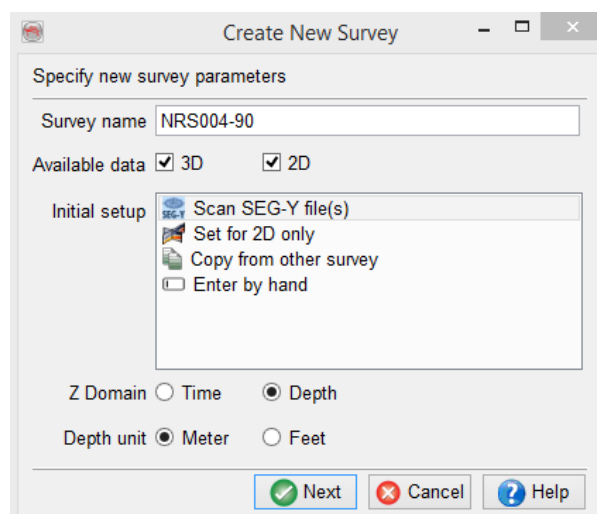


Figure 3.6 The procedure of setting the parameters of “Create New Survey” in OpendTech®

- 5.) In “**Edit Survey Parameters**”, set the parameters following figure 3.9 and select “**OK**”.
- 6.) In the “**Survey Setup and Selection**”, click “**Select**” and “**Yes**” respectively.
- 7.) In “**Import 2D Line**”, exam “**Importing and Line name**”, create name of “**Output 2D line (attribute)**” and click “**OK**”.
- 8.) In “**Elements**” of OpendTech®, add “**2D Line**” and select “**attribute**” that was created from previous procedure.
- 9.) After the first 2D line can be displayed in OpendTech®, other 2D lines in each model will be imported by OpendTech® respectively following the next procedures below.
 - 9.1.) On the menu bar, select “**Survey**”, “**Import**”, “**Seismic**”, “**SEG-Y**” and “**2D...**” respectively.
 - 9.2.) Next, choose another SEG-Y file from NRS004-90 or NRS005-60 that need to be sorted correctly.
 - 9.3.) Repeat procedure “**3 to 4**”, and then the next procedure will follow below;
 - 9.3.1.) In “**Import SEG-Y Data**”, Select “**Edit**”.
 - 9.3.2.) In “**Manipulate SEG-Y File**”, add “**tracr**” and plus 50 in “**Formula for ‘tracr’**”. In addition, choose the location and create the name of “Output File” (01_0002+50) shown in figure 3.10.
 - 9.3.3.) In “**Import SEG-Y Data**”, change the “**Data format**” to “**5-IEEE float (32 bits)**” again and select “**Select**” respectively.
 - 9.3.4.) In “**Import 2D Line**”, change the “**line name**” to be “**01_0002**” and choose the attribute that be created previously.
 - 9.3.5.) Add “**2D Line**” that have been created previously from the “**Elements**” of OpendTech®.
- 10.) Finally, repeat **the procedure 9** until the remaining 2D lines of NRS004-90 or NRS005-60 will have been added into OpendTech®.

When all of 2D lines have been added already, their pre-rifts (may include syn-rifts) of each model will be interpreted by “**Horizon tracking**” in OpendTech®.

Procedure (Horizon tracking)

- 1.) In the “**Elements**”, select “**2D Horizon**” and “**Track New**”.
- 2.) Next, choose “**Event**” and set “**Event Type**” to be “**Zero Crossing +-**” respectively.
- 3.) Then, close a window of the horizon tracking settings.
- 4.) Finally, track the top horizons of pre-rifts (or syn-rifts) carefully.

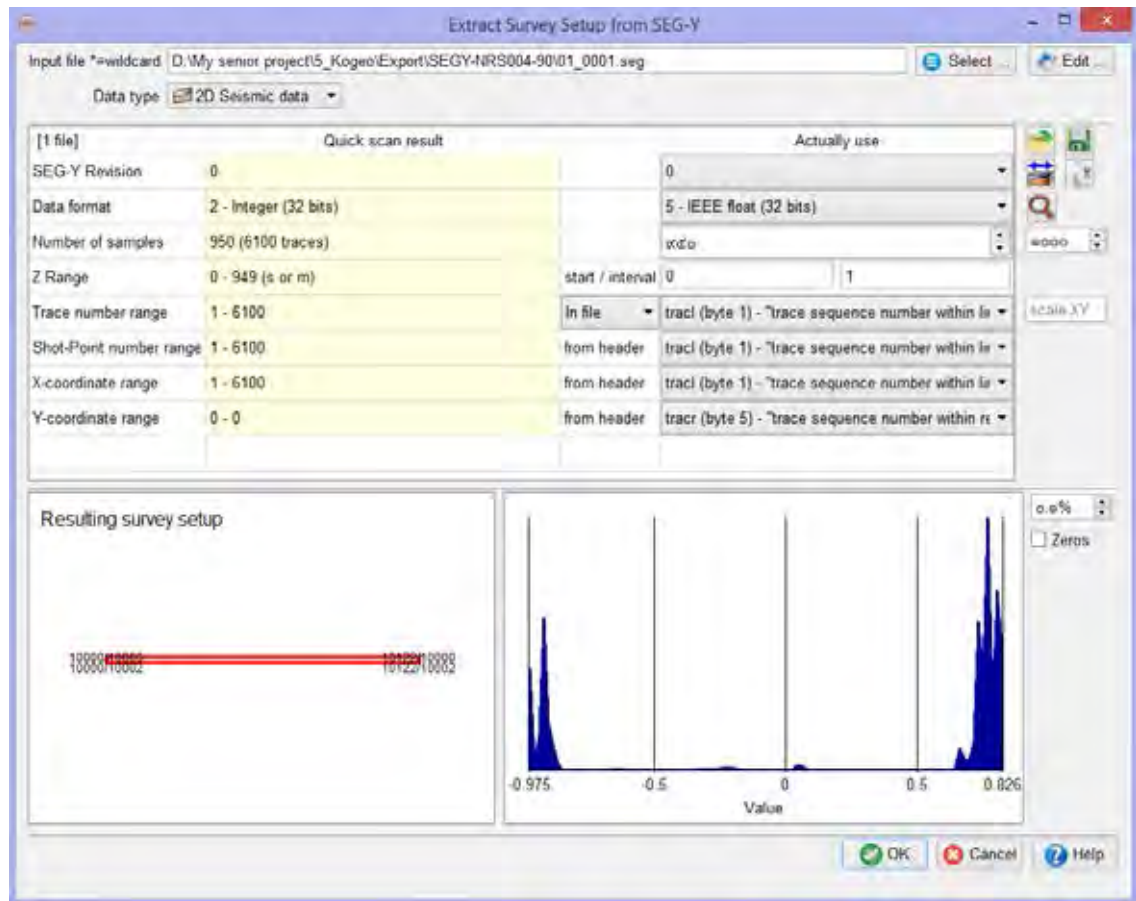


Figure 3.7 The procedure of setting the parameters in “Extract Survey Setup from SEG-Y file” for importing the SEG-Y file into OpenTect®.

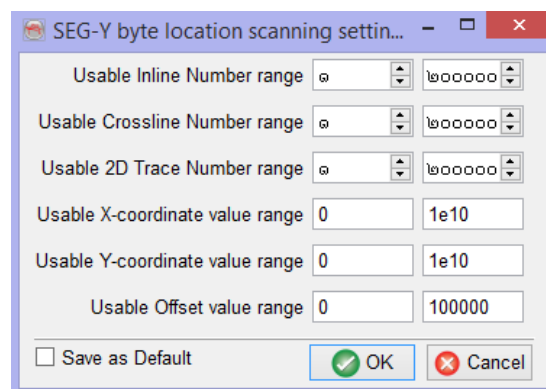


Figure 3.8 The procedure of setting the parameters in “SEG-Y byte location scanning setting”.

Survey name: NR-S004-90

Location on disk: D:\opendtect

Survey type: Both 2D and 3D

Ranges/coordinate settings: Enter below

Survey ranges:

- In-line Range: 00000 to 00000 Step: 0
- Cross-line range: 00000 to 00000 Step: 0
- Z range: 0 to 949 Step: 1 meter

Display depths in: meter feet

Seismic Reference Datum (m): 0

Coordinate settings: Easy Advanced Define Coordinate System ...

First In-line/Cross-line: 10000 10000 = (X,Y) 1 0

Another position on above In-line: 10000 10002 = (X,Y) 1 100

Position not on above In-line: 10122 10002 = (X,Y) 6101 100

Buttons:

Free space on disk: 333.50 GB

Figure 3.9 The procedure of setting the parameters in “Edit Survey Parameter”.

Manipulate 'D:\My senior project\1_NRS004-90\SEGY-NRS004-90\01_0002.seg'

Text Header:

Binary header: [Rev 0] 950 samples (4-byte), interval=1 Change ...

Trace headers:

- fldr
- tracr
- ep
- cdp
- cdpt
- trid
- nvs
- nhs
- duse
- offset
- gelev
- selev

tracr = tracr+50

	Byte	Value
tracr	5	50
fldr	9	0
tracf	13	0
ep	17	0
cdp	21	0

Output file: D:\My senior project\1_NRS004-90\SEGY-NRS004-90\01_0002+50.seg Select ...

Buttons:

Figure 3.10 The procedure of defining the value for locating the section of SEG-Y file to OpendTech®.

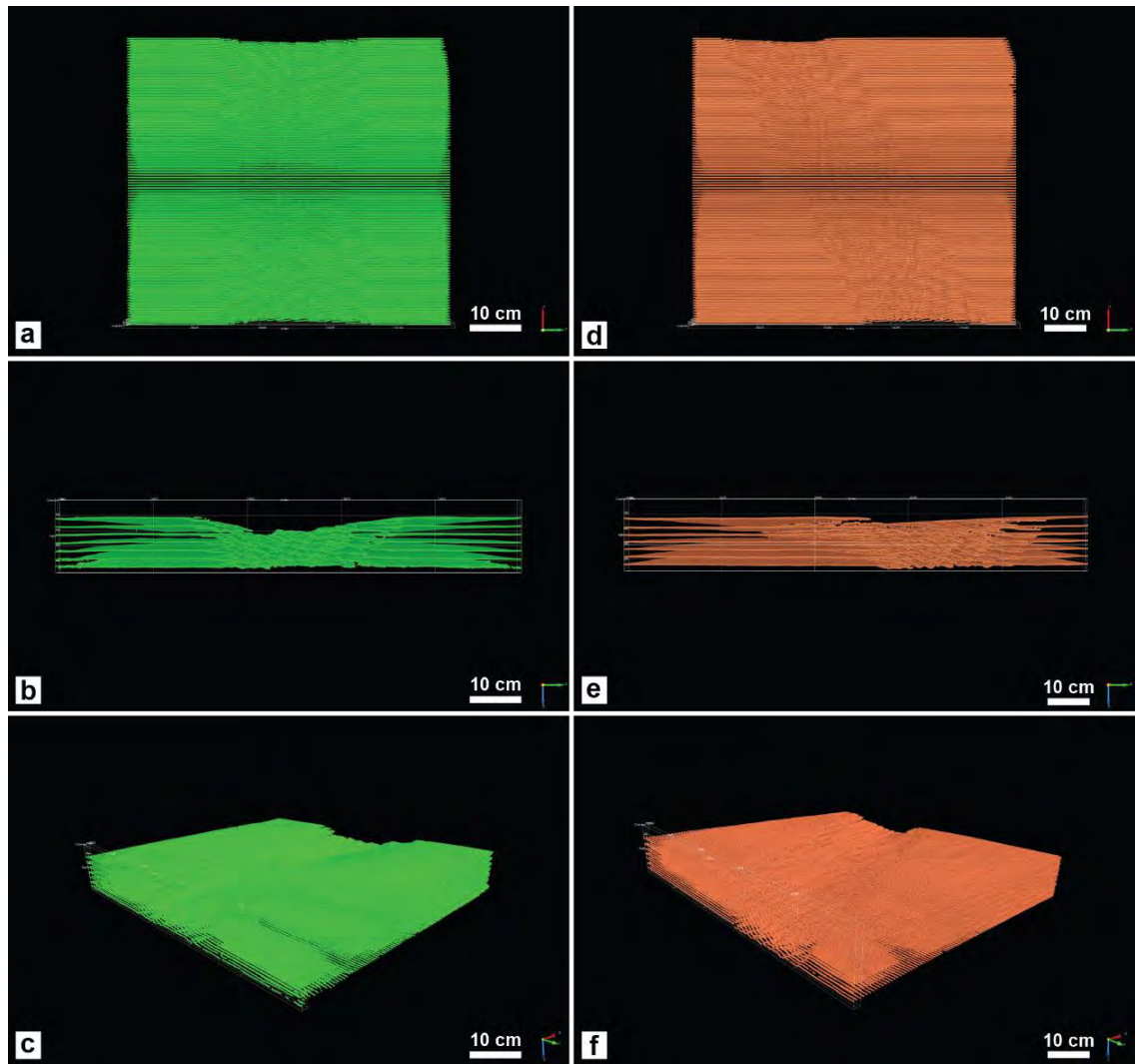


Figure 3.11 The 2D horizon lines from NRS004-90 (a, b and c) and NRS005-60 (d, e and f) that were shown in the map visualization (a and d), the north visualization (b and e) and the oblique visualization (c and f) in OpendTect®. These images were interpreted from the SEG-Y files of model section images from both models.

- **Exporting SEG-Y files from OpendTech® to Move™**

This procedure will explain about the methodology of exporting data from the horizons that were tracked in OpendTech® to Move™. Thus, this procedure will be essential about another process which will be used to create the horizon surfaces and also interpret the structural surfaces of each model in Move™.

Procedure

- 1.) Choose “**Survey**” on the menu bar.
- 2.) Next, select “**Export**”, “**Horizon**”, “**ASCII2D**” and “**Bulk 2D Horizons...**” respectively.
- 3.) Finally, set the parameters and create the name of “**Output ASCII File**” in “**DAT File (.dat)**” following figure 3.12 because this file can be corrected in the excel about the X-Y-Z ratio of model before this file will be imported to Move™.

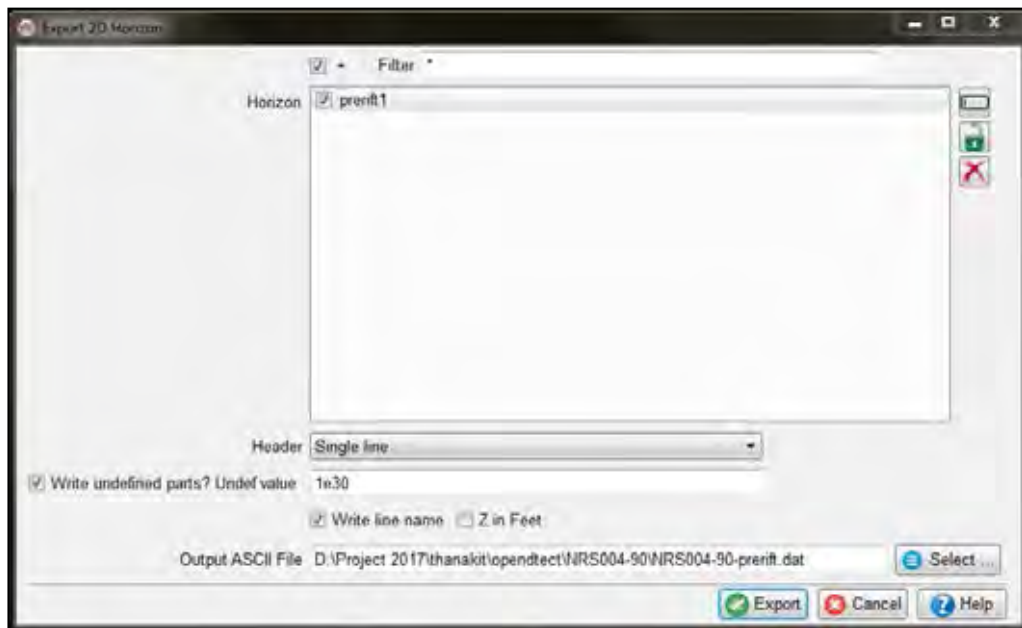


Figure 3.12 The procedure of setting the parameters in “Export 2D Horizon”.

- **DAT files correction in excel**

In this correction, the data had been corrected about the ratio of model to be appropriate with the ratio in Move™ before they were imported.

Procedure

- 1.) Insert the “**DAT file**” that has been exported by Excel already.
- 2.) Next, create new column of X, Y, Z value which were multiplied by 10.
- 3.) Calculate the values of the new column.
- 4.) Finally, save and export new DAT files.

- **Importing DAT files to Move™**

In this procedure, the correcting DAT files will be imported to Move™, and then all surfaces from each horizon interpreted from OpendTect® will be display in this software.

Procedure

- 1.) Open Move™.
- 2.) Choose “**File**”, “**Insert**”, and select the location of the DAT file that was corrected from previous procedure respectively.
- 3.) Set the parameters in the table will be shown in figure 3.13.

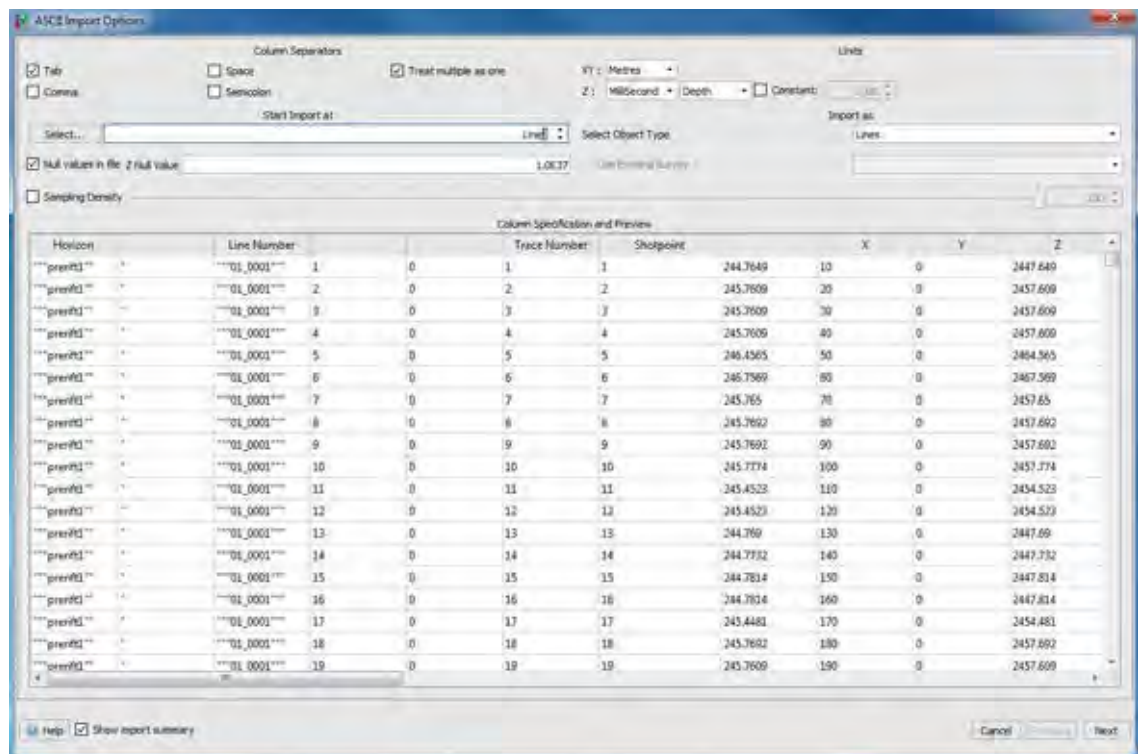


Figure 3.13 The procedure of setting the parameters in “ASCII Import Options”.

- **Horizon interpretation (syn-rift) in Move™**

After the pre-rift surfaces have been interpreted by OpendTech® and have been imported to Move™ already, the horizons of syn-rift will be interpreted and created by Move™ since the problem of the wave phase.

Thus, this procedure will also explain about the methods of importing resizing images, digitizing horizons of syn-rifts and creating horizon surfaces of syn-rifts.

Procedure (importing resizing images)

- 1.) In Move™, choose “**File**” and “**New**” respectively.
- 2.) Next, set parameters of “**Coordinate System**” following figure 3.14 and select “**OK**”.
- 3.) After that select “**Insert**” and choose the resizing image respectively.
- 4.) Then, set all parameters following this procedure below;
 - 4.1.) select “**As an image**” and “**Next**” in Import Type.
 - 4.2.) In Image Name and Region, create “image name”, select “**Import Sub-region**” and select “**Next**” respectively.
 - 4.3.) In Image Location, select “Vertical extents” and “**Create Section with Image**”.
 - 4.4.) In Reference Settings, all images of each model were set the scale of X, Y and Z (X = width of a model, Y= position of image section which was cut from scaled physical model and Z = depth of the model) in “**Bottom Right**”. Then, select “**Load**” to import the image section in Move™.
- 5.) Finally, repeat the procedure 3 to 4 for importing all resizing images of each model to Move™.

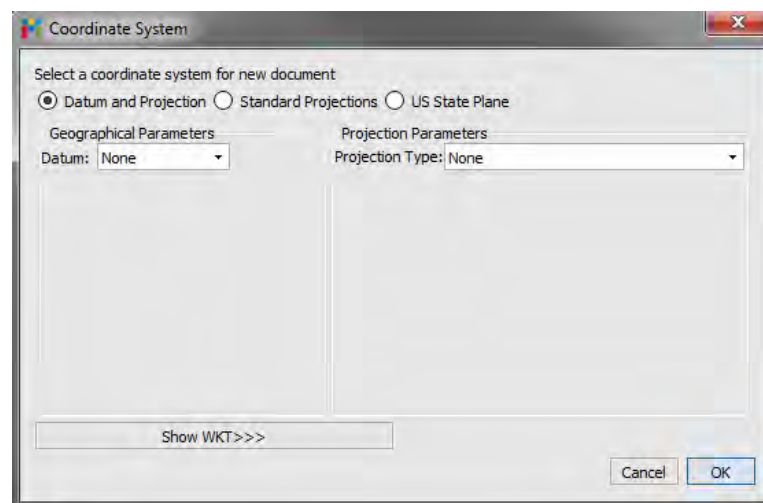
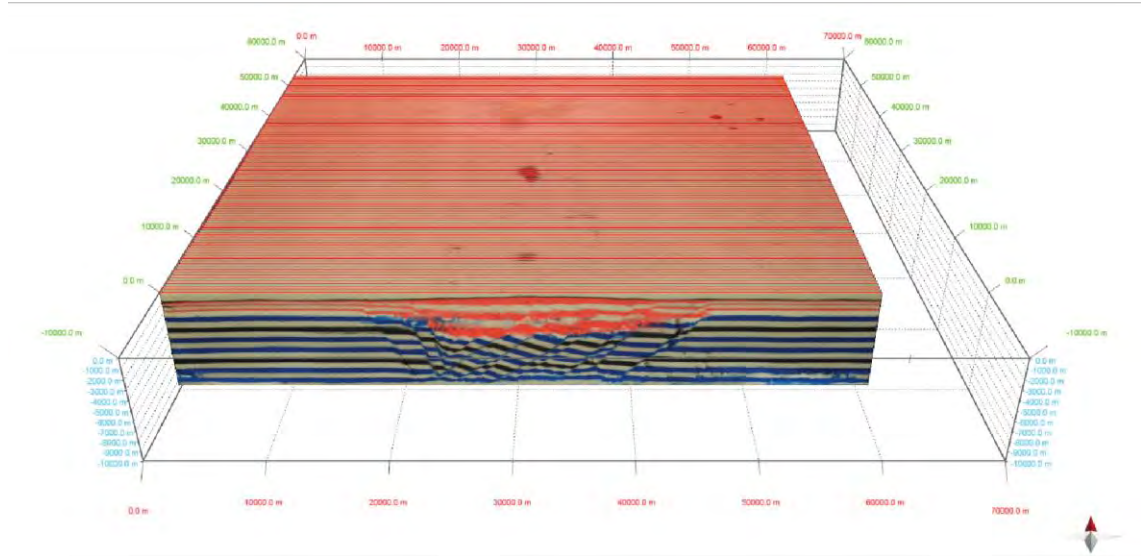


Figure 3.14 The procedure of setting the parameters in “Coordinate System”.

a) Model Section Images of NRS004-90 (orthogonal rift model)



b) Model Section Images of NRS005-60 (oblique rift model)

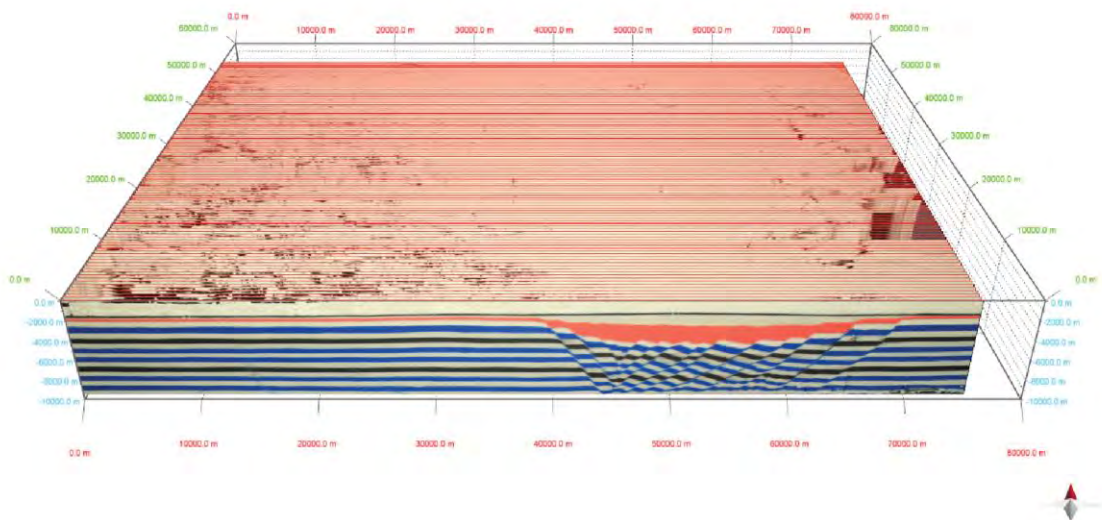


Figure 3.15 The model section images of both models: (a) NRS004-90 and (b) NRS005-60 that were used in the procedure of the digitizing horizons and faults.

Procedure (digitizing horizon of syn-rift)

- 1.) In digitizing the horizons, on the Model Building tab, select “**Horizon**”.
- 2.) Then, select “**Snap to Point**”.
- 3.) Under “**Horizon Assignment**”, select “**Horizon_01**”.
- 4.) Click to digitize the Horizon_01 in the footwall of the section. Start by hovering the cursor over the footwall cut-off of the Horizon_01. The cursor will change to a circle, indicating that the horizon will be snapped to the fault. Click to start digitization and continue clicking until the horizon is snapped to the western post. Right-click to end digitization.
- 5.) Next, digitize the Horizon_01 in the hanging wall of the section. Use the same method as specified in the previous step.
- 6.) Then, digitize the Horizon_01 in the other sections of NRS004-90. Using the previously same methods (1-6).
- 7.) In another horizon, **repeat the previous method (1-6)**, but the horizon assignment will be changed to other horizons such as “**Horizon_02**”.

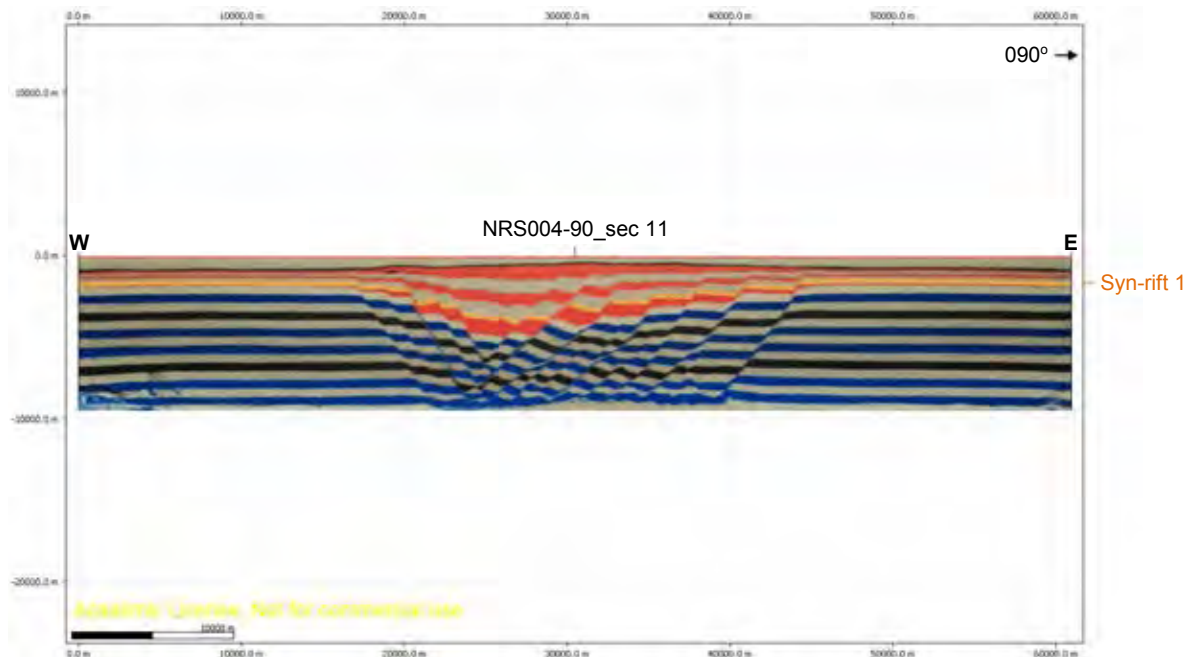


Figure 3.16 The 2D cross-section image (sec 11) of NRS004-90 that was digitized the horizon of syn-rift 1.

Procedure (creating surface of horizon)

- 1.) Choose **“MODEL BUILDING”** and select **“Surface”** in **“Surfaces/Volumes”** respectively.
- 2.) On **“Create Surface”**, select **“Create Surface from Lines”**.
- 3.) On **“Model Browser”**, select a set of the horizon lines (Horizon_01, Horizon_02, Horizon_03,...) in **“Sets”**.
- 4.) On **“Create Surface”**, add the **“horizon lines”** into **“Select Lines”**.
- 5.) Next, set all parameters following figure 3.17.
- 6.) Finally, click **“Create surface”**.

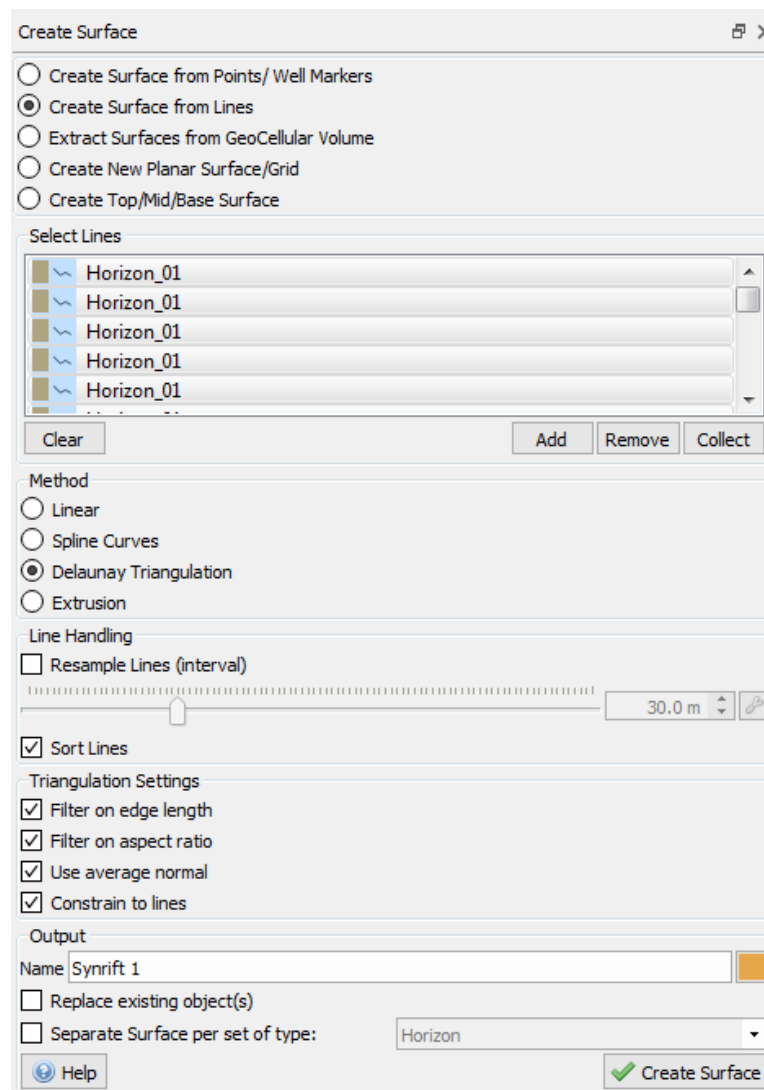
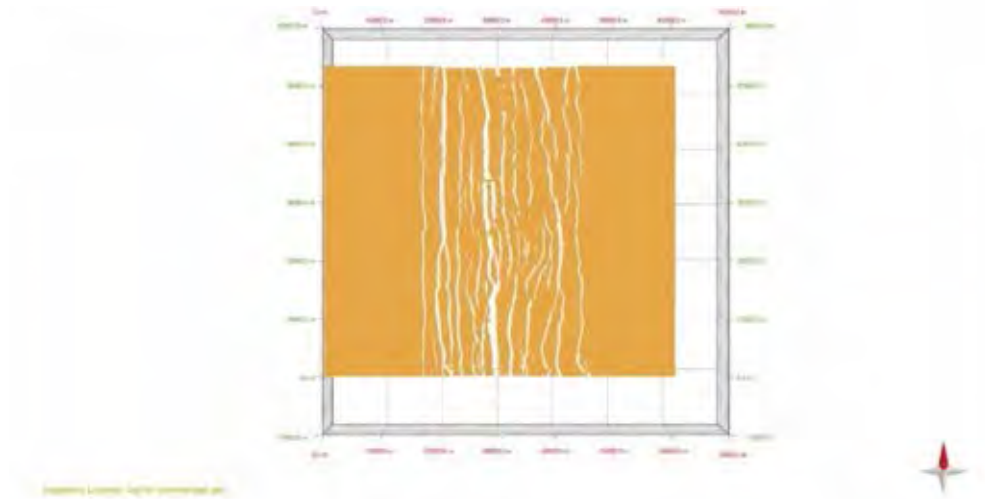
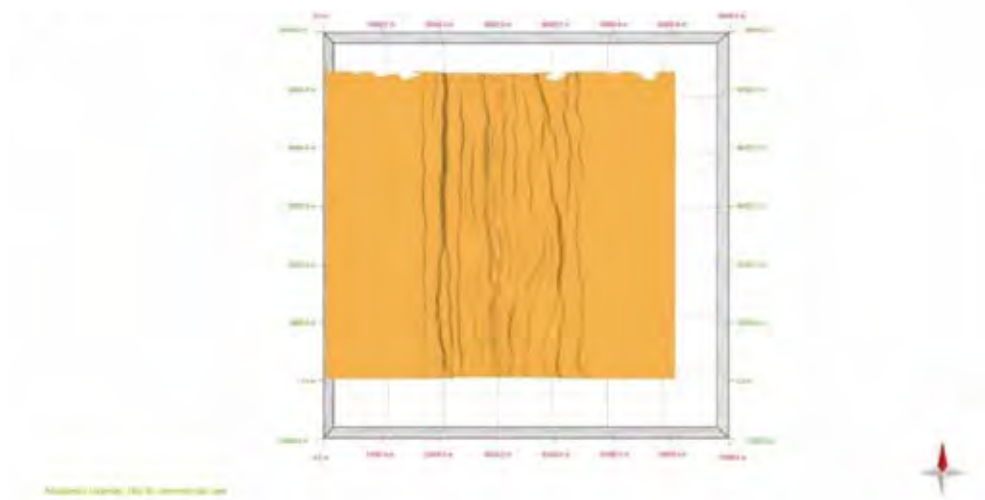


Figure 3.17 The procedure of setting the parameters in “Create Surface” of syn-rift 1.

a) Horizon Lines of Syn-rift 1 from NRS004-90 (map view)



b) Horizon Surface of Syn-rift 1 from NRS004-90 (map view)



c) Horizon Surface of Syn-rift 1 from NRS004-90 (oblique view)

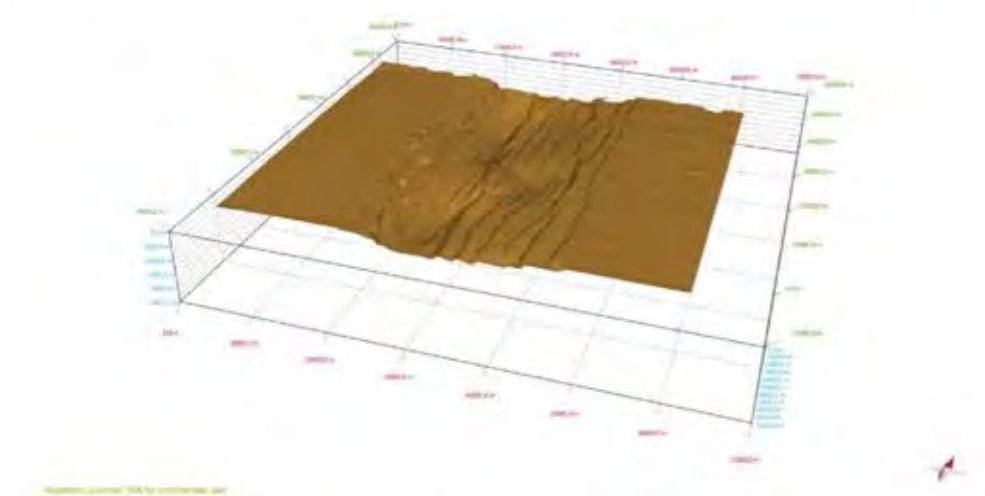


Figure 3.18 (a) Horizon lines of the syn-rift 1 digitized already. (b) and (c) a horizon surface of the syn-rift 1 created from the horizon lines of syn-rift 1.

- **Examining scale of model**

In Move™, the scale of each model is very significant for the next procedures that are discussion and interpretation. Thus, after horizon surfaces were generated already, these horizon surfaces must be examined the scale of the surfaces which were imported from the DAT file (pre-rifts from OpendTech®) and were created by Move™ (syn-rifts) every time before the next procedure will be run.

Procedure

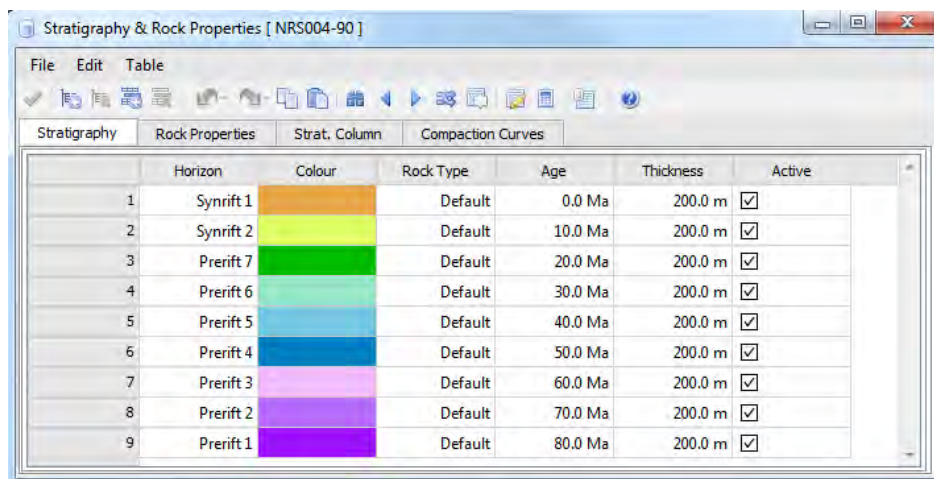
- 1.) Choose **“MODEL BUILDING”** on the menu bar.
- 2.) Select **“Advance”** that is in **“Transform”**.
- 3.) Next, add the surface that would like to transform the scale of model.
- 4.) In **“Transformation and Scale Using 2 Points”** to set the value of the new surface.
- 5.) After that, set the new X, Y and Z values.
- 6.) Click **“Transform”**.

- **Setting the stratigraphy**

This procedure will determine the stratigraphy of all horizons of each model since depths of the stratigraphy will be used in the procedure of fault analysis. Thus, determining stratigraphy of each horizon surface will be significant procedure which can absolutely create the potential analysis.

Procedure

- 1.) Choose **“DATA & ANALYSIS”** on the menu bar.
- 2.) Then, select **“Stratigraphy”**.
- 3.) Determine the numbers of horizons and create the name of each horizon.



	Horizon	Colour	Rock Type	Age	Thickness	Active
1	Synrift 1	Orange	Default	0.0 Ma	200.0 m	<input checked="" type="checkbox"/>
2	Synrift 2	Yellow	Default	10.0 Ma	200.0 m	<input checked="" type="checkbox"/>
3	Prerift 7	Green	Default	20.0 Ma	200.0 m	<input checked="" type="checkbox"/>
4	Prerift 6	Light Green	Default	30.0 Ma	200.0 m	<input checked="" type="checkbox"/>
5	Prerift 5	Light Blue	Default	40.0 Ma	200.0 m	<input checked="" type="checkbox"/>
6	Prerift 4	Blue	Default	50.0 Ma	200.0 m	<input checked="" type="checkbox"/>
7	Prerift 3	Purple	Default	60.0 Ma	200.0 m	<input checked="" type="checkbox"/>
8	Prerift 2	Dark Purple	Default	70.0 Ma	200.0 m	<input checked="" type="checkbox"/>
9	Prerift 1	Dark Blue	Default	80.0 Ma	200.0 m	<input checked="" type="checkbox"/>

Figure 3.19 Setting stratigraphy of NRS004-90 that was defined from amounts of horizons.

- **Changing horizons name in object types**

In changing horizon name in object types, it is easy procedure but is very significant to protect a confusing problem that can happen since a lot of data in Model Browser.


Procedure

- 1.) Choose “**Model Browser**”.
- 2.) Select and change the names of horizon in “**Mesh surface**” to be similar the names of the horizons that were set in the stratigraphy respectively.

- **Changing the color map**

This procedure will change the color of surface map that will be created the elevation of surface following the shades of color.

Procedure

- 1.) Choose “**DATA & ANALYSIS**” on the menu bar.
- 2.) Select “**Colour Map**” in “Display”.
- 3.) Add the surface that would like to change.
- 4.) Set the parameters following figure 3.20.
- 5.) After that, click “ **Expand Colour Map to Selection**”.
- 6.) Click “**Apply**”.

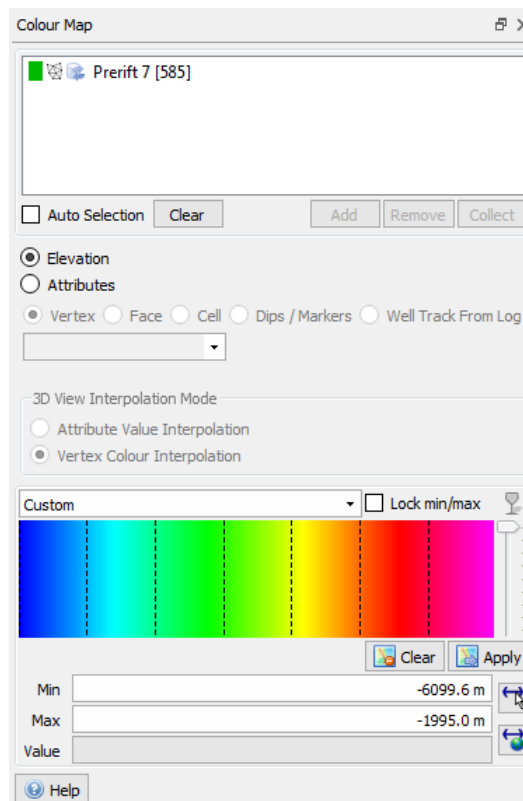
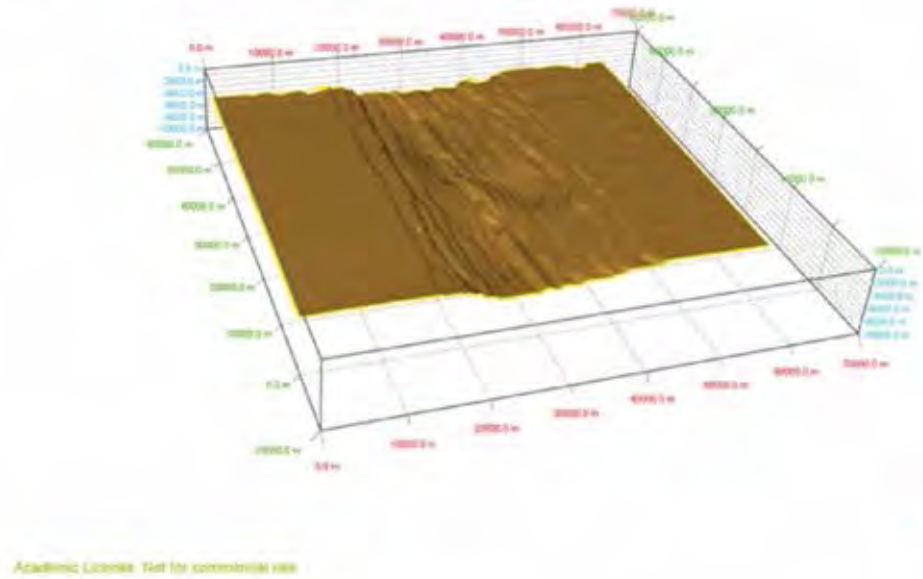


Figure 3.20 The procedure of setting the parameters in “Color Map”.

a) Non-Changing Color Map of NRS004-90 (oblique view)



b) Changing Color Map of NRS004-90 (oblique view)

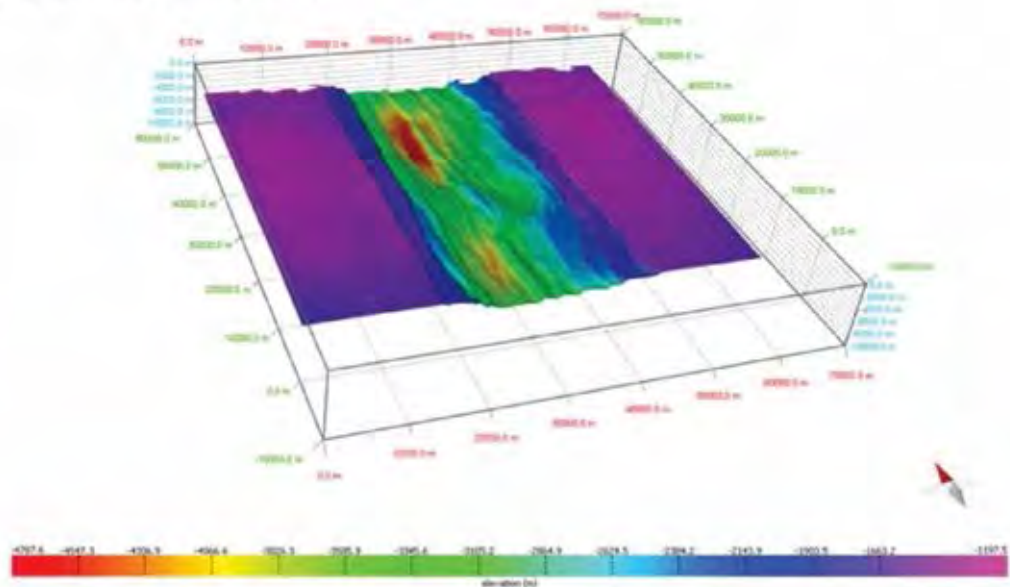



Figure 3.21 The surface map of syn-rift 1 from NRS004-90: (a) the surface map that wasn't changed the color map and (b) the surface map that was changed the color map.

- **Surface Correction**

After changing the color maps, there may be some distortions occurring from importing the data from OpendTech®. Thus, this process will develop the data to be better before changing the color map again. Also, this procedure can help about the procedure of fault analysis.

Procedure

- 1.) Zoom the distortion area on surface.
- 2.) Select “ **Object Loop Selection**”.
- 3.) Press shift to activate and draw around the distortion area.
- 4.) Press “**Delete**” on a keyboard.
- 5.) Repeat the procedure of “**Changing the Color Map**” again.

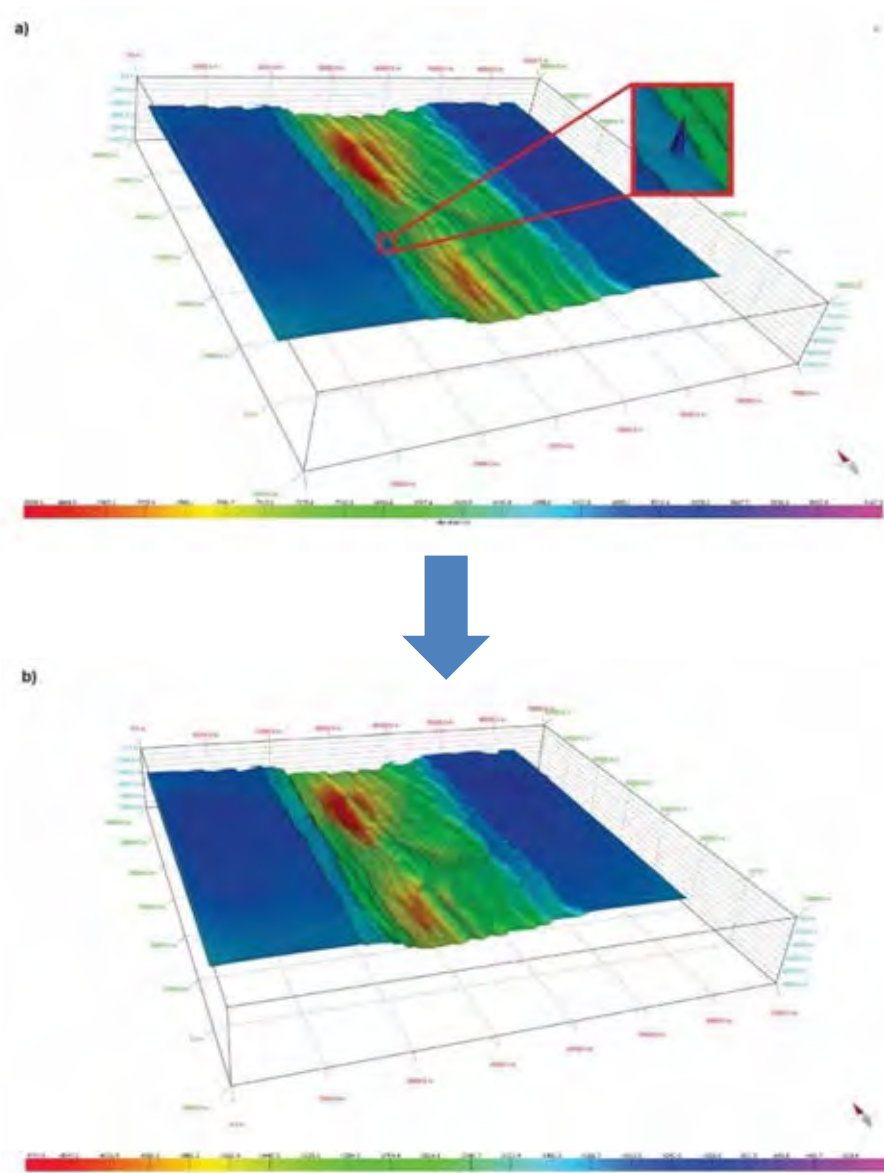


Figure 3.22 (a) The surface correction of some surface that has a distortion coming from the creating surface and (b) the new surface that has been corrected already.

- **Adjusting smooth surface of horizon surfaces**

This procedure will develop or prepare the surfaces of each horizon before analyzing data. The horizon surfaces that came from DAT files of OpendTech® will be adjusted because they might affect with the procedure of the fault interpretation and the trimming in fault analysis (Fig 3.24).

The procedure of adjusting smooth surface can be divided into 2 methods. The first method, the horizon surfaces will be adjusted by the function in Move™. The second one will use the Petrel to help adjusting the smooth of horizon surfaces (This methodology was explained by the procedure of the fault interpretation that used the function of “Move™ link for Petrel”).

Procedure (Move™)

- 1.) Choose “**MODEL BUILDING**” on menu bar.
- 2.) Select “**Smooth**” in “**Modify Data**”.
- 3.) Add the horizon surface that would like to adjust the quality of surfaces.
- 4.) Set the parameters following in figure 3.23.

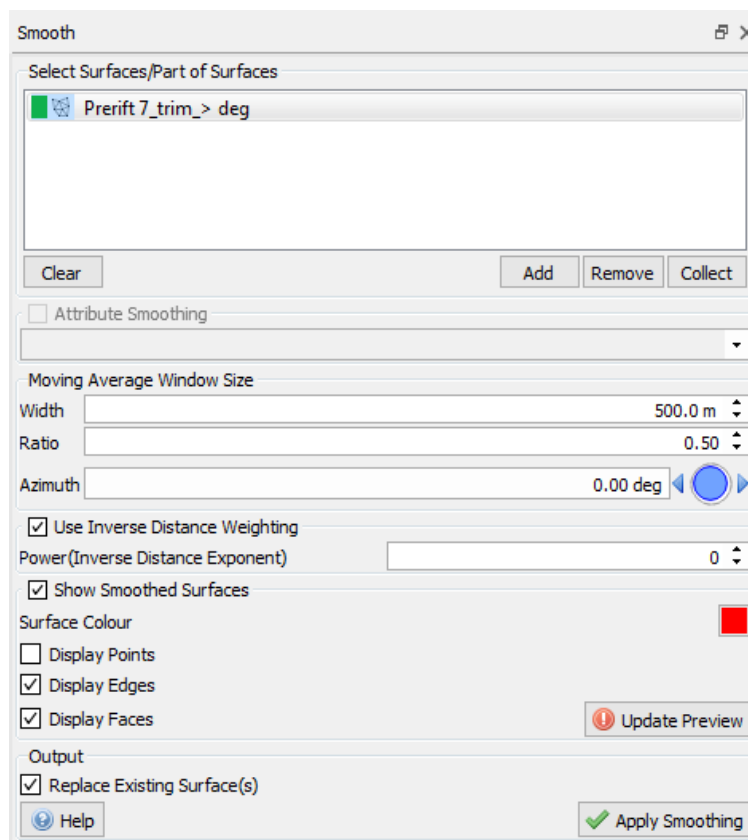
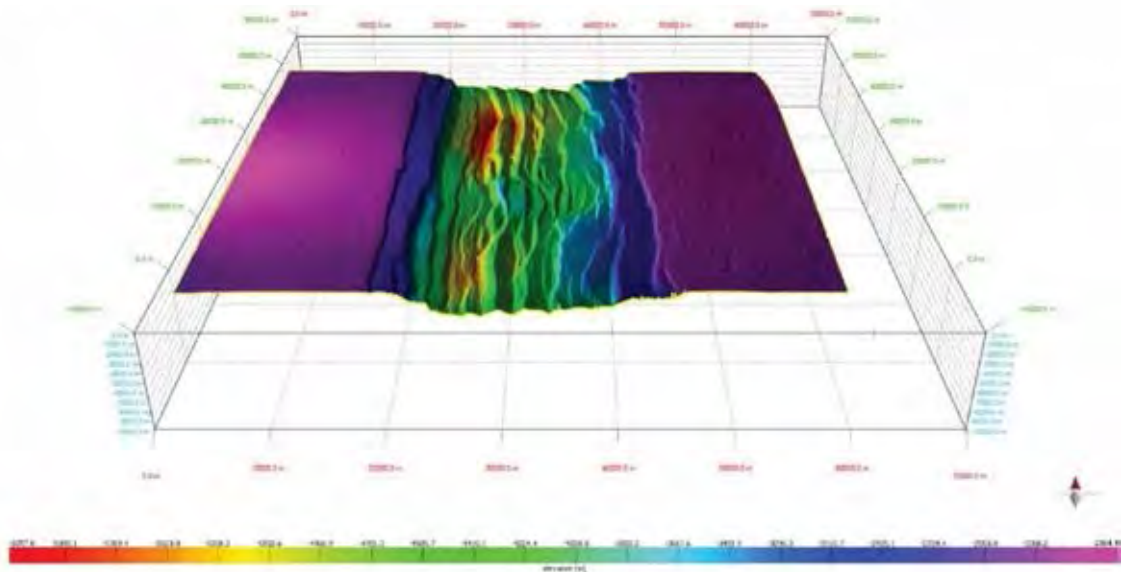


Figure 3.23 The procedure of setting the parameters in “Smooth”.

a) The Non-Smooth Horizon Surface of Syn-rift 1



b) The Smooth Horizon Surface of Syn-rift 1

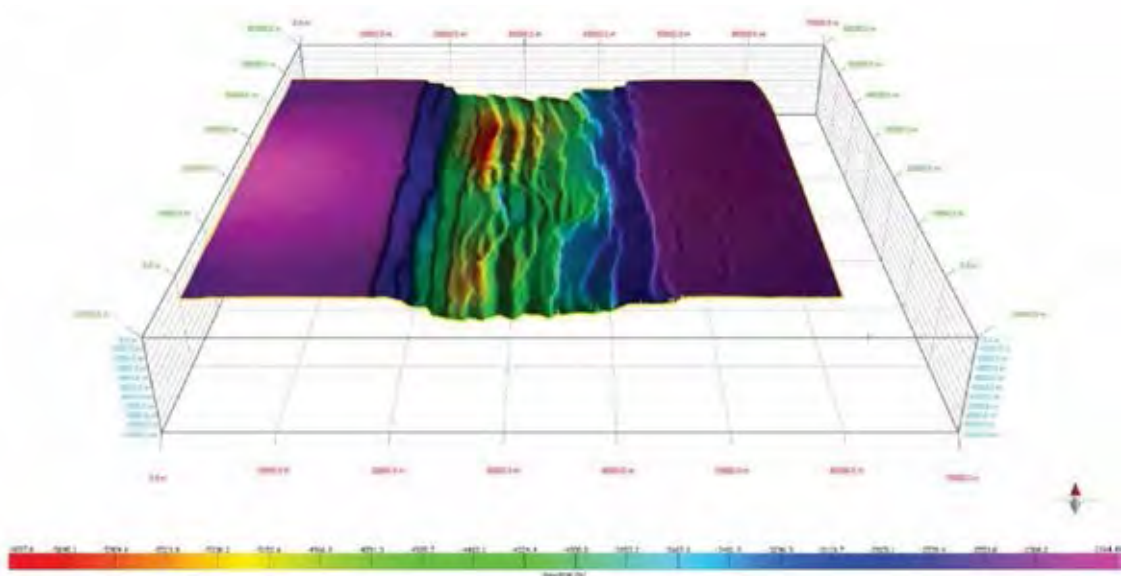


Figure 3.24 (a) The horizon surfaces of syn-rift 1 from NRS004-90 before will be adjusted to be a smooth surface and (b) the horizon surface of syn-rift 1 from NRS004-90 after has been adjusted to be the smooth surface already.

3.3.2 3D fault surface generation (fault interpretation)

After the horizon surfaces were created perfectly, the next procedure is the interpretation of 3D internal structures that are faults. Thus, this procedure will can be divided into 2 methods that have different techniques used for the interpretation of faults because some models have a complex internal structure that occurred in rift basin, so each model should choose the best technic that depends on the suitability for the interpretation.

The first one is the method of digitizing faults in the model sections from Move™ (manual-interpretation). This method will choose the fault that was represented from each model for the digitization on every model section having propagation of this fault (Fig 3.26), and then this fault will be created to be the fault surface (Fig 3.27).

The another one is the method using the relationship between the Petrel and Move™. In this method, the faults occurring in the model of the rift basin will be interpreted by cutting off of the dip angle and the dip azimuth of the horizon surfaces (Fig 3.28). Then, these horizon surfaces will be converted from the mesh files to the point cloud files and will be created the fault surface from the point cloud files respectively. Next, they will be linked to Move™ with the Petrel to transfer the fault surface for adjusting the quality of the fault surface. Lastly, the adjusting surfaces will be transferred back into Move™ for using in the next procedure of the structural analysis.

Moreover, these interpretations will be selected the faults that are representative of each model to use for studying the relationship that occurred since the factors of the shape of pre-existing structural discontinuities and metamorphic fabrics under rift basin and the direction of extensional force which controlled the fault patterns in the rift basin.

Procedure (Move™)

- 1.) First of all, choose “**MODEL BUILDING**” on menu bar and select “**Fault**” in “**Create Lines**” respectively.
- 2.) Then, set the parameters following this procedure below
 - 2.1.) Toggle “**Snap to Point**” and set the color of fault line.
 - 2.2.) Under Displacement, toggle Normal Slip (since this is an extensional fault) from the list.
- 3.) Under digitization of fault, Left-click along the length of each fault that was selected for interpretation, and then right-click to end digitization of each section.
- 4.) In creating fault surface, choose “**MODEL BUILDING**” and select “**Surface**” in “**Surfaces/Volumes**”.
- 5.) On “**Create Surface**”, toggle “**Create Surface from Lines**”.
- 6.) On “**Model Browser**”, select a set of the fault lines in “**Sets**”.
- 7.) On “**Create Surface**”, add the “**fault lines**” into “**Select Lines**”.

- 8.) Next, set all parameters following figure 3.25.
- 9.) Finally, click **“Create surface”**.

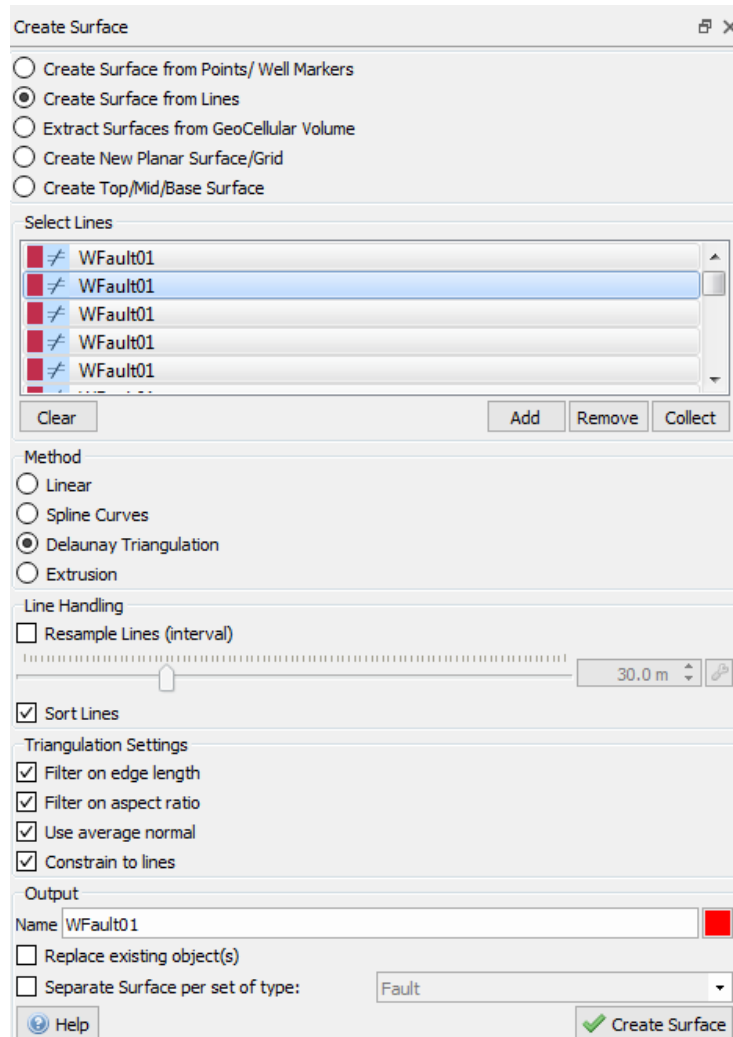


Figure 3.25 The procedure of setting the parameters in “Create Surface” to create the surface from the fault lines.

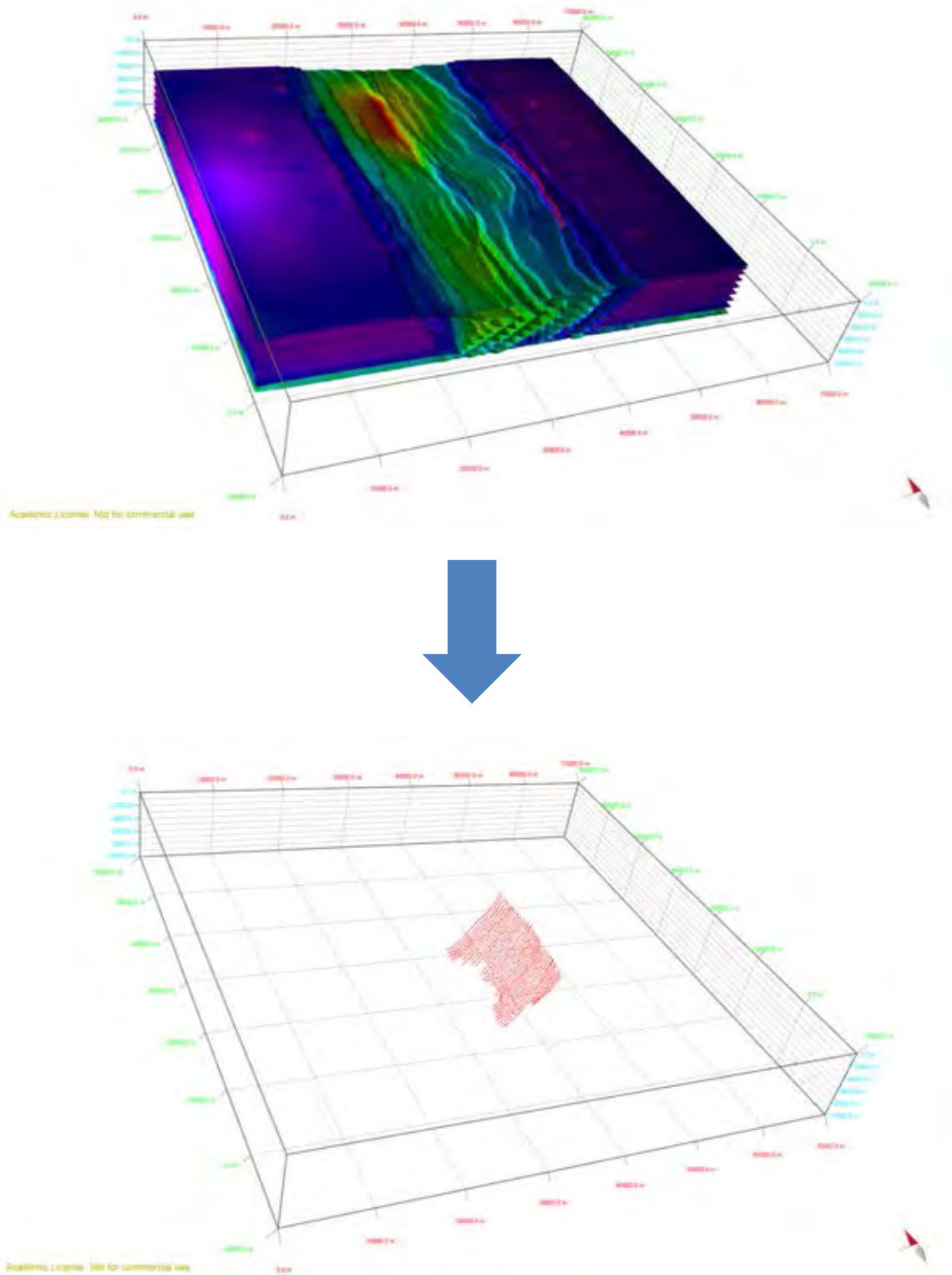


Figure 3.26 The fault lines of WFault01 (west dipping fault) that were digitized from the horizon surfaces and the model sections in NRS004-90.

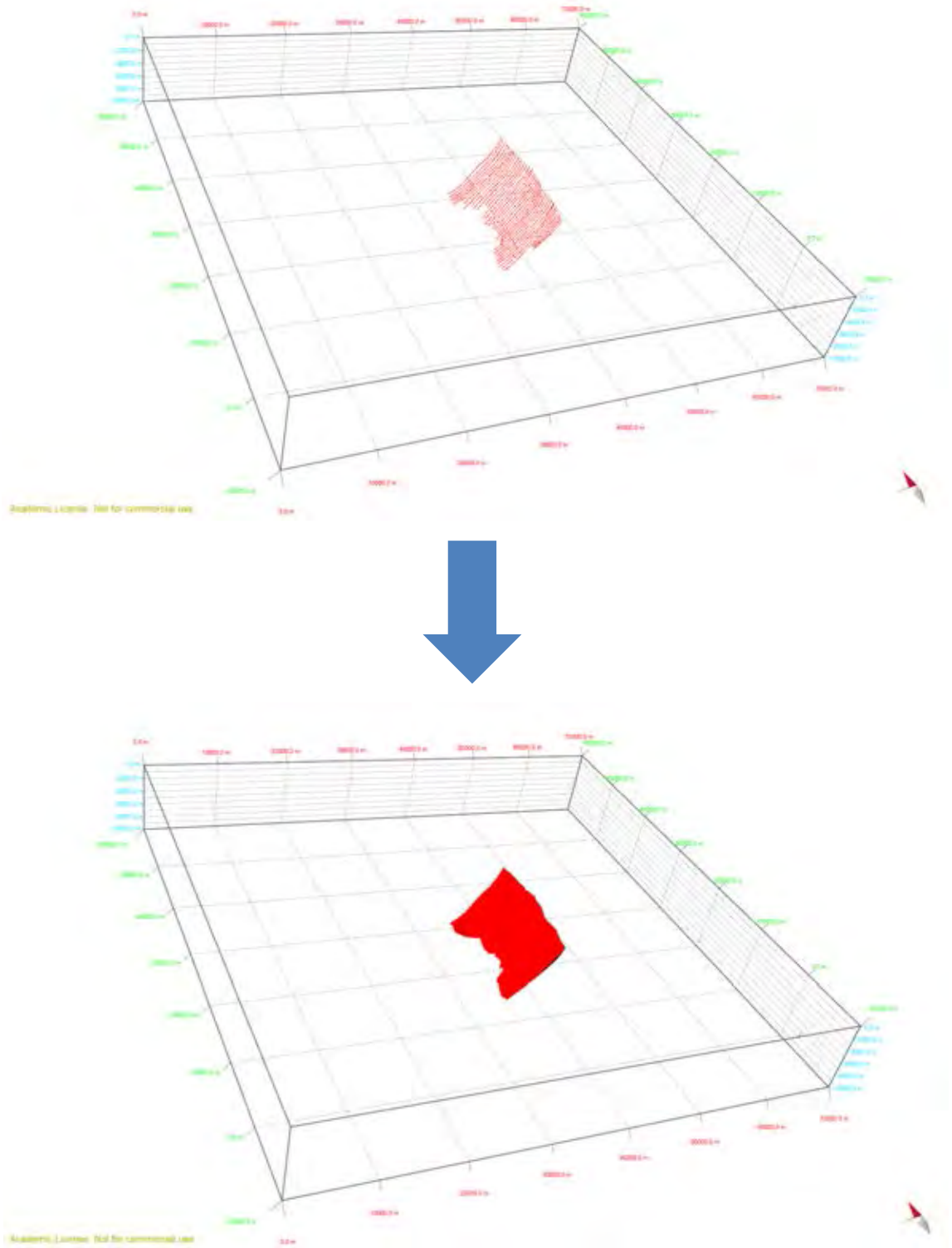


Figure 3.27 Creating fault surface (below) from fault lines (above) of WFault01 in NRS004-90.

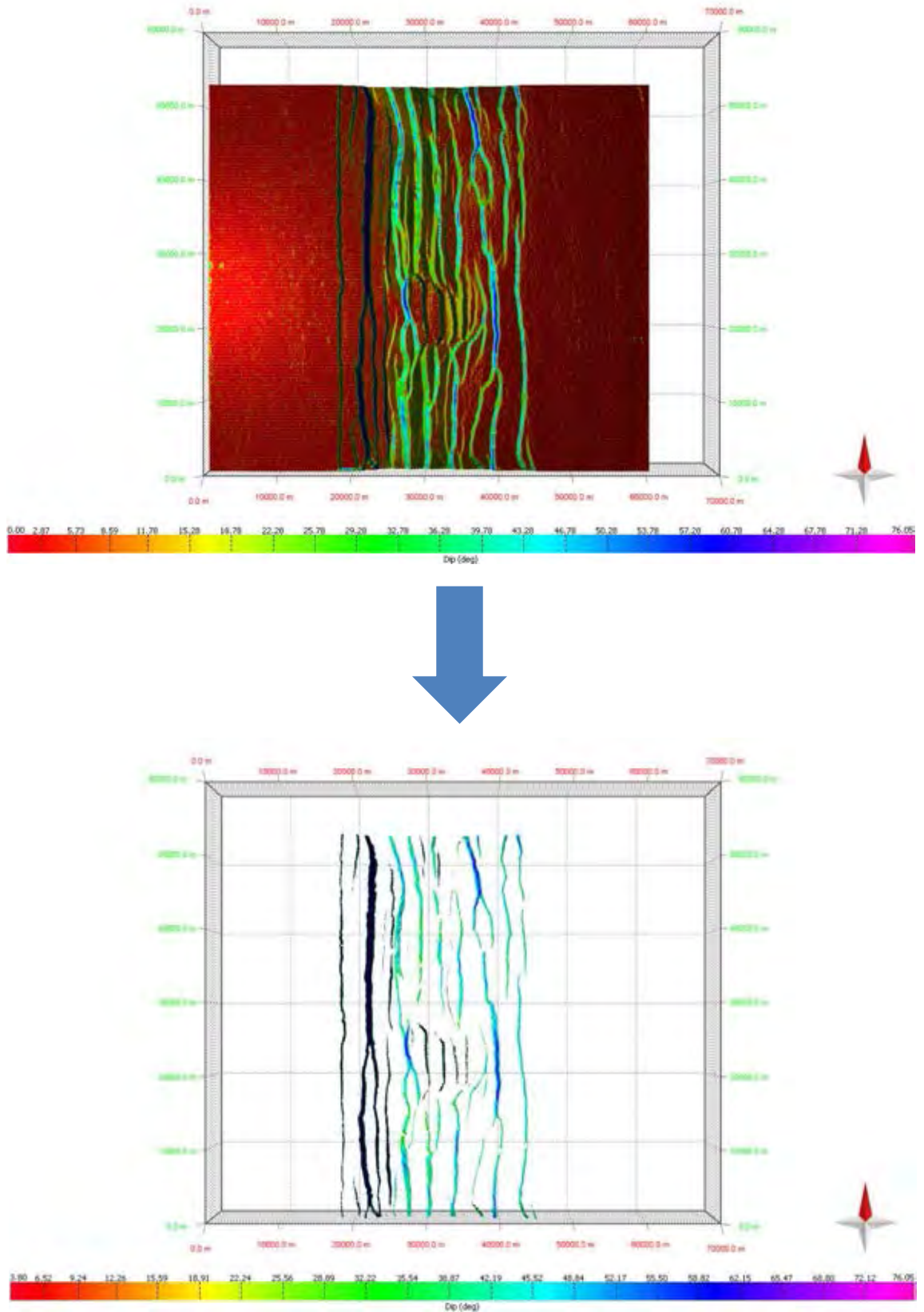


Figure 3.28 The method using the relationship between the Petrel and Move™. In this method, the faults occurring in the model of the rift basin will be interpreted by cutting off of the dip angle and the dip azimuth of the horizon surfaces.

procedure (Move™ link for Petrel)

- 1.) In installing Move™ link for Petrel, the Move™ Link or Petrel can be installed via the Ocean Plug-in Manager using (*.pip) files. Alternatively, Windows Installer (*.msi) files are also supplied. Both file types are provided for Petrel 2014, 2015 and 2016.

Installation using the ocean plug-in manager in Petrel 2014-2016

- 1.1.) In Petrel, navigate to Options in the File menu.
- 1.2.) Select Plug-in Manager.
- 1.3.) Select Install plug-in.
- 1.4.) Brows to the correct MoveLink *.pip from the installation disk.
- 1.5.) Close Petrel
- 1.6.) When Petrel is restarted, the Move Link button will be available in the Home panel.

Installation using the Microsoft Installer (msi) files.

- 1.1.) With Petrel closed, navigate to the correct *.msi file on the installation disk.
- 1.2.) Double click on the file, and follow the instruction.
- 1.3.) When Petrel is opened, the Move Link button will be available.



Figure 3.29 In UX mode, the Move Link button will be visible in the Home panel.



Figure 3.30 Using the Classic user interface, it appears as a tool Button appended to the File Group the File Group

- 2.) In the Move Link for Petrel, communication between Move and Petrel is established via Transmission Control Protocol (TCP). To start a Move for Petrel Session, it is necessary to start a TCP server in Petrel so that Petrel will respond to requests from Move™.

Connect Petrel to the TCP Server, to start the server in Petrel:

- 2.1.) In Petrel, click “**Move Link**”.

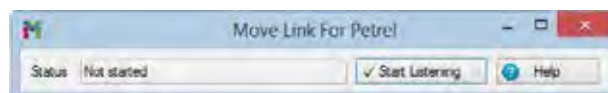


Figure 3.31 Move Link for Petrel tab before connect Petrel with the TCP Server.

- 2.2.) Click **“Start Listening”** - the dialog will indicate that Petrel is now listening to requests from Move™.

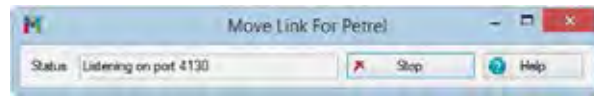


Figure 3.32 Move Link for Petrel tab after connected Petrel with the TCP Server.

Once Petrel has been set up to listen to Move™, the link is controlled from Move™.

Connect Move™ to Petrel

- 2.3.) Click on **“Move Link for Petrel”**, located on the **“Modules”** tab. If this button is not enabled, the Move Link to Petrel license will not have been checked out.



Figure 3.33 The location of “Move Link for Petrel” on the “Modules” tab.

- 2.4.) The Move Link for Petrel window will open. In the **“Connection”** sheet, click **“Connect”**.



Figure 3.34 Move Link for Petrel tab before connect Move™ with Petrel.

- 2.5.) Move will establish a connection with Petrel, and the connection status will be updated accordingly.



Figure 3.35 Move Link for Petrel tab after connected Move™ with Petrel.

Once a connection has been established, the “**Petrel to Move**” and “**Move to Petrel**” sheets in the tool will become active.

- 3.) Transferring data to Petrel is controlled via the Move™ to Petrel sheet. Within this sheet, there are two trees that display the folders within the Petrel Project, where objects may be transferred to. The Input Tree contains folders that will accept the transfer of Point Clouds, PolyLines, Grid and Mesh Surfaces, while the Models Tree displays containers for GeoCellular Volumes.

To transfer objects from Move™ to Petrel

- 3.1.) Select the objects to be transferred.
- 3.2.) Select the destination folder within the appropriate tree - “**Transfer Selected Objects to Petrel**” will be active, as shown in figure 3.36.
- 3.3.) Click “**Transfer Selected Objects to Petrel**”.
- 3.4.) The selected objects will appear in the Petrel project, and will belong to the Petrel Link Session, as shown in figure 3.37. This can be verified using the Petrel to Move™ sheet.

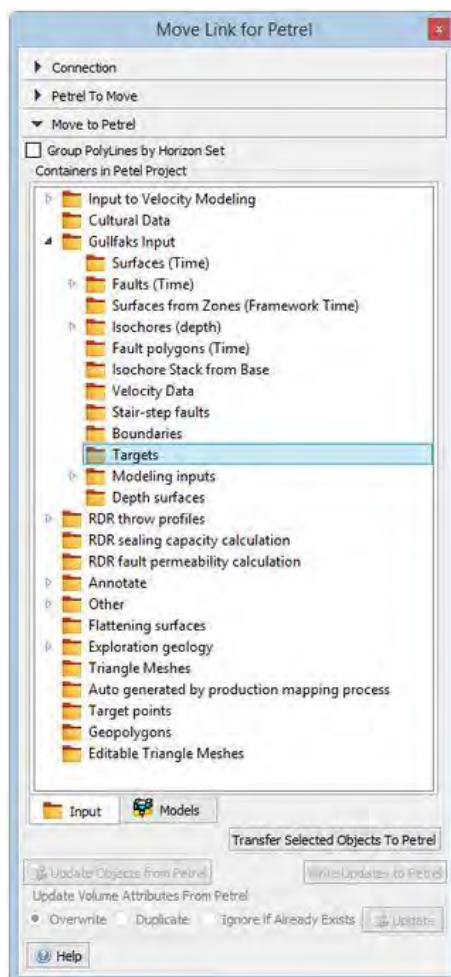


Figure 3.36 The destination folder within the appropriate tree.

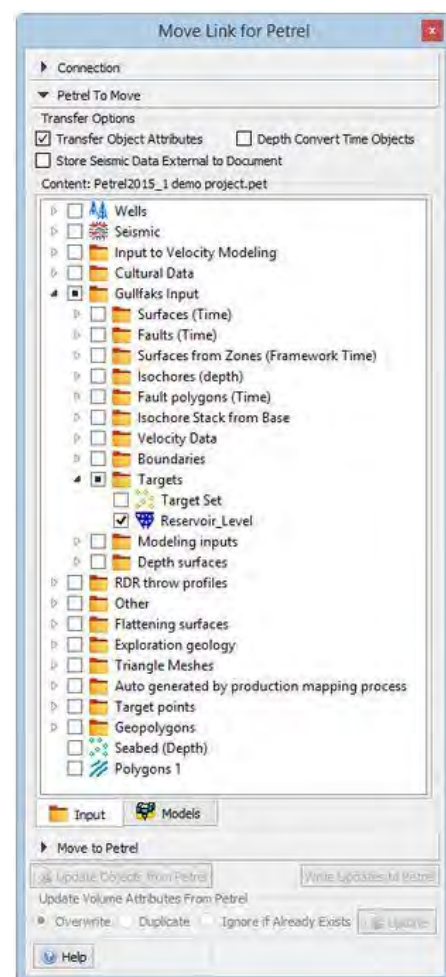


Figure 3.37 The objects in the Petrel project that were appeared in Move™.

- 4.) Convert the mesh files to the point cloud files in Petrel for adjusting the quality of the horizon surfaces.
 - 4.1.) Choose a horizon mesh file from **“Input”**.
 - 4.2.) Right click at this horizon mesh file for converting to the point cloud file.
 - 4.3.) Within **“the Make Surface”** on utilities, toggle **“Automatic (from input data/boundary)”** on grain size and position. After that, select **“Apply”** for creating the mesh file, as shown in figure 3.38.
 - 4.4.) Next, select the surface created from previous method to set the colors on **“Setting”** and toggle **“Local (private) color table”** and **“Limited defined in color table”**, and then select MAX and MIN for calibrating the surface map, as shown in figure 3.39.
 - 4.5.) Choose a horizon mesh file from **“Input”** and right click at this horizon mesh file for converting to the point cloud file. Finally, this point cloud file will be linked into Move™ for the next step.
- 5.) In Move™, the point cloud files will be generated to be the horizon mesh surfaces, and then these surfaces will be created the Geometry Surface for preparing to create the surface of fault.
 - 5.1.) In Move™, choose the point cloud files on **“Move link for Petrel”**.
 - 5.2.) Create the horizon surfaces from point cloud files following **“the procedure of Creating Surface of Horizon”** (within **“Create Surface”**, toggle on **“Create Surface from Point”**).
 - 5.3.) Then, create dip surface from **“Geometry Surface”** (look at procedure of structural analysis), and then cut off the dip surface of each horizon surface that is less than 15 degrees.
- 6.) In cutting off method, all of horizon surfaces will be cut off by the geometry surface of dip azimuth and dip respectively. Thus, these cutting off surfaces will be representative of faults occurring in the rift basins
 - 6.1.) In the method of cutting off dip azimuth, the horizon surfaces will be created to be the dip azimuth surface from the geometry surface (see the procedure of Surface Geometry, and toggle azimuth on **“Property to Analyze”**), and then these horizon surfaces that have different dip azimuth from the dip azimuth of fault plane will be cut off, as shown in figure 3.40.
 - 6.2.) In the method of cutting off dip, the horizon surfaces that were cut off from the previous method of cutting off dip azimuth will be created to be the dip surface from the geometry surface (see the procedure of Surface Geometry), and then the horizon surfaces that have dip angle less than 30 degrees will be cut off since these surfaces must adjust the quality before they will be used to create the fault surfaces (Fig 3.41).

- 7.) The mesh files of the horizon surface that were cut off from previous method will be converted to be the point cloud files. Then, these point cloud files will be created to be the fault surfaces.
 - 7.1.) In **“Object types”**, right click horizon surface that has been cut off already from previous method.
 - 7.2.) Right click and select **“Create Points at Face Center”** for converting from mesh files to be point cloud files.
 - 7.3.) In creating the surface of fault from the point cloud files, select **“surface”** on **“MODEL BUILDING”**.
 - 7.4.) Add the point cloud files that would like to create the fault surface.
 - 7.5.) Next, set all parameters following below:
 - In **“Create Surface”**, toggle **“Create Surface from Points and Well Markers”**.
 - In **“Method”**, toggle **“Delaunay Triangulation”**.
 - In **“Line Handing”**, toggle **“Sort Lines”**.
 - In **“Triangulation Setting”**, toggle all parameters.
 - 7.6.) Create the name and select **“Create Mesh Surface”** respectively for creating the fault surface.

After all of fault surfaces have been created from the procedure of fault interpretation already, these surfaces are typically not smooth. Thus, they should adjust the quality to be the smooth surface because they are significant for the procedure of the structural analysis such as a throw profile.

- 8.) This method will use the linking between the Petrel and Move™ to adjust the quality of the fault surface to be smooth.
 - 8.1.) Linking Move™ with Petrel for transferring the mesh files of the fault surface from Move™ to petrel.
 - 8.1.1.) In **“Data transfer”**, select “Move Link for Petrel” and connect it with Petrel.
 - 8.1.2.) In **“Object types”**, select the mesh files of the fault surface that was created from previous method.
 - 8.1.3.) Within **“Move link for Petrel”**, create a folder used for transferring between Move™ and Petrel, and then select this folder.
 - 8.1.4.) Click on **“Transfer Selected Object to Petrel”** to transfer this file to Petrel.

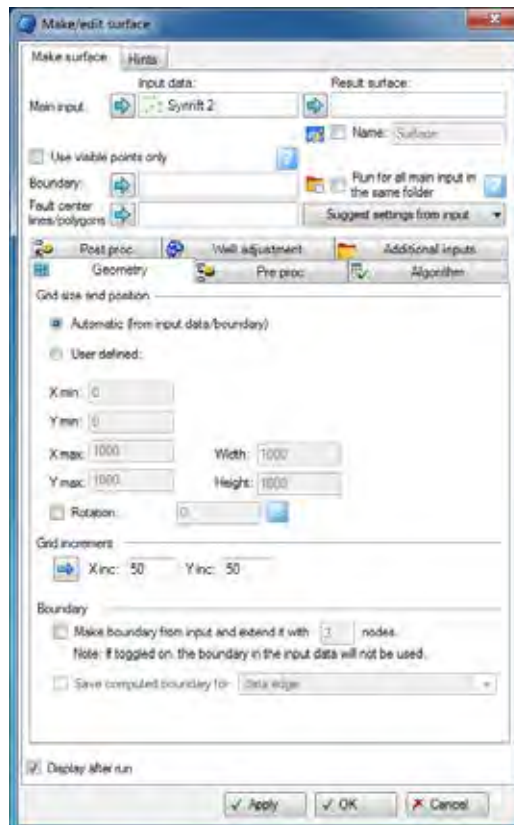


Figure 3.38 The procedure of setting the parameters in “Make/edit surface” of syn-rift 2.

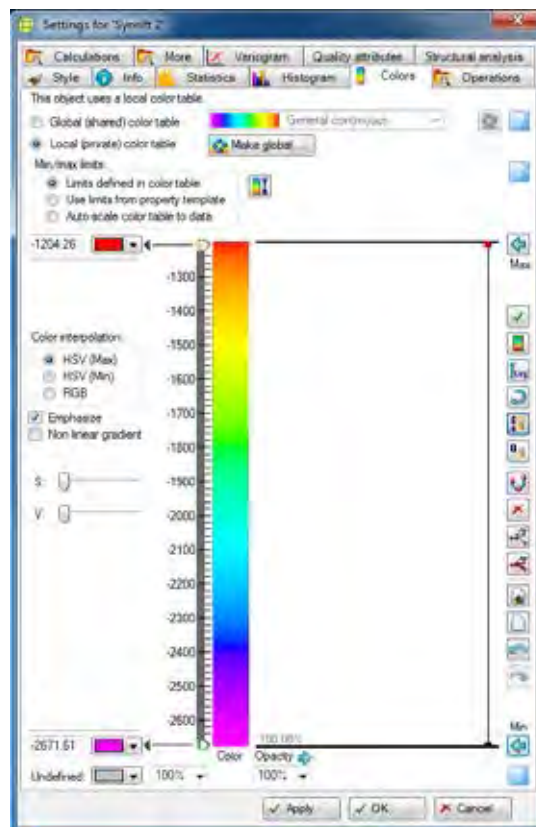


Figure 3.39 The procedure of setting the parameters in “Color” of syn-rift 2.

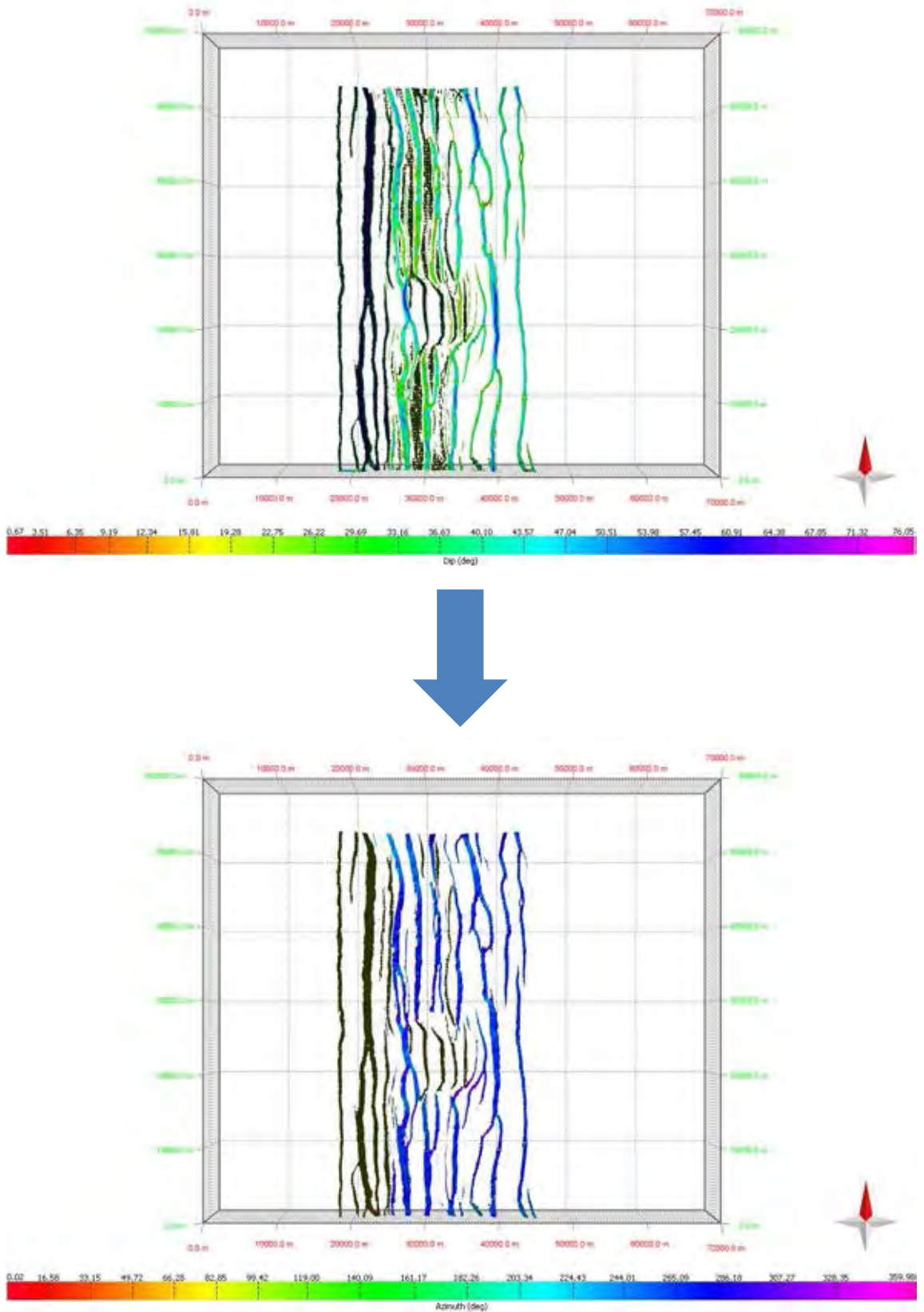


Figure 3.40 A horizon surface of pre-rift 6 in NRS004-90 was created to be the dip azimuth surface (above) and this dip azimuth surface having different dip azimuth from the dip azimuth of fault plane was cut off by the procedure of cutting off dip azimuth (below).

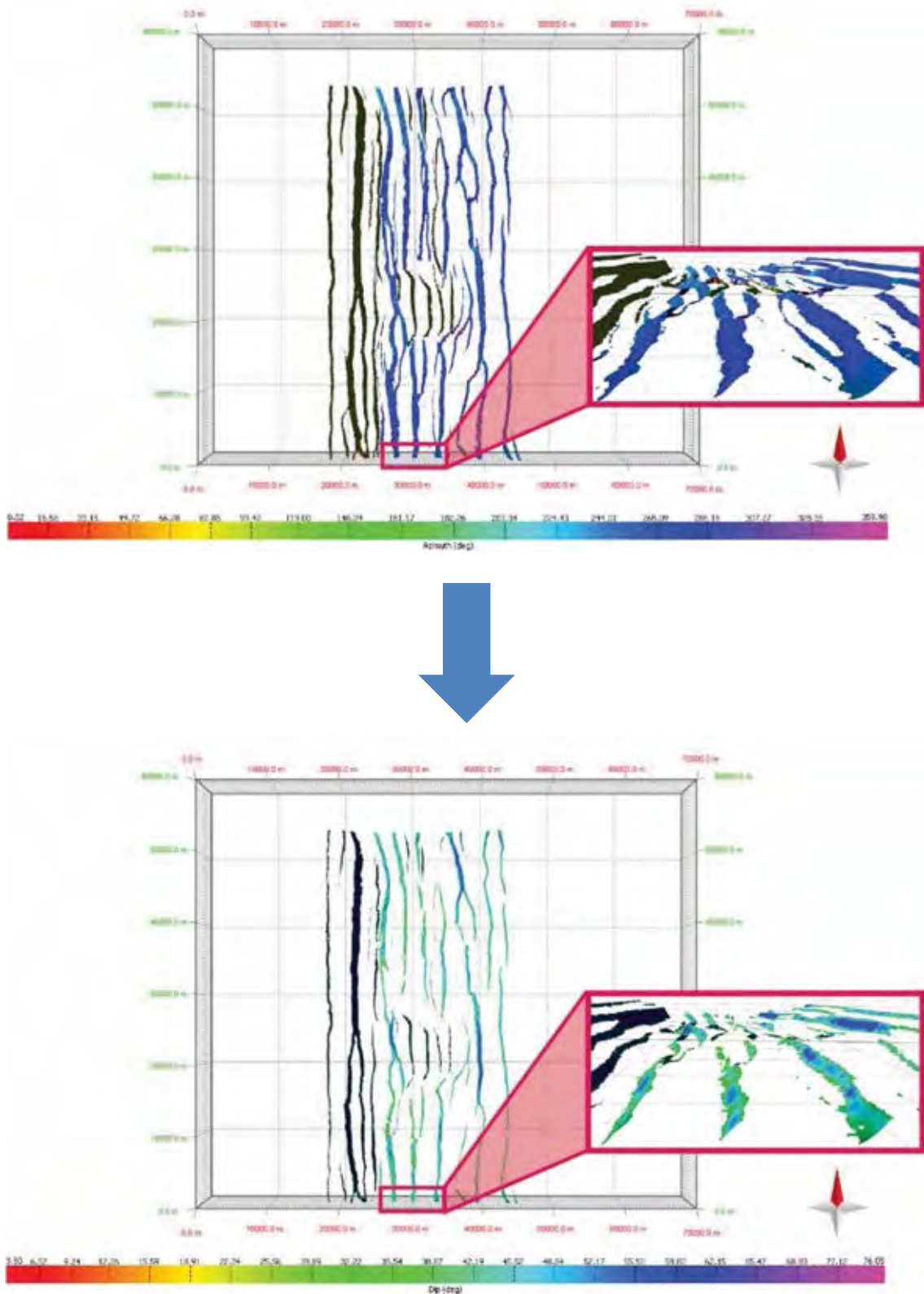


Figure 3.41 A horizon surface of pre-rift 6 in NRS004-90 will be created to be dip azimuth surface (above) and the horizon surfaces that have dip angle less than 30 degrees will be cut off by the procedure of cutting off dip for using in the procedure of fault analysis (below).

- 8.2.) In this method, the fault surfaces will be converted from the mesh files to the point cloud files and will be created the fault surfaces in the Petrel.
- 8.2.1.) Right click on the input file of the fault surface and select **“Convert to point”** respectively for converting the mesh file to point cloud file.
 - 8.2.2.) Creating the fault surface from the point cloud files, select **“Make Surface”** on “Fracture Modeling”, set the parameters in **“Make/edit surface”** following figure 3.42 and click **“Apply”** respectively.
- 8.3.) After the fault surfaces have been created from previous method already, these surfaces will be adjusted the quality of the surfaces to be smoother.
- 8.3.1.) In **“Input”**, select the mesh file of the fault surface
 - 8.3.2.) Then, right click on this mesh files and select **“Setting”** respectively.
 - 8.3.3.) Within **“Operations”**, select **“smooth”** in **“Surface-operation”**.
 - 8.3.4.) Finally, set the appropriate value of **“Iteration & Filter width”** to adjust the fault surface to be smooth and click **“OK”** respectively.
- 8.4.) These fault surfaces will be converted from the mesh files to the point cloud files in the petrel (similar method in 8.2.1). These point cloud files will be representative of the fault surfaces that will be used to create the surfaces in Move™.
- 8.5.) In **“Input”**, select the point cloud files that are representative of the fault surfaces to transfer these files from the Petrel to Move™. This may take several seconds depending on the number of objects in the project. These objects will be automatically updated when the project content is changed from within Petrel.
- 8.6.) To transfer an object from Petrel to Move™, in the tree view, click on the check box next to the objects to be transferred. To transfer a group of objects, click the check box for the containing folder (Fig 3.43).
- 8.7.) As a transfer may take a long time, clicking on **“Cancel”** will interrupt the transfer.

- 9.) The last method of this method is the creating the fault surface from the point cloud files that came from the Petrel (similar method in 7.3 to 7.6). Also, these fault surfaces can be created the properties of the surface geometry that can use to study about characteristics of the fault surfaces

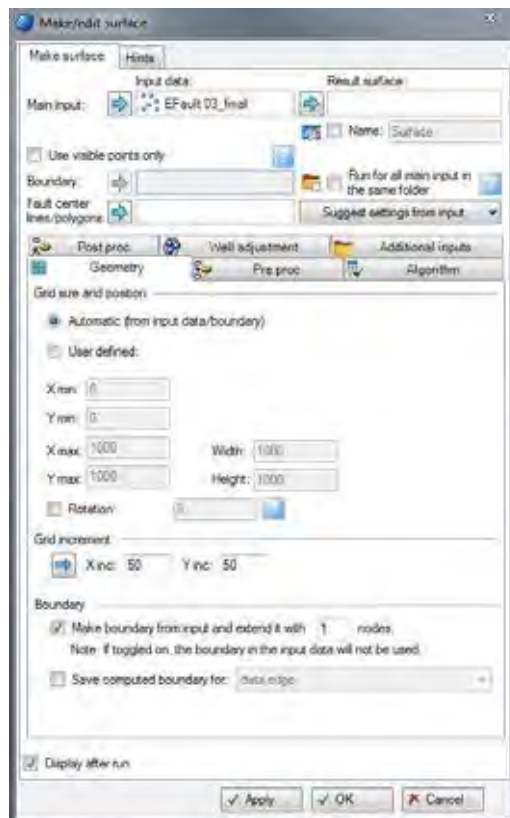


Figure 3.42 The procedure of setting the parameters in “Make/edit surface” of EFault 03

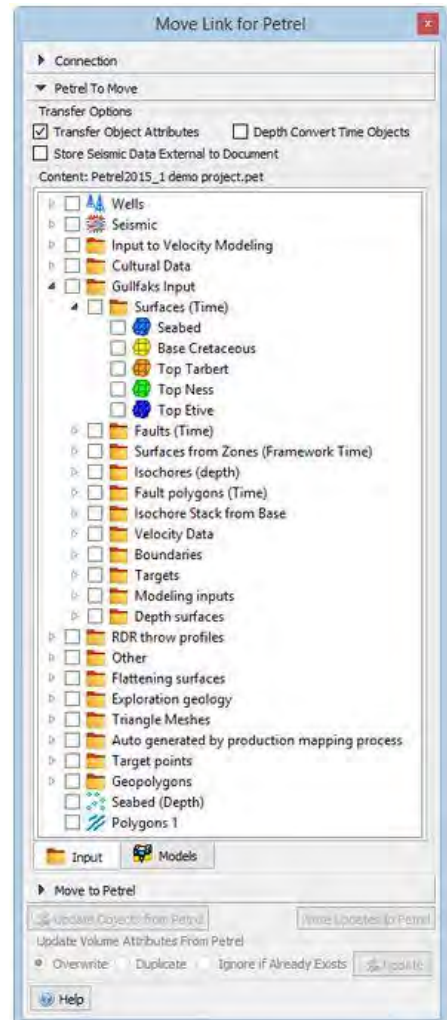


Figure 3.43 The objects from Petrel that would like to transfer from Petrel to Move™.




3.4 Fault analysis

The fault analysis is the analysis about a relationship of fault length and throw for studying throw profiles and a fault scaling from each scaled physical model. Thus, this process can be divided into 2 significant methods: the surface geometry analysis and the fault analysis that will be used to analyse the 3D fault model of rift basins from the scaled physical models.

The Surface Geometry Analysis will create the dipping surface, and then this surface of each horizon will be used to trim in the dipping area because this technique will help to improve the method of the fault analysis.

The Fault Analysis will define the distance of trim and inclusion between a fault plane and surfaces. Then, this method will be used to analyse and create for Throw Profiles which is a ratio of throw to fault length and Fault Scaling which is the ratio of maximum throw to fault length.

Procedure (surface geometry analysis)

- 1.) Choose “**DATA & ANALYSIS**” on menu bar and select “**Surface Geometry**” respectively.
- 2.) Add the horizon surfaces that have been adjusted the quality of the smooth surfaces already.
- 3.) Under “**Property to Analyse**”, toggle “**Dip**”, and then choose the color (rainbow) that will be used to display the dipping of the surface.
- 4.) After setting all parameters already, select “ **Expand Color Map to selection**” . Then, select “**Apply**” and “**Create vertex Attribute**” respectively.
- 5.) Next, select “ **Toggle Attribute Selection Filter**”.
- 6.) In “**Restrict to Objects**”, add the surface that has been changed the geometry of surface already and define the value of dip surface that would like to cut off.
- 7.) Choose “ **Object Loop Selection**” (Press Shift to activate) and draw around the surface.
- 8.) Press “**Delete**” on your keyboard.

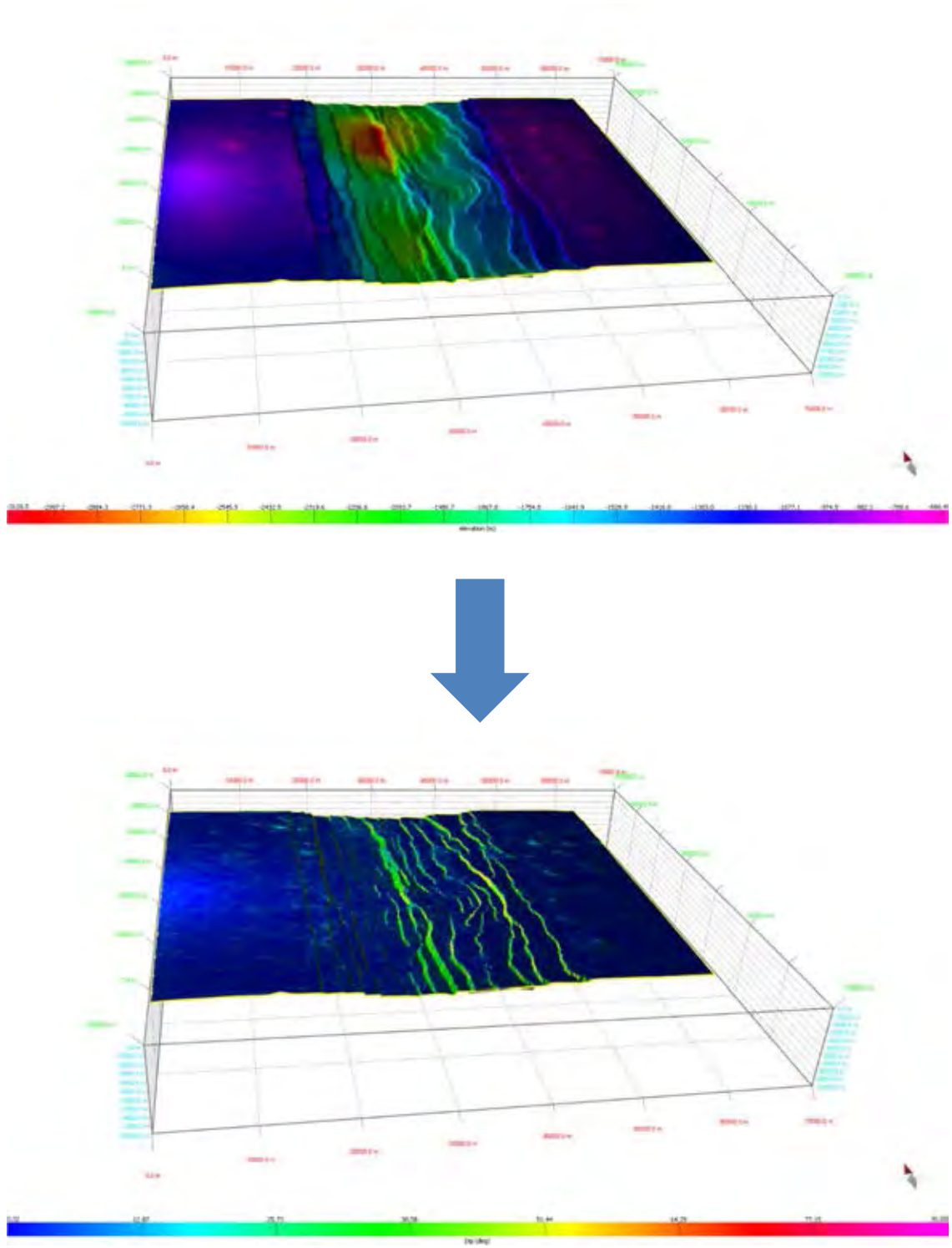


Figure 3.44 The procedure of the surface geometry analysis that created the dipping of surface in NRS004-90.

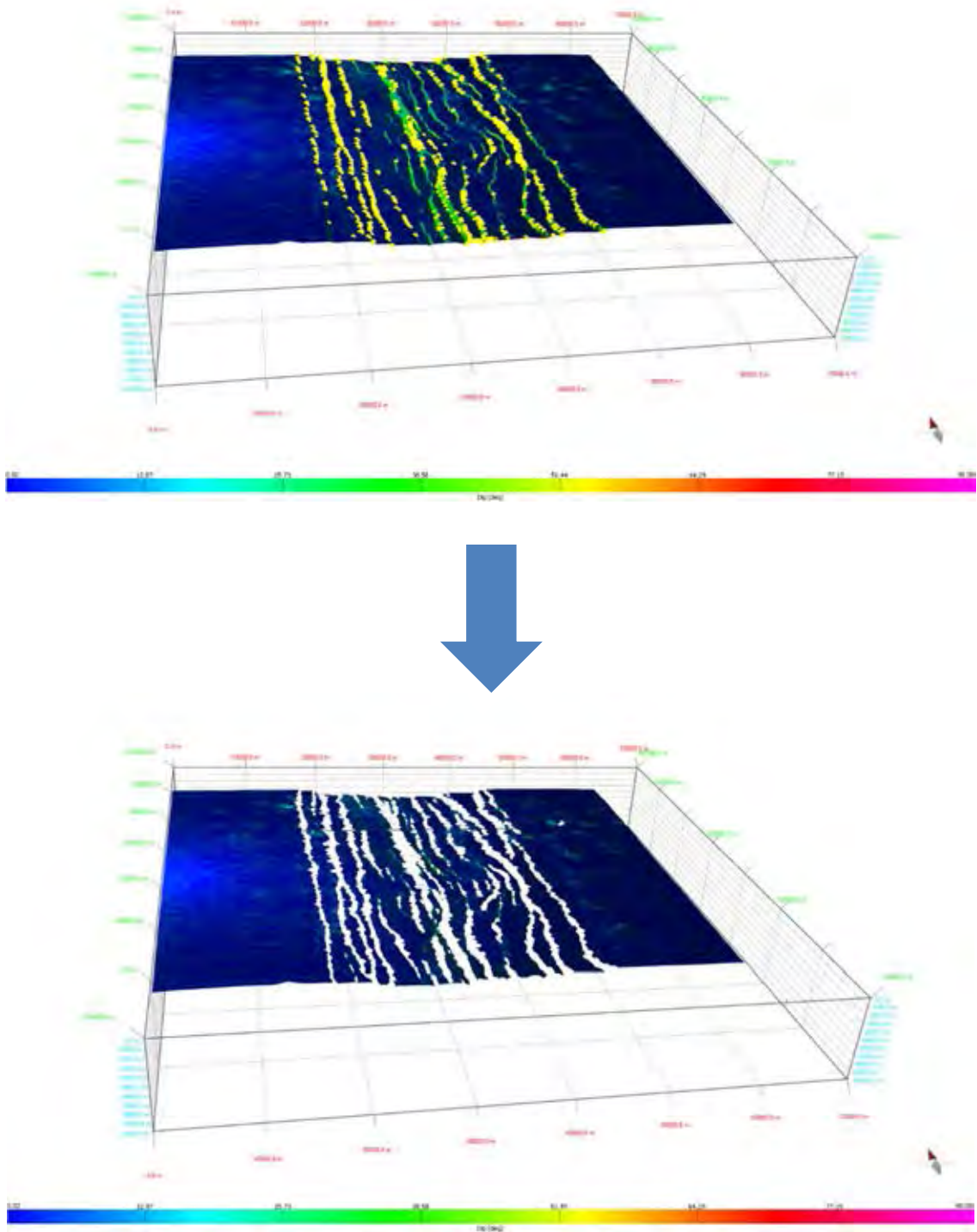


Figure 3.45 The procedure of the surface geometry analysis that trimmed the dipping surface in NRS004-90 for using in the fault analysis.

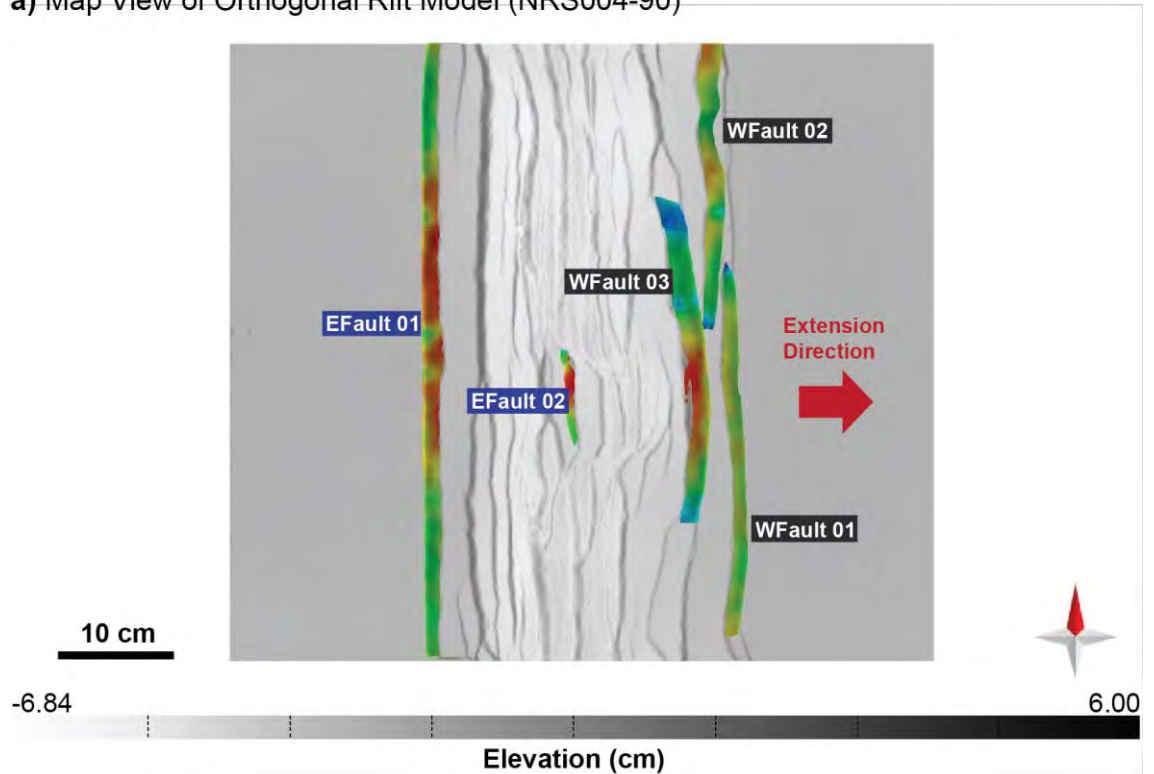
Procedure (Fault Analysis)

- 1.) Choose **“MODULES”** on the menu bar.
- 2.) Select **“Fault Analysis”** in **“Advance Modules”**.
- 3.) In **“Faults”**, Add the surface of fault that would like to analyst and set **“Trim and Inclusion”** that are appropriate between a horizon surfaces and a fault plane.
- 4.) In **“Horizons”**, Add the surfaces of horizon that would like to analyst, and then select **“Create Cut-Off Lines”**.

After the previous method (1-4), the surface of fault will display the lines that represent hangingwall (dashed line) and footwall (solid line) of the horizon surfaces shown in figure 3.47a. Moreover, this analysis will show the result of the throw profiles and fault scaling.

- 5.) In **“Fault Analysis”**, select **“Displacement Analysis”** and **“Create Throw”** respectively.
- 6.) Finally, the results of the fault analysis will be shown by graphs of throw profile and fault scaling in figure 3.47b and 3.48 respectively.

a) Map View of Orthogonal Rift Model (NRS004-90)



b) Oblique View of Orthogonal Rift Model (NRS004-90)

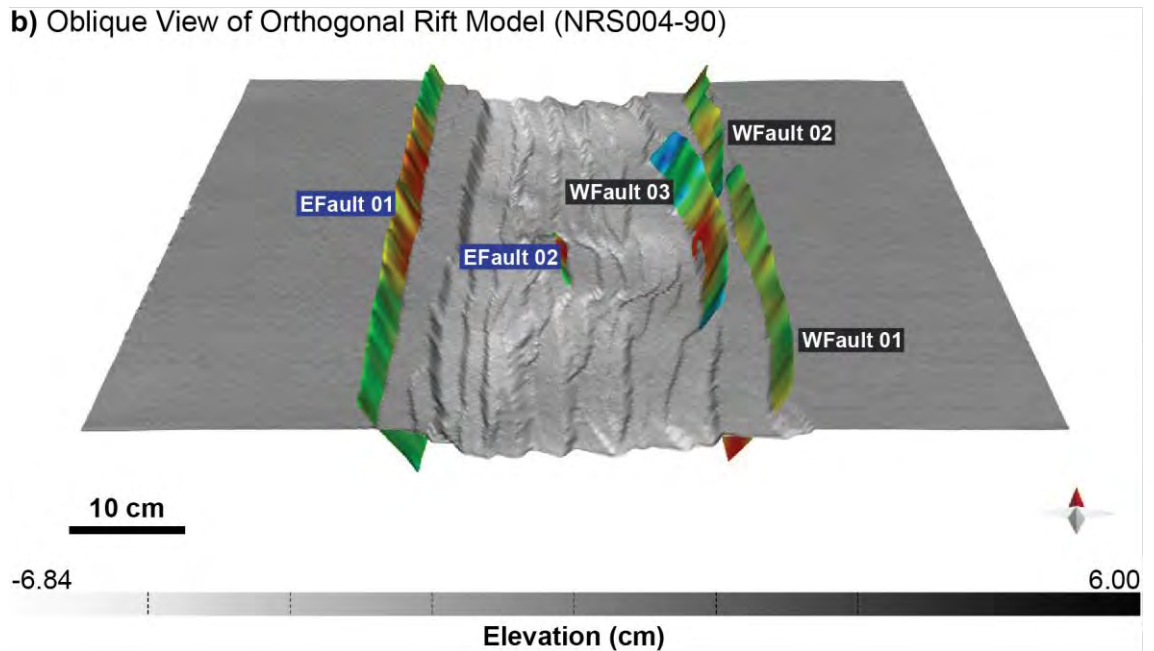


Figure 3.46 (a) and (b) show map and oblique visualization of faults map of orthogonal rift model respectively that display fault surfaces of East dipping faults (EFault 01 and EFault 02) and West dipping faults (WFault 01, WFault 02 and WFault 03).

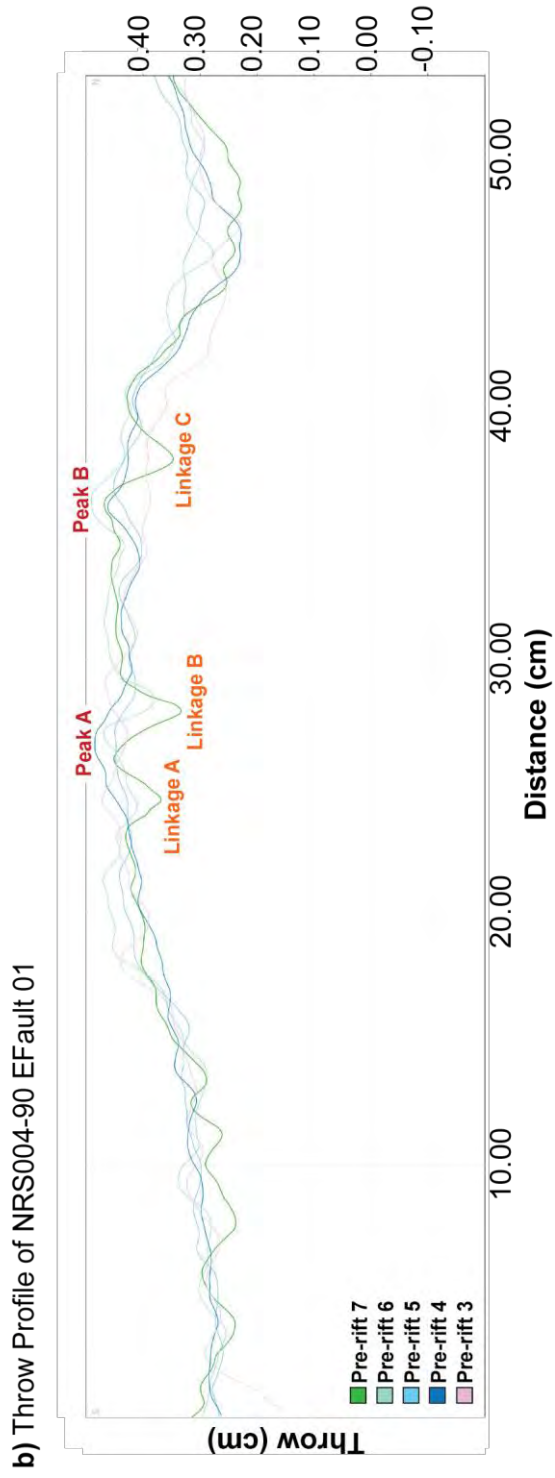
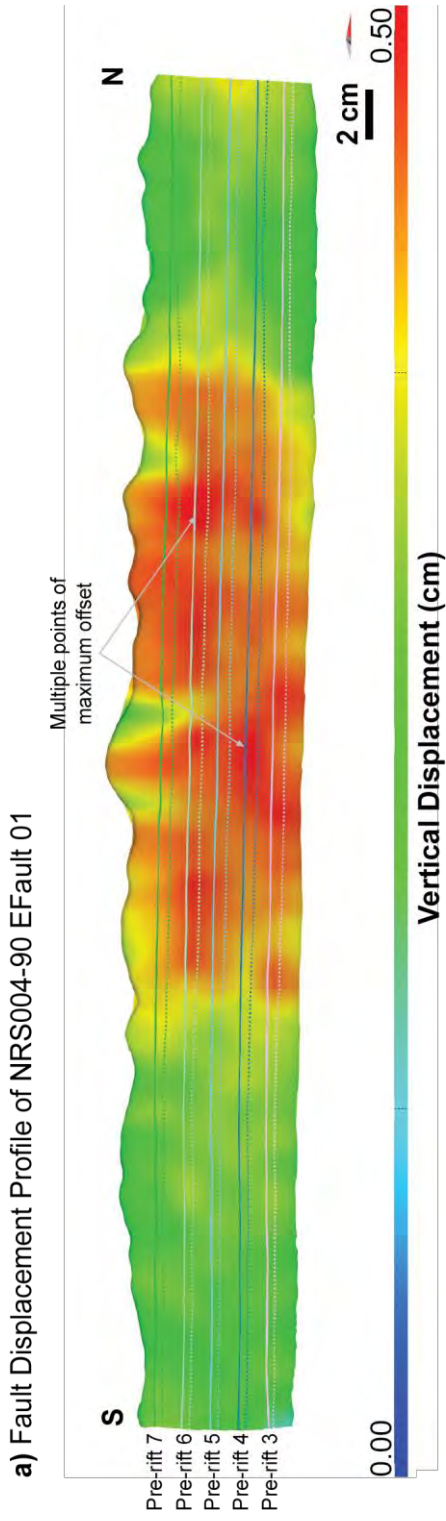


Figure 3.47 (a) A fault throw profile of EFault01 in orthogonal rift model that was a result from the procedure of the fault analysis. (b) A graph of throw profile that is the ratio of throw (cm) to fault distance (cm).

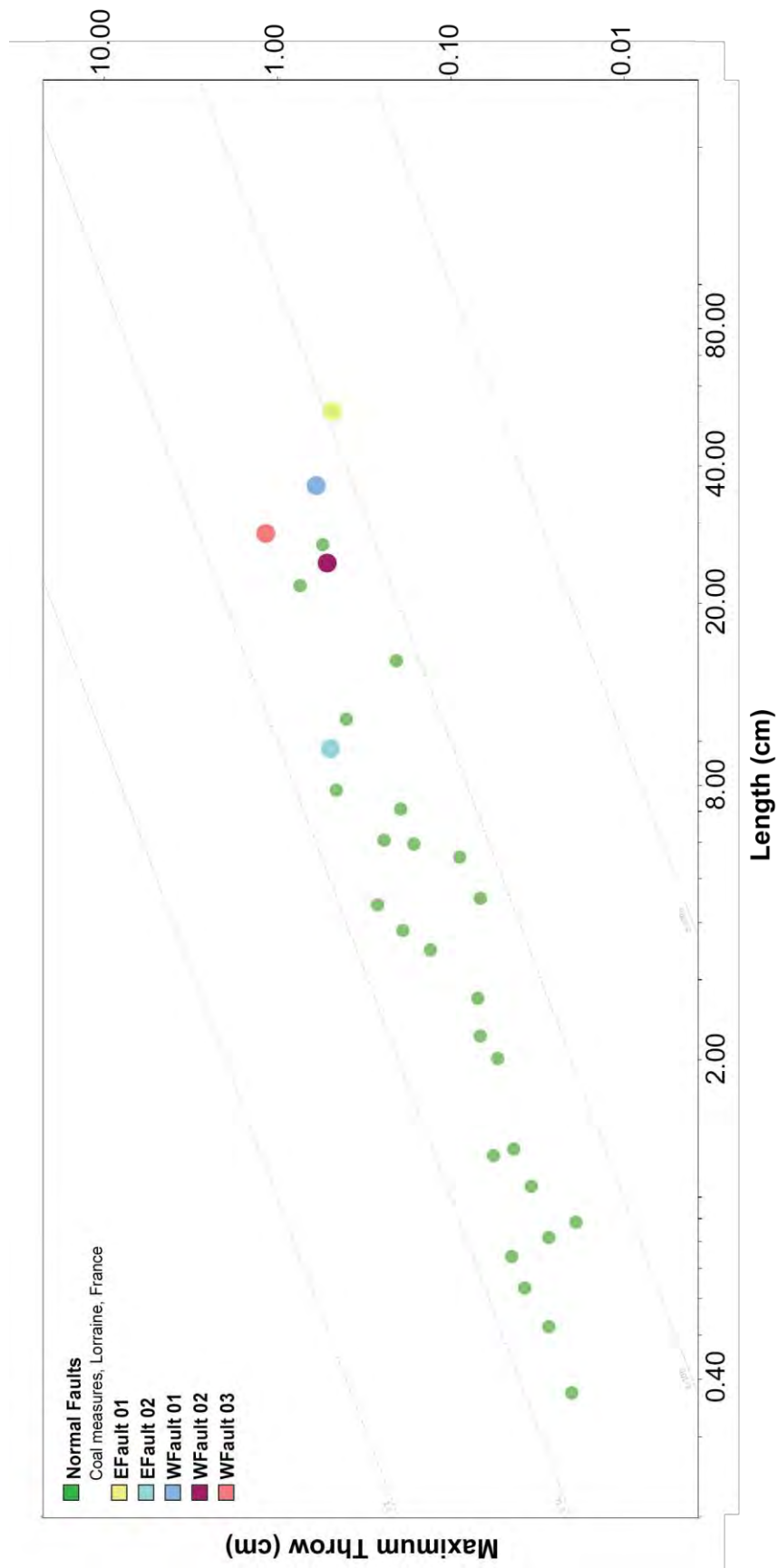


Figure 3.48 A fault scaling of faults in orthogonal rift model that was a result from the procedure of the fault analysis.

Chapter 4

Results

4.1 Introduction

In this study, the results of creating the 3D internal structures of rift basins from scaled physical models having extension direction to be perpendicular (NRS004-90 or orthogonal rift model) and 60 degrees (NRS005-60 or oblique rift model) to the pre-existing structure beneath the basins, which are horizon surfaces and fault surfaces. Besides, the results of analyzing the internal structures between the horizon surfaces and the fault surfaces can be presented by Fault Displacement Profile or Fault Throw Profile that is the plots created by projecting the throw between a set of horizon cut-off lines from single or multiple faults onto a normalized (and for multiple faults, common) plane. In addition, another result is Fault Scaling that is the proportion between the length of fault and the maximum throw accommodated on that fault.

In the orthogonal rift model and the oblique rift model, there are 9 horizon surfaces that consist of 7 pre-rifts and 2 syn-rifts, as shown in figure 4.1 and 4.16. Moreover, the faults can be divided into 2 sets that are west dipping normal faults (opposite dip azimuth to the extension direction) and east dipping normal faults (similar dip azimuth to the extension direction) used to study about the relationship of fault displacement in both models from the fault throw profiles. Furthermore, these faults can be used to analyst about the direction of stress and including the architecture of the pre-existing structure beneath the rift basin.

The faults of both models were selected to create the 3D fault surfaces, there are five faults (Fig 4.4) in the orthogonal rift model and four faults in the oblique rift model (Fig 4.19) that were chosen to analyst about the fault displacement profiles or the fault throw profiles of seven pre-rifts and two syn-rifts. Hangingwall and footwall were marked on these faults for each horizon surface, with the resulting amounts of throw shown by color changes on fault planes. Dashed lines and solid lines that were appear on the fault surfaces represent the hangingwall and the footwall of each horizon surface respectively.

4.2 Orthogonal rift model (NRS004-90)

4.2.1 Fault systems

The three dimension of orthogonal rift model are characterized by long, straight segmented normal faults in N-S striking of both intra-rift faults and rift-border faults (Fig 4.1) that are perpendicular to the extension direction and parallel to the pre-existing structure beneath the basin in the scaled physical models. No strike-slip or oblique-slip transfer faults were found in this model.

The dip directions of both faults were divided into two sets, which are the same direction (east dipping faults) and opposite direction (west dipping faults) to the extension direction. In addition, the dip angle of faults occurring in intra-rift zone are lower than border-rift zone, as shown in figure 4.2, but the dip angles of faults in this model have a high angle in upper zones and continuously decrease in lower zones. Moreover, the mean directions of fault orientation analyzed from rose diagrams from the west dipping faults and the east dipping faults (Fig 4.3) are 178 degrees and 358 degrees respectively.

The fault linkages in this model having both lateral fault linkages and vertical fault linkages occurring during extension and they can be observe from both map views and oblique views of the 3D orthogonal rift model and cross-section views of model section images respectively. The fault linkages occurring from overlapping fault tips of rift-border faults and intra-rift faults in this model. Hence, these are causes of forming relay ramp structure in this orthogonal rift model. Moreover, along the strike of intra-rift faults in the orthogonal rift model that have the half-graben structure located in north and south trend around the intra-rift zone. The offsets of depocenters are accomplished by accommodation zones formed by interlocking conjugate fault arrays besides, the elevation map shown in figure 4.1 can be observed the location of accommodation zones located in the intra-rift zone.

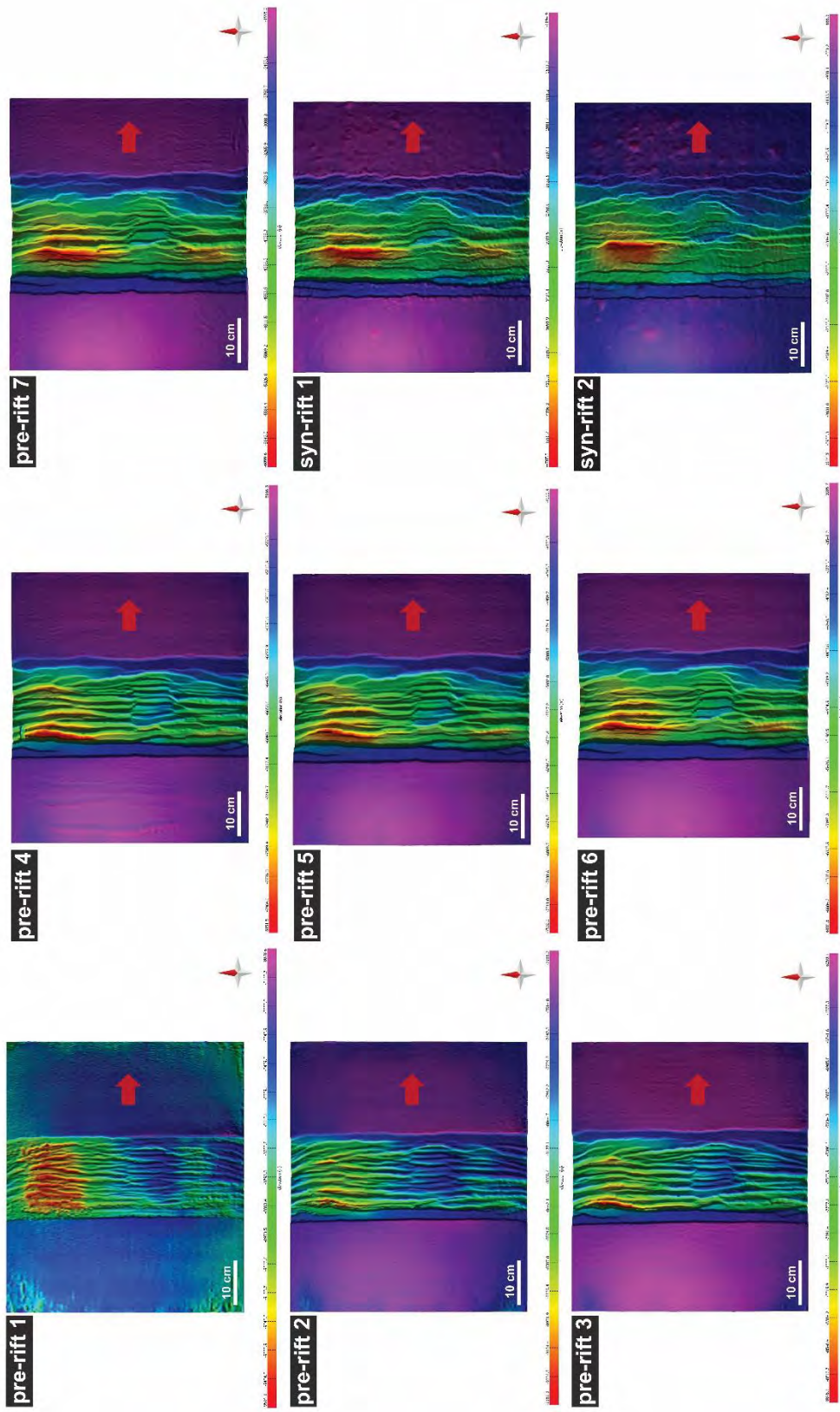


Figure 4.1 The map visualization of elevation maps from orthogonal rift model that consists of pre-rift 1 to pre-rift 7 and syn-rift 1 to syn-rift 2. These elevation map present pattern of fault system and other structures occurring in the rift basin.

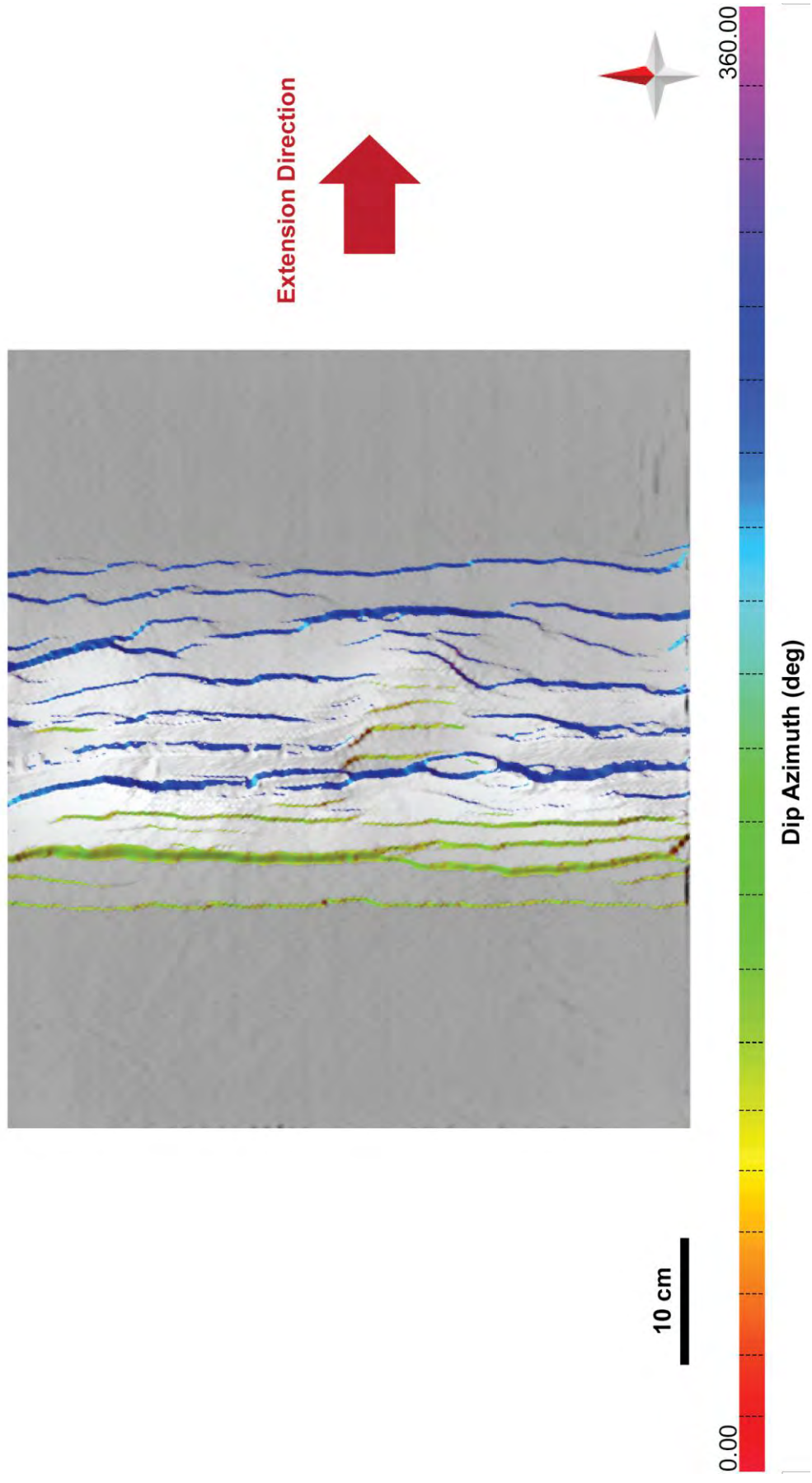


Figure 4.2 The dip azimuth map of pre-rift 7 from orthogonal rift model that present the west dipping faults (blue) and the east dipping faults (green) occurring in the rift basin.

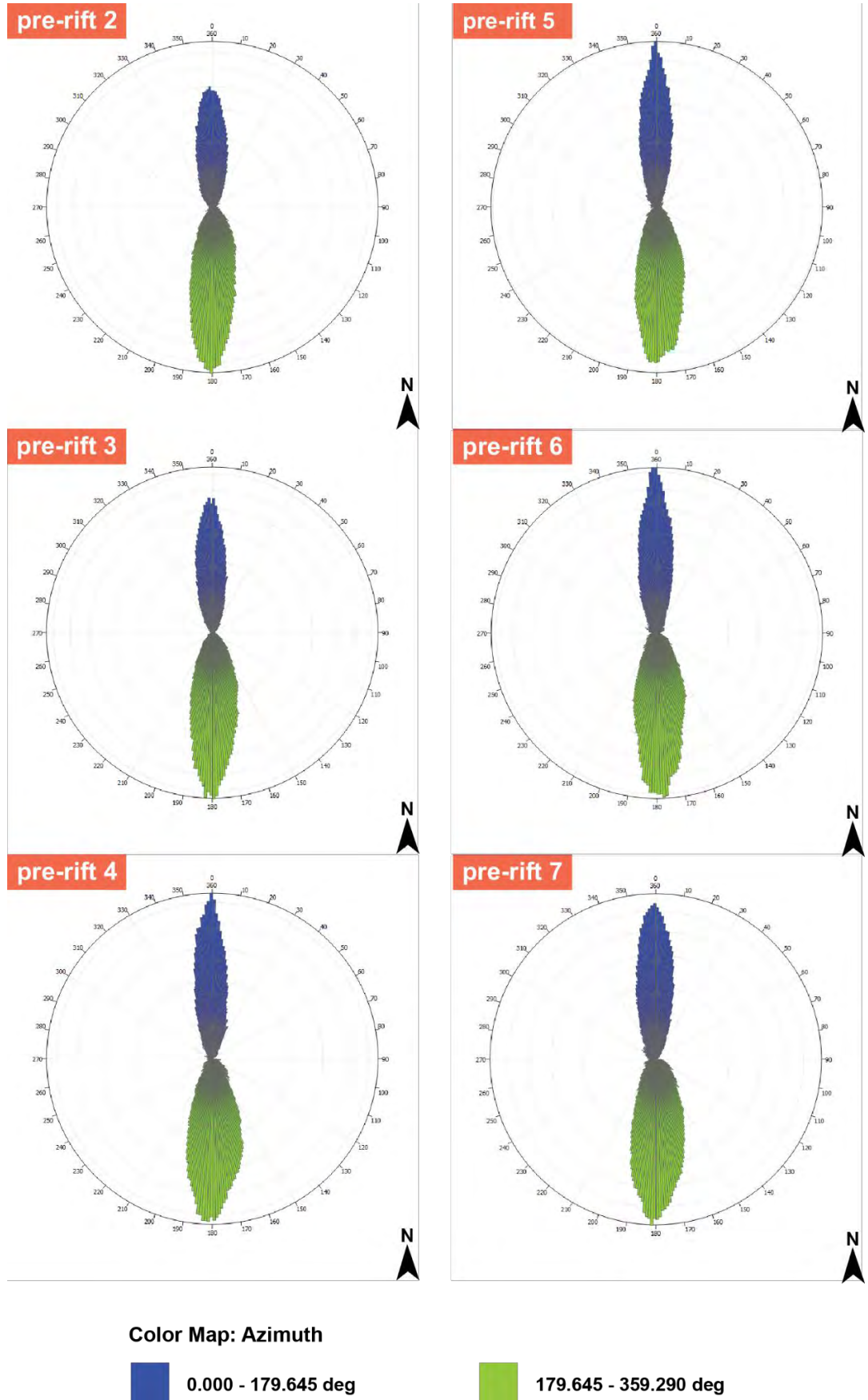


Figure 4.3 The rose diagrams of pre-rift 2 to pre-rift 7 from orthogonal rift model that present the N-S striking of faults pattern in the rift basin. These rose diagrams also show the intensity of mesh files of east dipping faults and west dipping faults that were separated by the green color and the blue color respectively.

4.2.2 Fault analysis

Figure 4.4 shows an oblique 3D visualization of Pre-rift 6 horizon surfaces mapped in the orthogonal rift model that consists of East dipping faults (EFault 01 and EFault 02) and West dipping faults (WFault 01, WFault 02 and WFault 03). Essential examples of displacement profiles on the west dipping faults and the east dipping faults are shown and described as follows.

4.2.2.1 East dipping fault displacement profiles

- ***EFault 01***

The dip angle of EFault 01 surface has a high angle (60-70 degrees) in an upper surface and continuously decreases to a low angle in a lower surface (45-60 degrees), as shown in figure 4.5a. In addition to, the dip azimuth is sub-parallel to parallel to the extension direction (Fig 4.5b).

The example of 3D EFault 01 (Fig 4.6a) shows an offset profile having N-S striking rift-border fault segmented. A graph in figure 4.6b shows a fault throw calculated from the horizon surfaces of pre-rift 3 to pre-rift 7. This graph also shows the largest amounts of offset at a pre-rift 4 (Peak A) and a pre-rift 6 (Peak B), with each maximum displacement up to 0.485 centimeters and up to 0.490 centimeters located in the center of the fault respectively. Moreover, the stage of early fault linkage can be observed from decreasing and increasing of pre-rift 4 line that almost unchanged, whereas the stage of late fault linkage can be observed from the rapid decreasing of Linkage A, B and C shown in a pre-rift 7 line.

In the fault scaling of EFault 01 (Fig 4.15), the length of this fault is 53.1482 centimeters, whereas the maximum throw is 0.4906 centimeters. The ratio of maximum throw to fault length shown in the graph of this fault scaling presents the location of similarly natural normal fault, which is coal measures located in Lorraine, France.

- ***EFault 02***

The dip angle of EFault 02 surface has a high angle (46-61 degrees) that continuously increase to northward in an upper-surface and a low angle in a lower surface (30-40 degrees), as shown in figure 4.7a. In addition to, the dip azimuth in the northward is more sub-parallel to parallel to the extension direction than southward (Fig 4.7b).

The example of 3D EFault 02 (Fig 4.8a) shows an offset profile having N-S striking intra-rift fault segmented. A graph in figure 4.8b shows a fault throw calculated from the horizon surfaces of pre-rift 3 to pre-rift 6. This graph also shows the largest amount of

offset at the pre-rift 6 (Peak), with the maximum displacement up to 0.499 centimeters located in the upper northward of fault. Moreover, this graph also shows the stage of early fault linkage that can be observed from decreasing and increasing of pre-rift lines that almost unchanged.

In the fault scaling of EFault 02 (Fig 4.15), the length of this fault is 9.5965 centimeters, whereas the maximum throw is 0.4999 centimeters. The ratio of maximum throw to fault length shown in the graph of this fault scaling presents the location of a similarly natural normal fault, which are coal measures located in Lorraine, France.

4.2.2.2 West dipping fault displacement profiles

- **WFault 01**

The dip angle of WFault 01 surface has a high angle (60-70 degrees) in an upper surface and continuously decreases to a low angle in a lower surface (45-60 degrees), as shown in figure 4.9a. In addition to, the dip azimuth is sub-parallel to parallel to the extension direction (Fig 4.9b).

The example of 3D WFault 01 (Fig 4.10a) shows an offset profile having N-S striking rift-border fault segmented. The graph in figure 4.10b shows a fault throw calculated from the horizon surfaces of pre-rift 3 to pre-rift 7. Besides, this graph shows the largest amounts of offset at the pre-rift 4 (Peak A) and the pre-rift 3 (Peak B), with each maximum displacement up to 0.522 centimeters and up to 0.615 centimeters located in both northward and southward of fault respectively. Moreover, this graph only shows the stage of early faults linkage because decreasing and increasing of pre-rift lines that almost unchanged.

In the fault scaling of WFault 01 (Fig 4.15), the length of this fault is 36.4502 centimeters, whereas the maximum throw is 0.6156 centimeters. The ratio of maximum throw to fault length shown in the graph of this fault scaling presents the location of a similarly natural normal fault, which are coal measures located in Lorraine, France.

- **WFault 02**

The dip angle of WFault 02 surface is 50 to 68 degrees, as shown in figure 4.11a. The dip azimuth is sub-parallel to parallel and oblique (because these zones are linkage zones) to the extension direction (Fig 4.11b).

The example of 3D WFault 02 (Fig 4.12a) shows an offset profile having N-S striking rift-border fault segmented. The graph in figure 4.12b shows a fault throw calculated from

the horizon surfaces of pre-rift 3 to pre-rift 7. This graph also shows the largest amounts of offset at the pre-rift 6 (Peak A) and the pre-rift 3 (Peak B and Peak C), with each maximum displacement up to 0.448 centimeters, 0.518 centimeters and 0.497 centimeters respectively, which are located in the northward and the center of fault. In this graph, the evolution of downward-fault development is shown by the zone of the Peak A that is a position of Linkage A (older pre-rifts) to be closer than Linkage B (younger pre-rifts), but on the other hand another upward-fault development is shown by the zones of Peak B and Peak C that are the position of Linkage B (younger pre-rift) to be closer than Linkage A (older pre-rift).

In the fault scaling of WFault 02 (Fig 4.15), the length of this fault is 24.8598 centimeters, whereas the maximum throw is 0.5184 centimeters. The ratio of maximum throw to fault length shown in the graph of this fault scaling presents the location of a similarly natural normal fault, which are coal measures located in Lorraine, France.

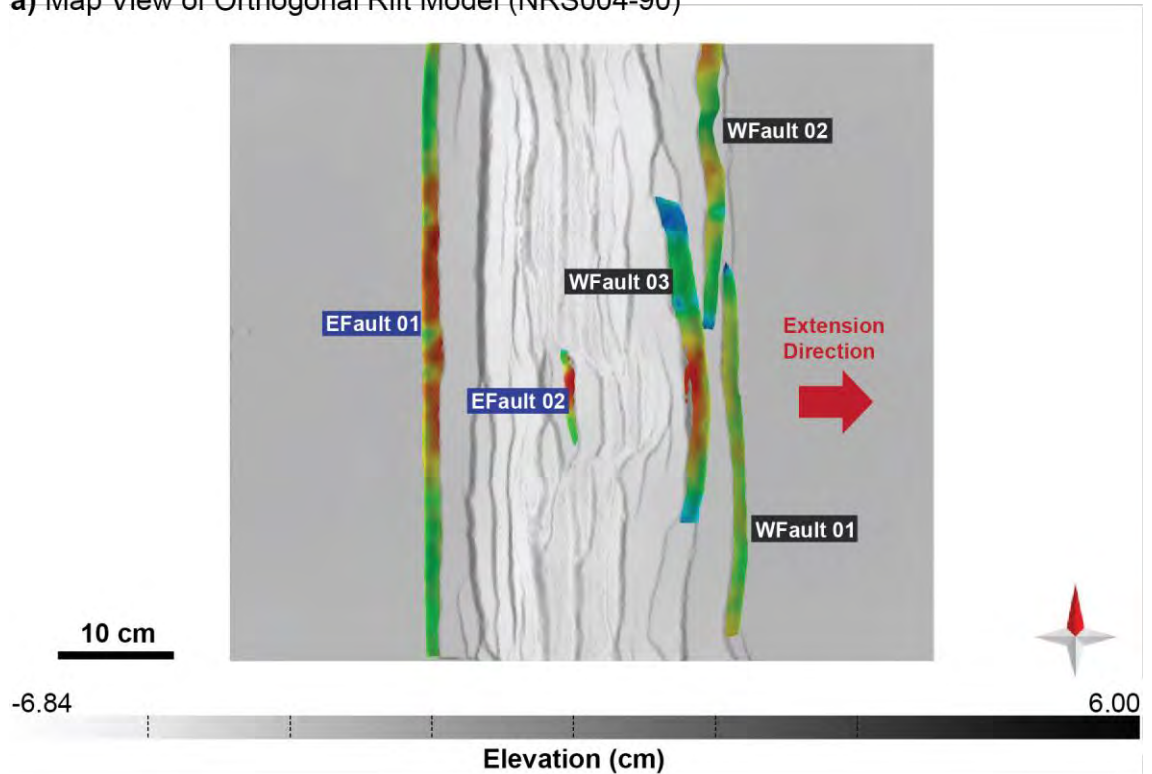
- **WFault 03**

The dip angle of WFault 03 surface has a high angle (60-70 degrees) in an upper surface and continuously decreases to a low angle in a lower surface (40-60 degrees), as shown in figure 4.13a. In addition to, the dip azimuth is sub-parallel to parallel and oblique (the zone of yellow color because this zone is a linkage zone) to the extension direction (Fig 4.13b).

The example of 3D WFault 03 (Fig 4.14a) shows an offset profile having N-S striking intra-rift fault segmented. The graph in figure 4.14b shows a fault throw calculated from the horizon surfaces of pre-rift 3 to syn-rift 1. Besides, this graph shows the largest amount of offset at the pre-rift 7 (Peak), with the maximum displacement up to 1.177 centimeters, which is located in the center of the fault. In this graph, the evolution of downward-fault development is shown by the zone of Peak that is the position of Linkage C (the oldest pre-rift) to be closer than Linkage B and Linkage C (younger pre-rifts) respectively.

In the fault scaling of WFault 03 (Fig 4.15), the length of this fault is 28.5450 centimeters, whereas the maximum throw is 1.1775 centimeters. The ratio of maximum throw to fault length shown in the graph of this fault scaling presents the location of a similarly natural normal fault, which are coal measures located in Lorraine, France.

a) Map View of Orthogonal Rift Model (NRS004-90)



b) Oblique View of Orthogonal Rift Model (NRS004-90)

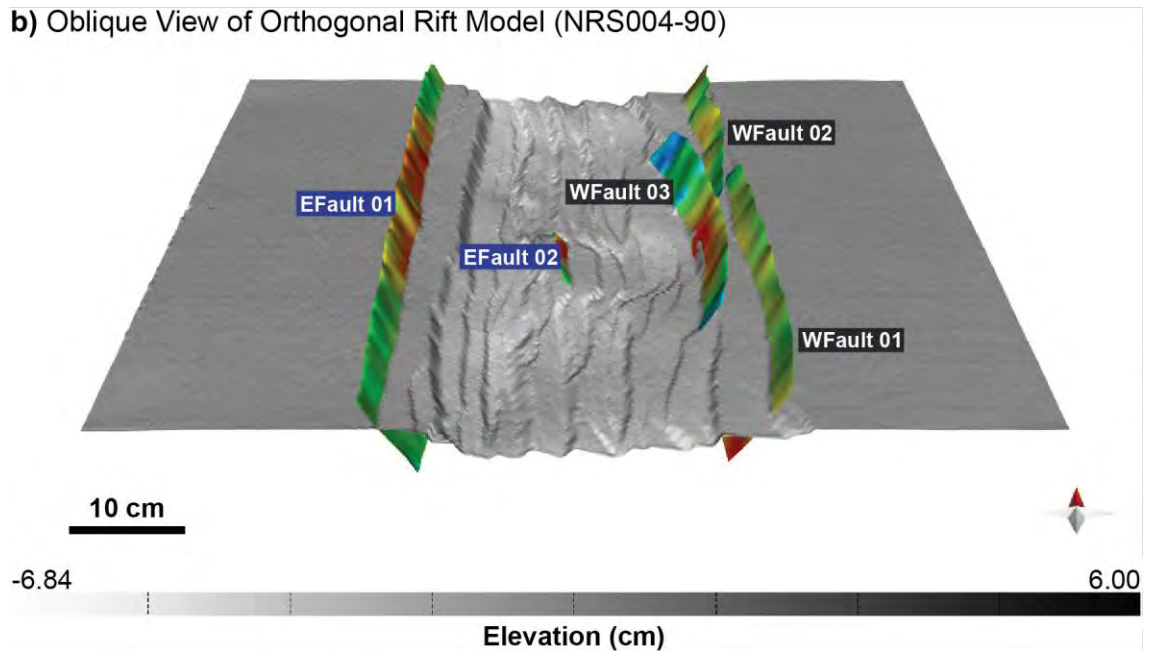


Figure 4.4 (a) The map visualization and (b) the 3D oblique visualization (looking N) of pre-rift 6 surface from orthogonal rift model that show the elevation map having west dipping fault surfaces (WFault 01, WFault 02 and WFault 03) and east dipping fault surfaces (EFault 01 and EFault 02) in the rift basin.

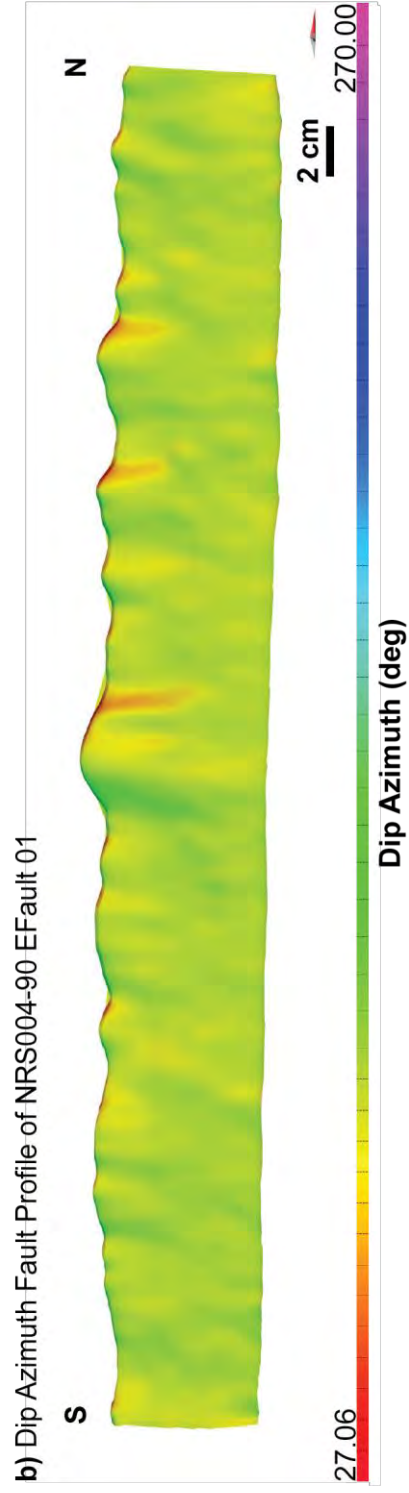
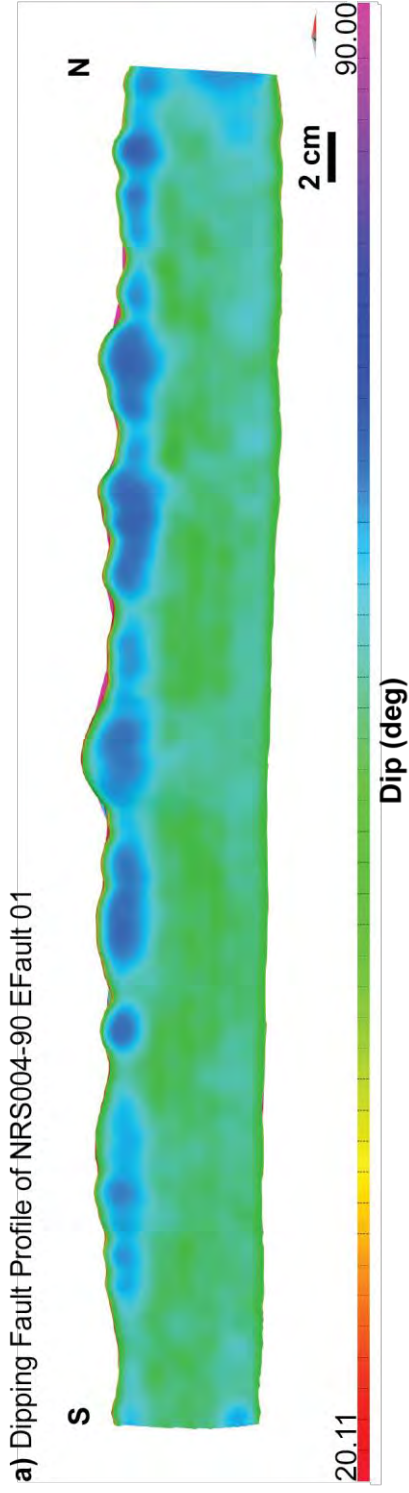


Figure 4.5 (a) The dipping fault profile of NRS004-90 EFault 01 (looking perpendicular to the strike) that shows the dip angle on fault surface of EFault 01. (b) The dip azimuth fault profile of NRS004-90 EFault 01 that shows the direction of dip azimuth on this fault surface.

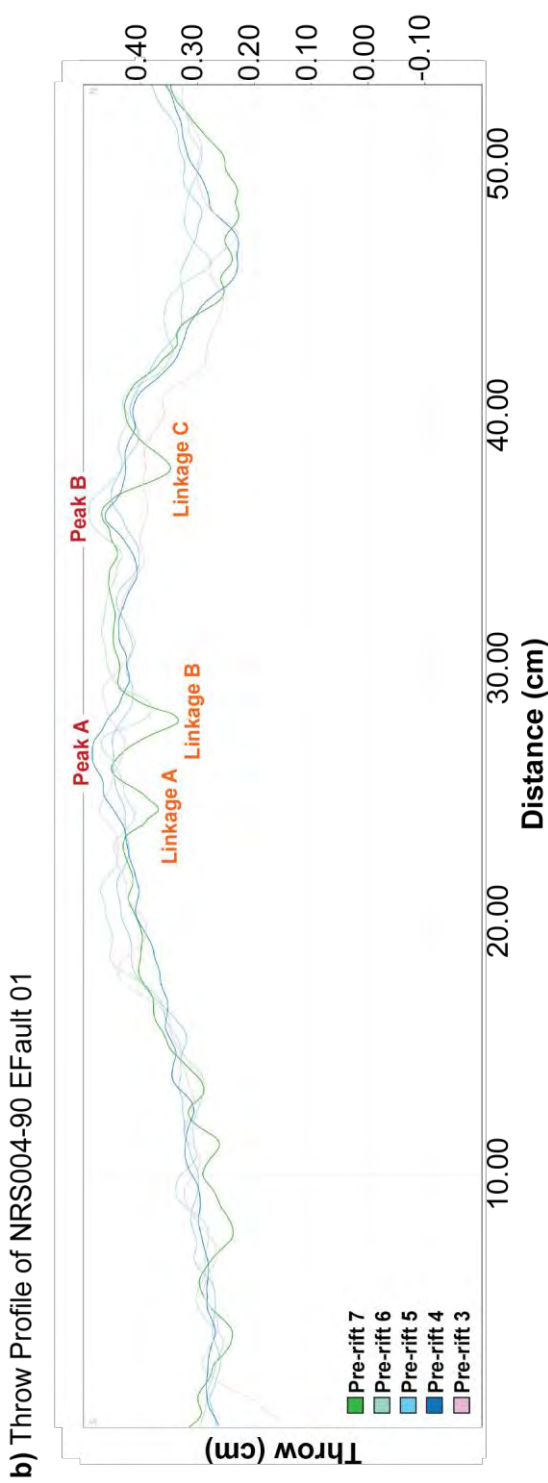
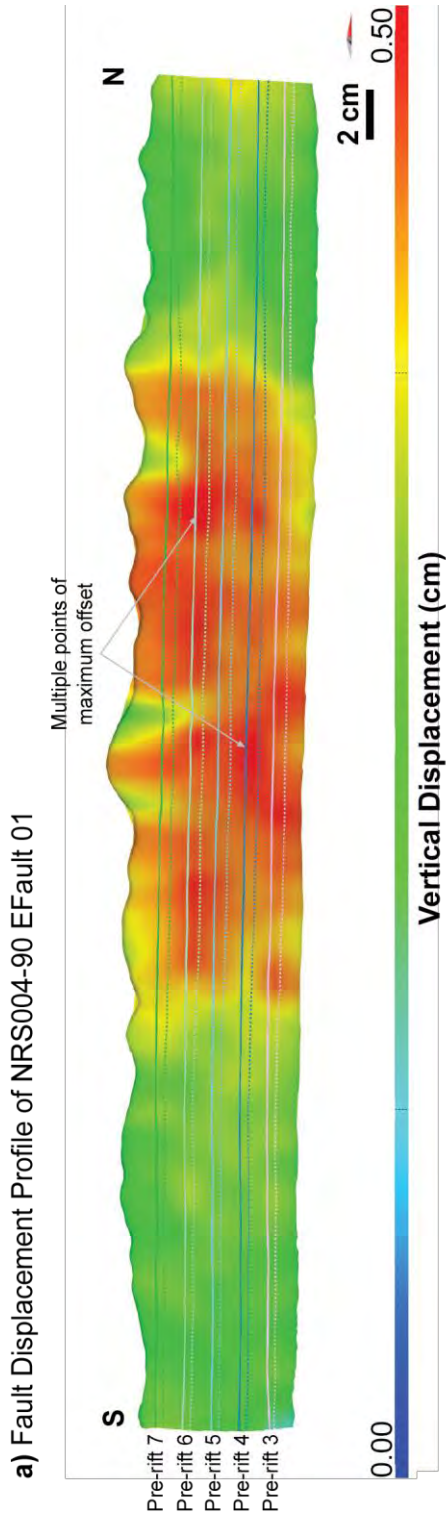
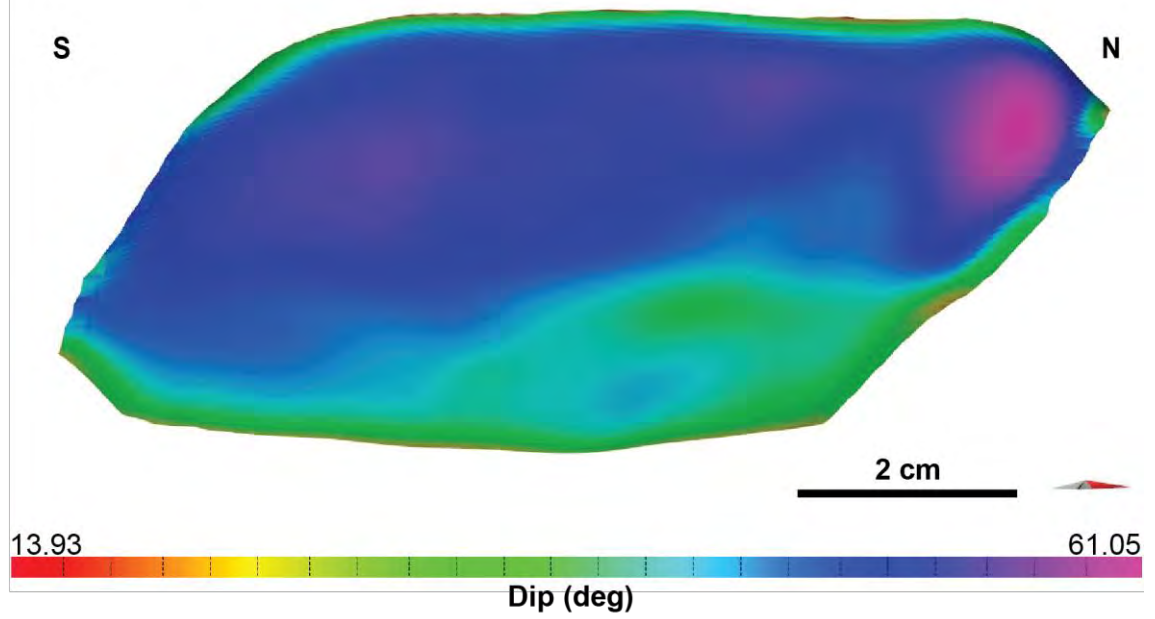


Figure 4.6 (a) Displacement profile of NRS004-90 EFault 01 (looking perpendicular to the strike). Line across the fault surface are hangingwall (dashed line) and footwall (solid lines) cutoffs from interpreted horizons. (b) Fault offset showing fault throw measured perpendicular to strike orientation along the fault. Fault location is shown in figure 4.4.

a) Dipping Fault Profile of NRS004-90 EFault 02



b) Dip Azimuth Fault Profile of NRS004-90 EFault 02

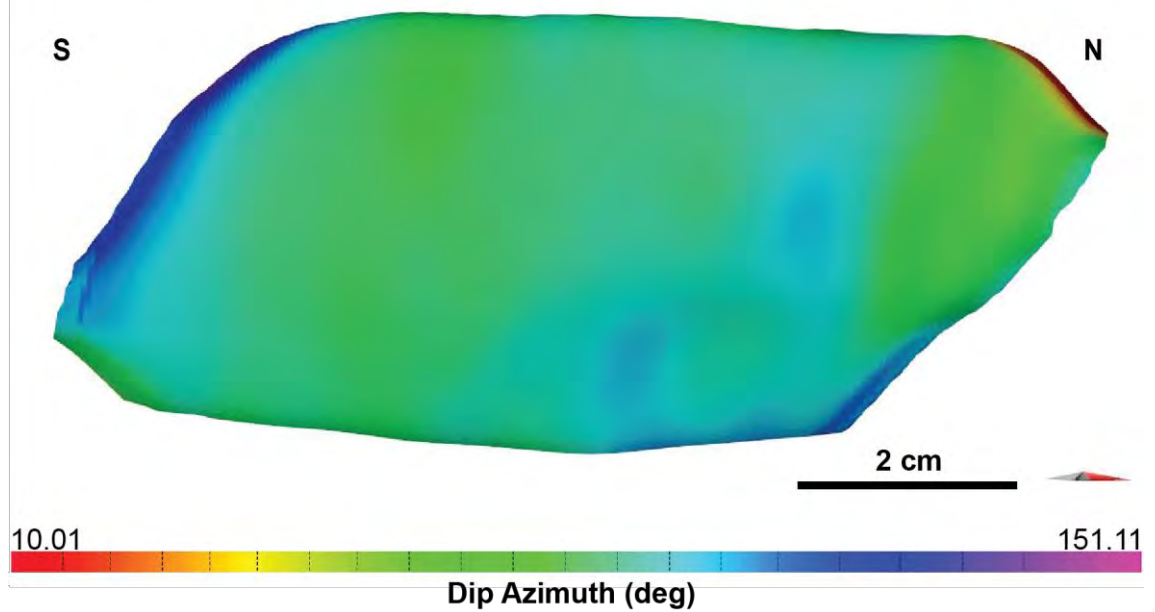
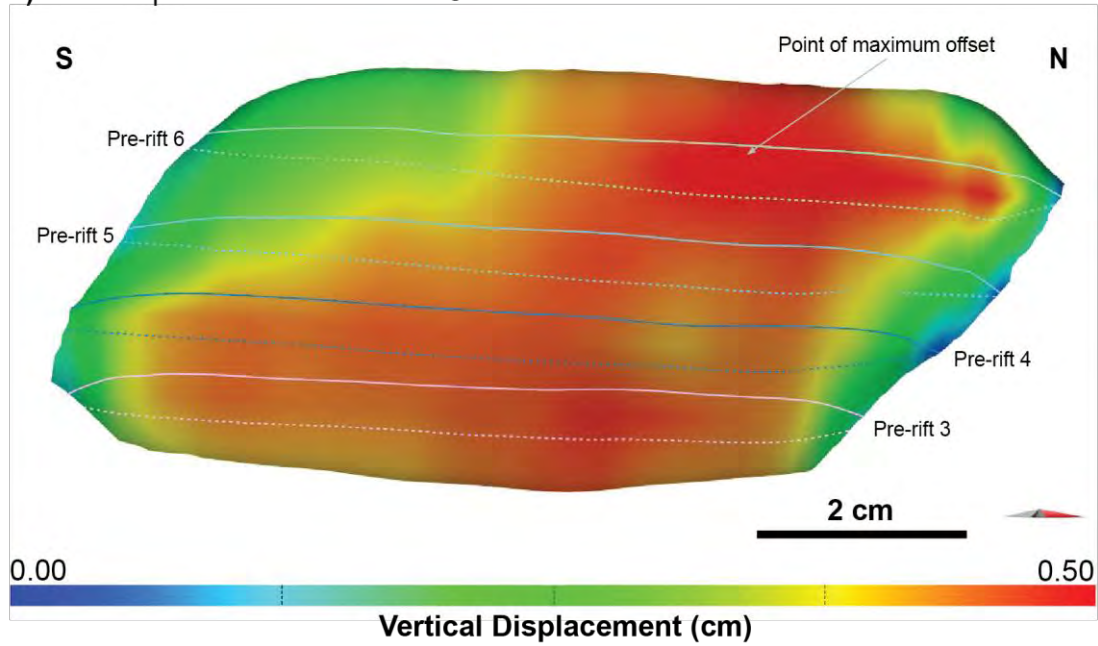


Figure 4.7 (a) The dipping fault profile of NRS004-90 EFault 02 (looking perpendicular to the strike) that shows the dip angle on fault surface of EFault 01. (b) The dip azimuth fault profile of NRS004-90 EFault 02 that shows the direction of dip azimuth on this fault surface.

a) Fault Displacement Profile of NRS004-90 EFault 02



b) Throw Profile of NRS004-90 EFault 02

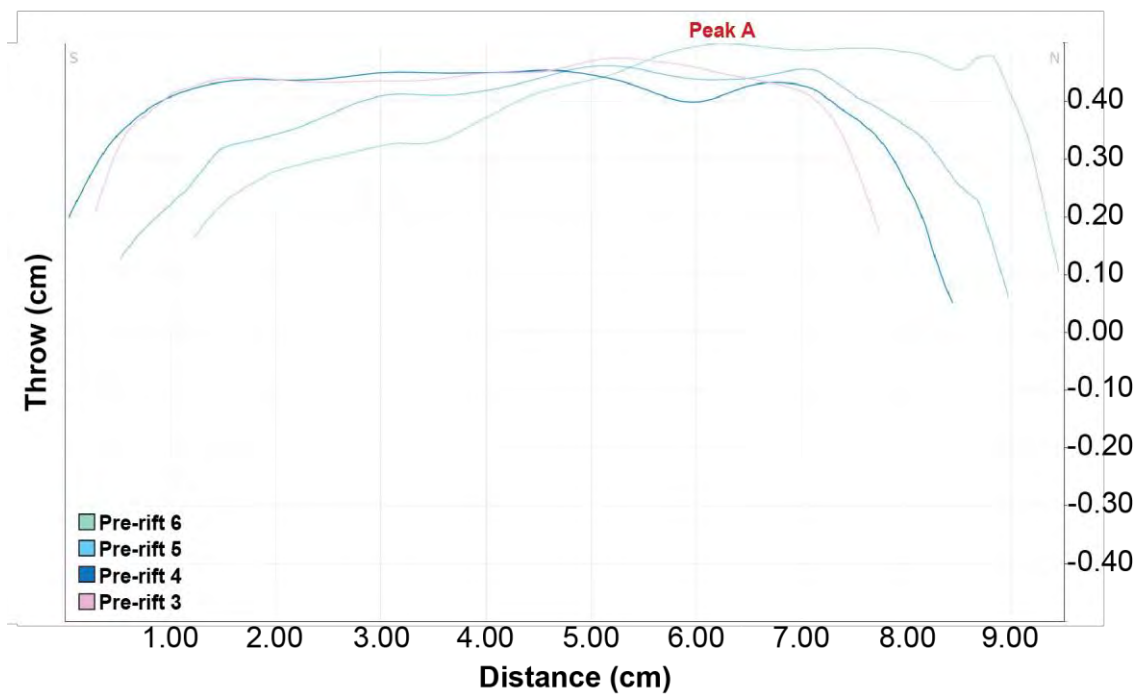


Figure 4.8 (a) Displacement profile of NRS004-90 EFault 02 (looking perpendicular to the strike). Line across the fault surface are hangingwall (dashed line) and footwall (solid lines) cutoffs from interpreted horizons. (b) Fault offset showing fault throw measured perpendicular to strike orientation along the fault. Fault location is shown in figure 4.4.

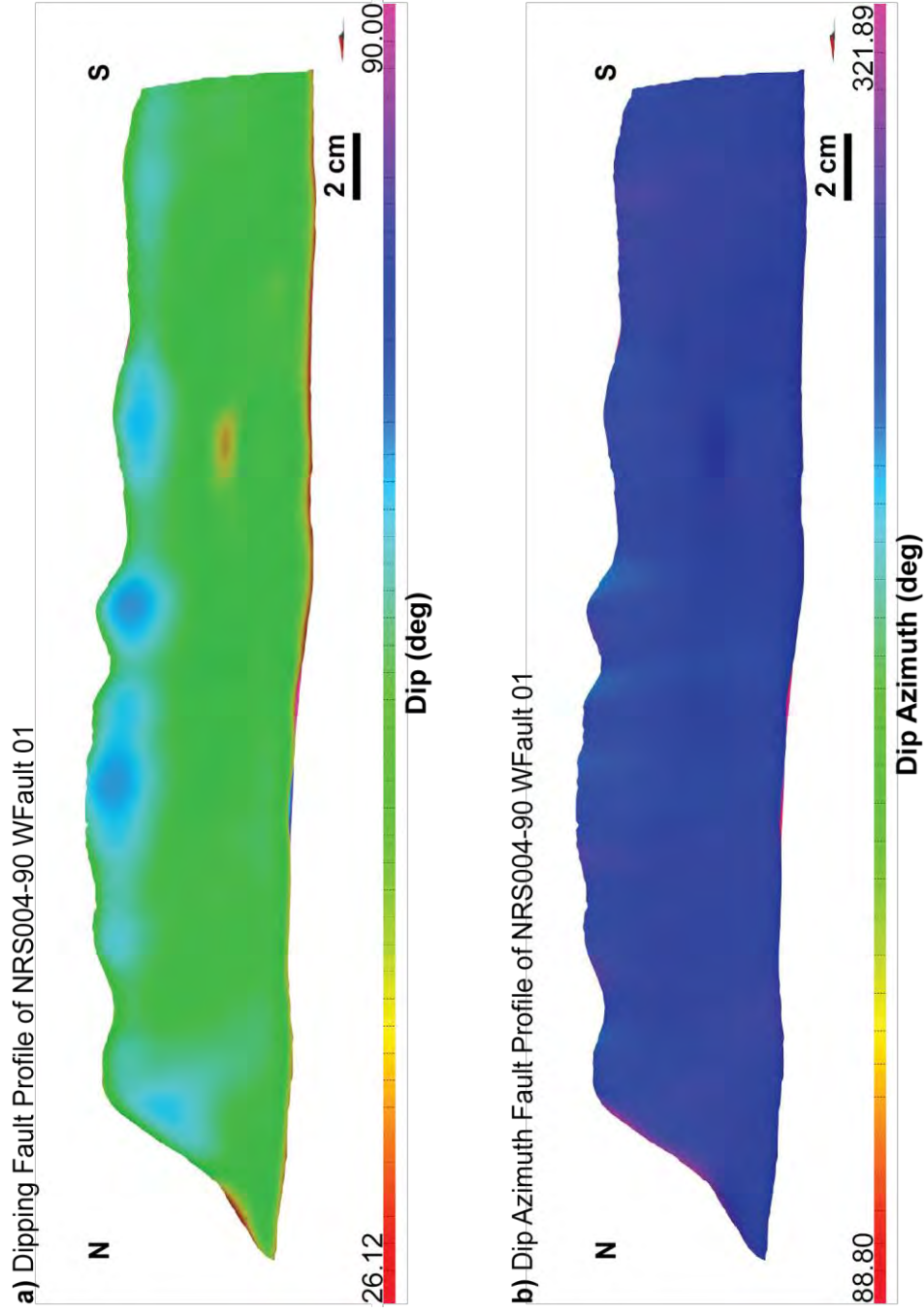
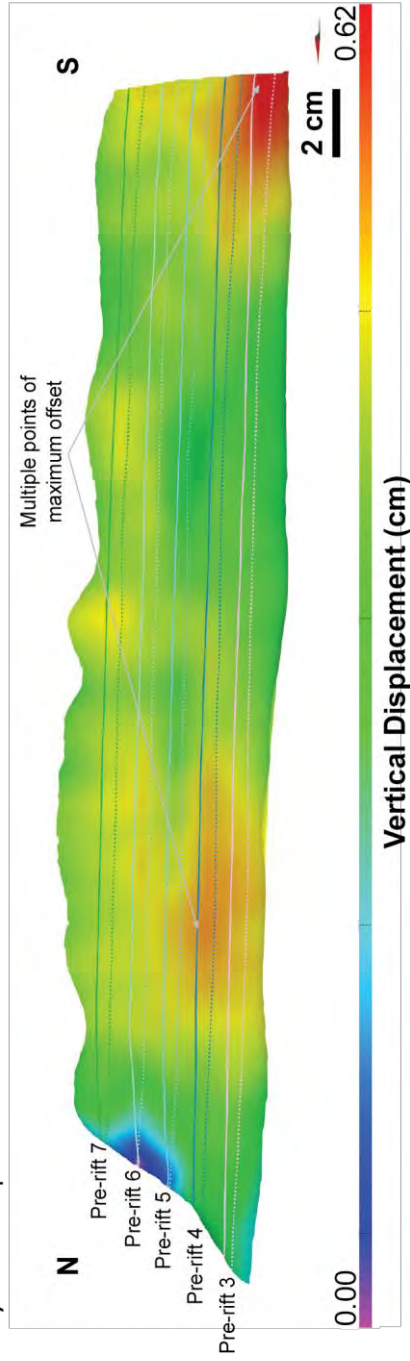


Figure 4.9 (a) The dipping fault profile of NRS004-90 WFault 01 (looking perpendicular to the strike) that shows the dip angle on fault surface of WFault 01. (b) The dip azimuth fault profile of NRS004-90 WFault 01 that shows the direction of dip azimuth on this fault surface.

a) Fault Displacement Profile of NRS004-90 WFault 01



b) Throw Profile of NRS004-90 WFault 01

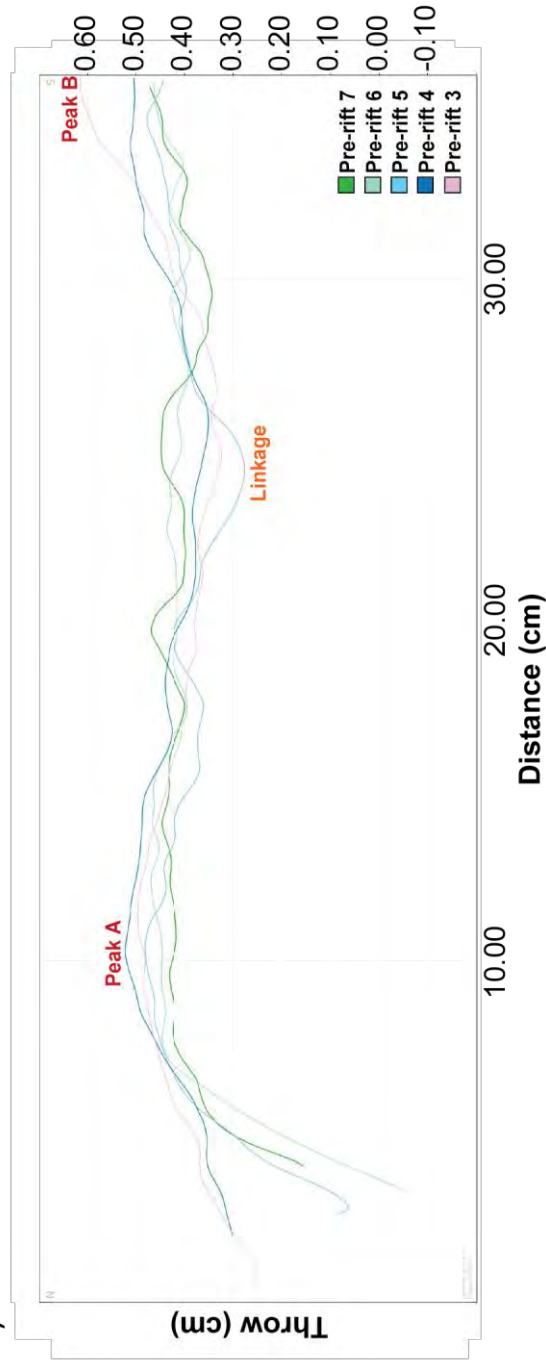
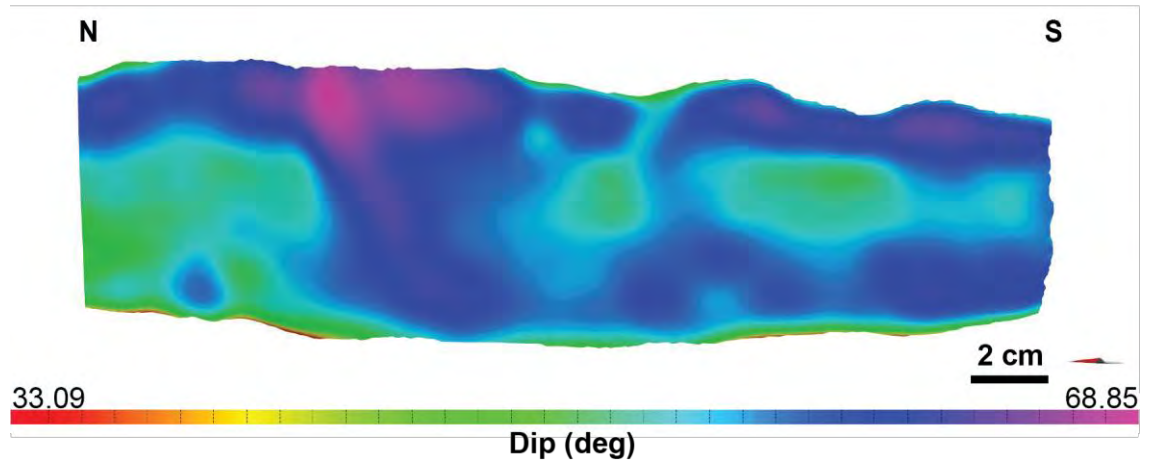


Figure 4.10 (a) Displacement profile of NRS004-90 WFault 01 (looking perpendicular to the strike). Line across the fault surface are hangingwall (dashed line) and footwall (solid lines) cutoffs from interpreted horizons. (b) Fault offset showing fault throw measured perpendicular to strike orientation along the fault. Fault location is shown in figure 4.4.

a) Dipping Fault Profile of NRS004-90 WFault 02



b) Dip Azimuth Fault Profile of NRS004-90 WFault 02

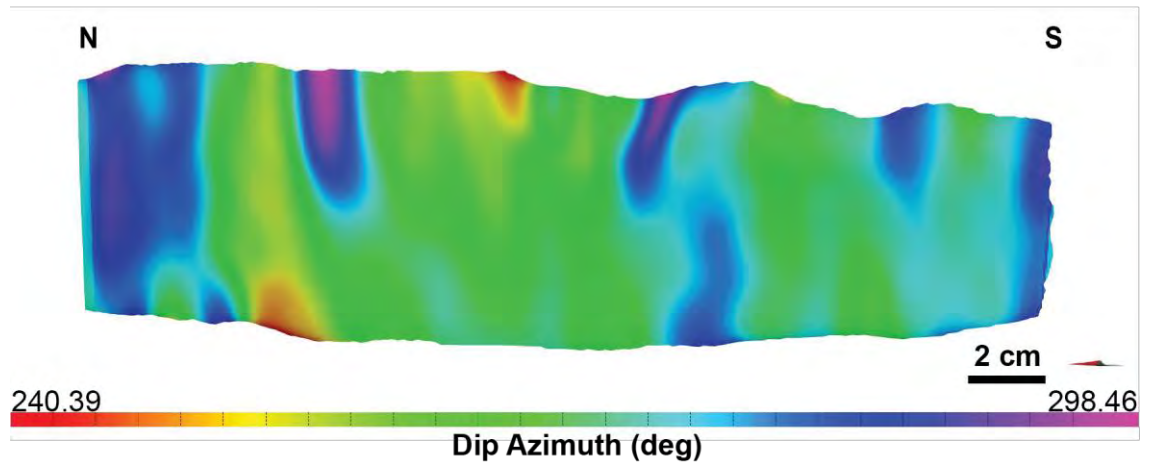
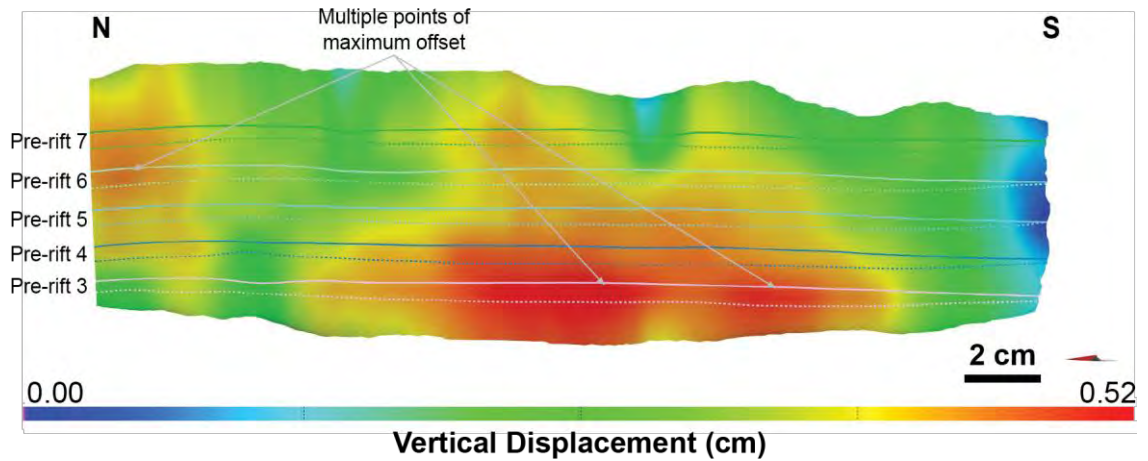


Figure 4.11 (a) The dipping fault profile of NRS004-90 WFault 02 (looking perpendicular to the strike) that shows the dip angle on fault surface of WFault 02. (b) The dip azimuth fault profile of NRS004-90 WFault 02 that shows the direction of dip azimuth on this fault surface.

a) Fault Displacement Profile of NRS004-90 WFault 02



b) Throw Profile of NRS004-90 WFault 02

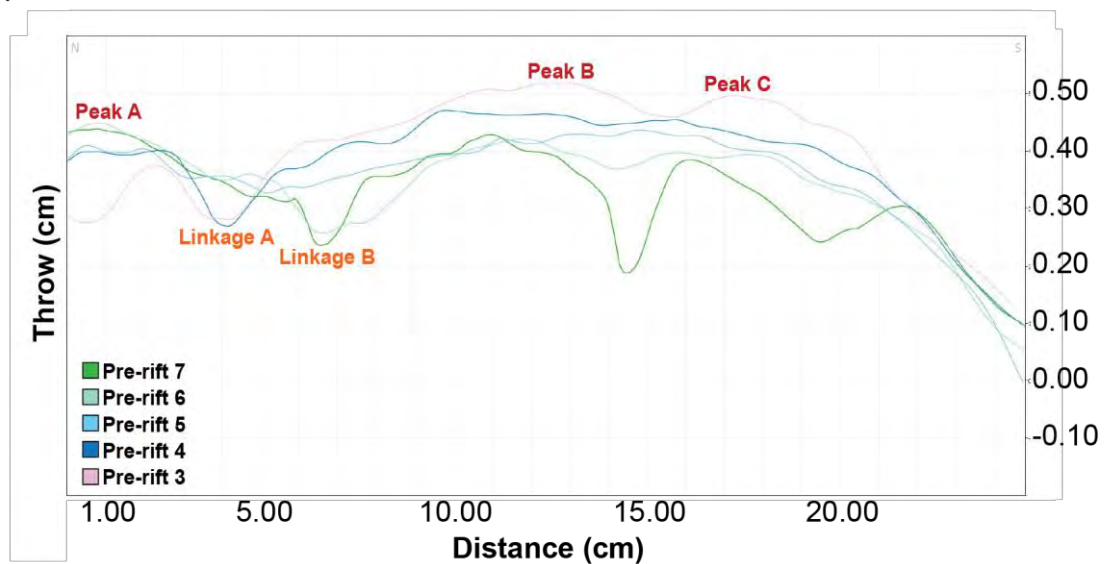
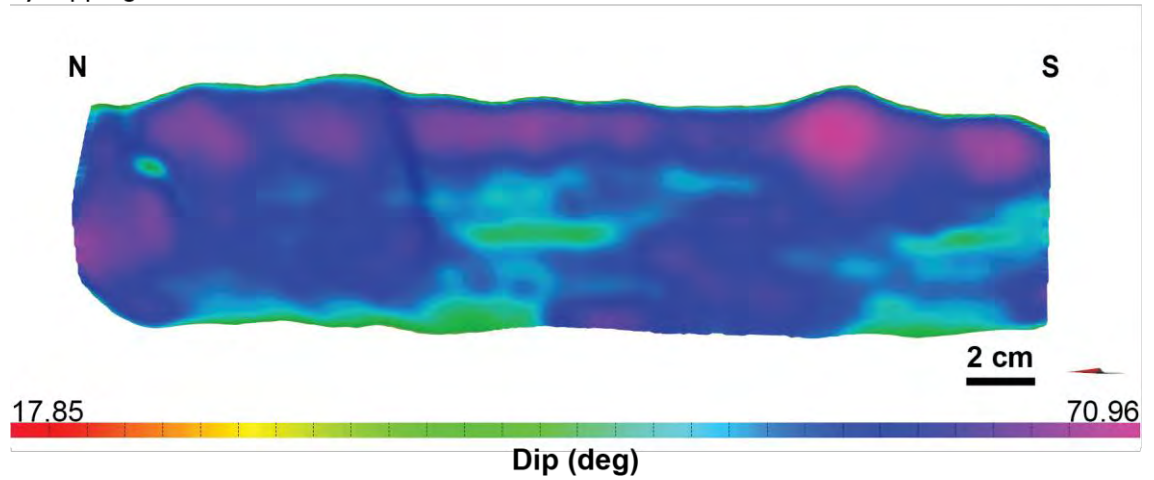


Figure 4.12 (a) Displacement profile of NRS004-90 WFault 02 (looking perpendicular to the strike). Line across the fault surface are hangingwall (dashed line) and footwall (solid lines) cutoffs from interpreted horizons. (b) Fault offset showing fault throw measured perpendicular to strike orientation along the fault. Fault location is shown in figure 4.4.

a) Dipping Fault Profile of NRS004-90 WFault 03



b) Dip Azimuth Fault Profile of NRS004-90 WFault 03

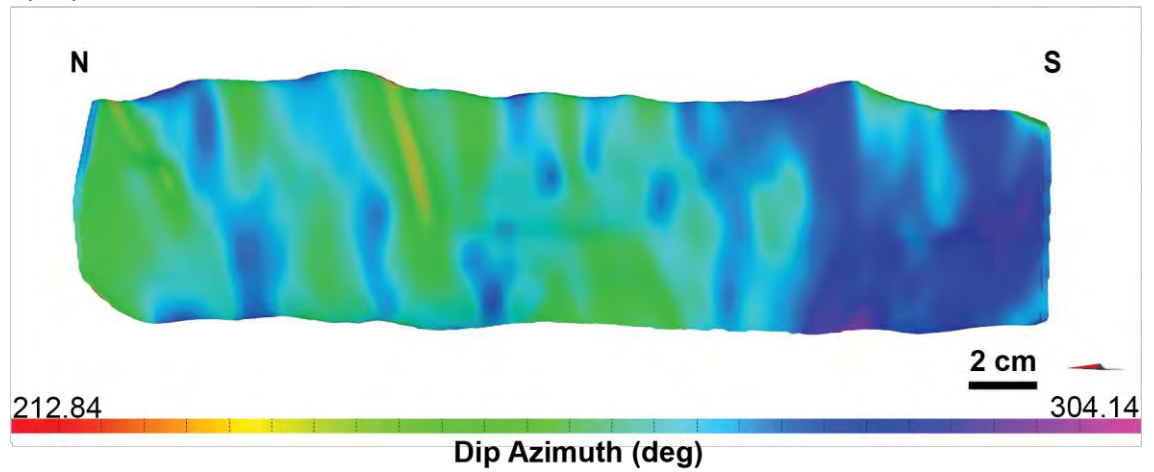
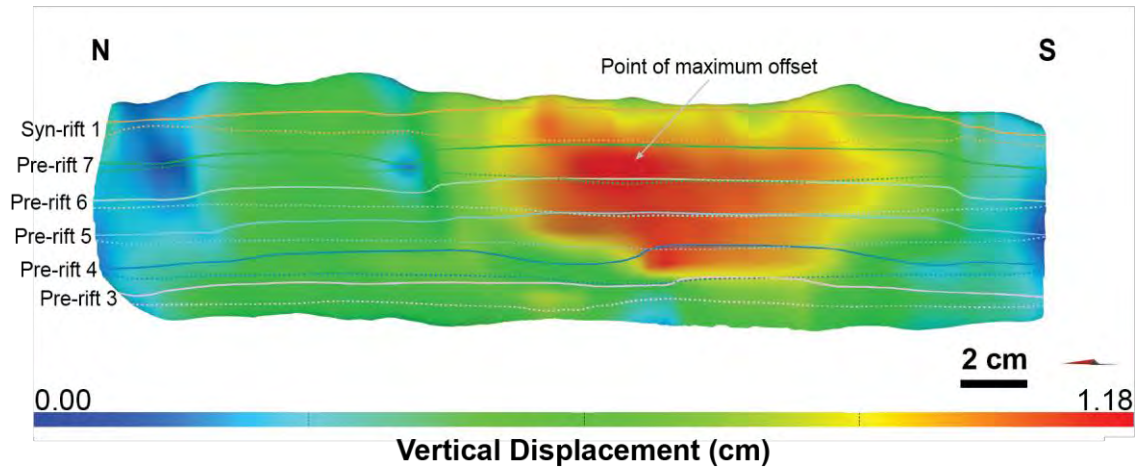


Figure 4.13 (a) The dipping fault profile of NRS004-90 WFault 03 (looking perpendicular to the strike) that shows the dip angle on fault surface of WFault 03. (b) The dip azimuth fault profile of NRS004-90 WFault 03 that shows the direction of dip azimuth on this fault surface.

a) Fault Displacement Profile of NRS004-90 WFault 03



b) Throw Profile of NRS004-90 WFault 03

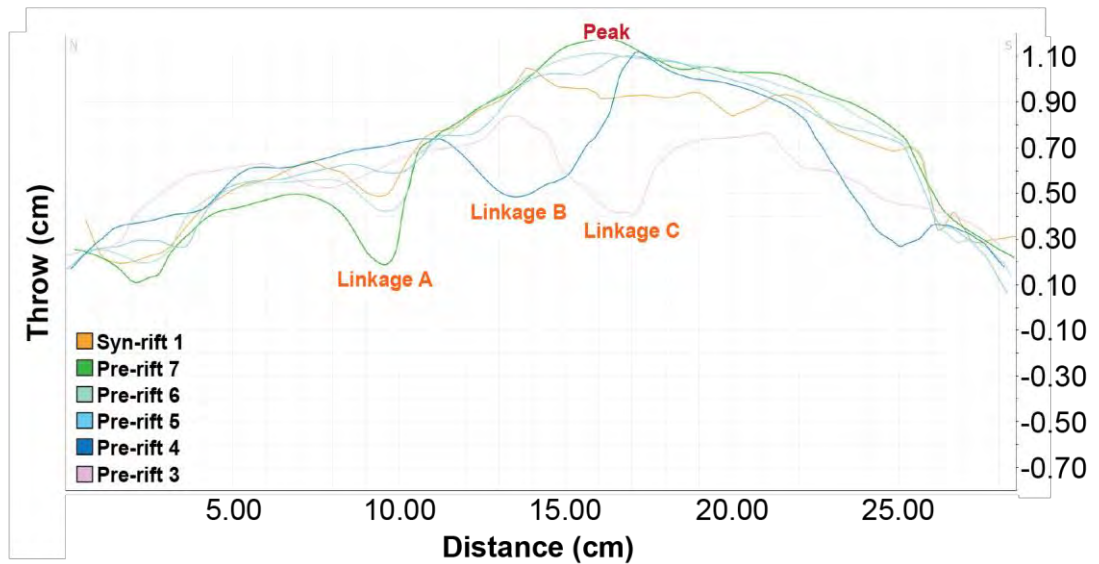


Figure 4.14 (a) Displacement profile of NRS004-90 WFault 03 (looking perpendicular to the strike). Line across the fault surface are hangingwall (dashed line) and footwall (solid lines) cutoffs from interpreted horizons. (b) Fault offset showing fault throw measured perpendicular to strike orientation along the fault. Fault location is shown in figure 4.4.

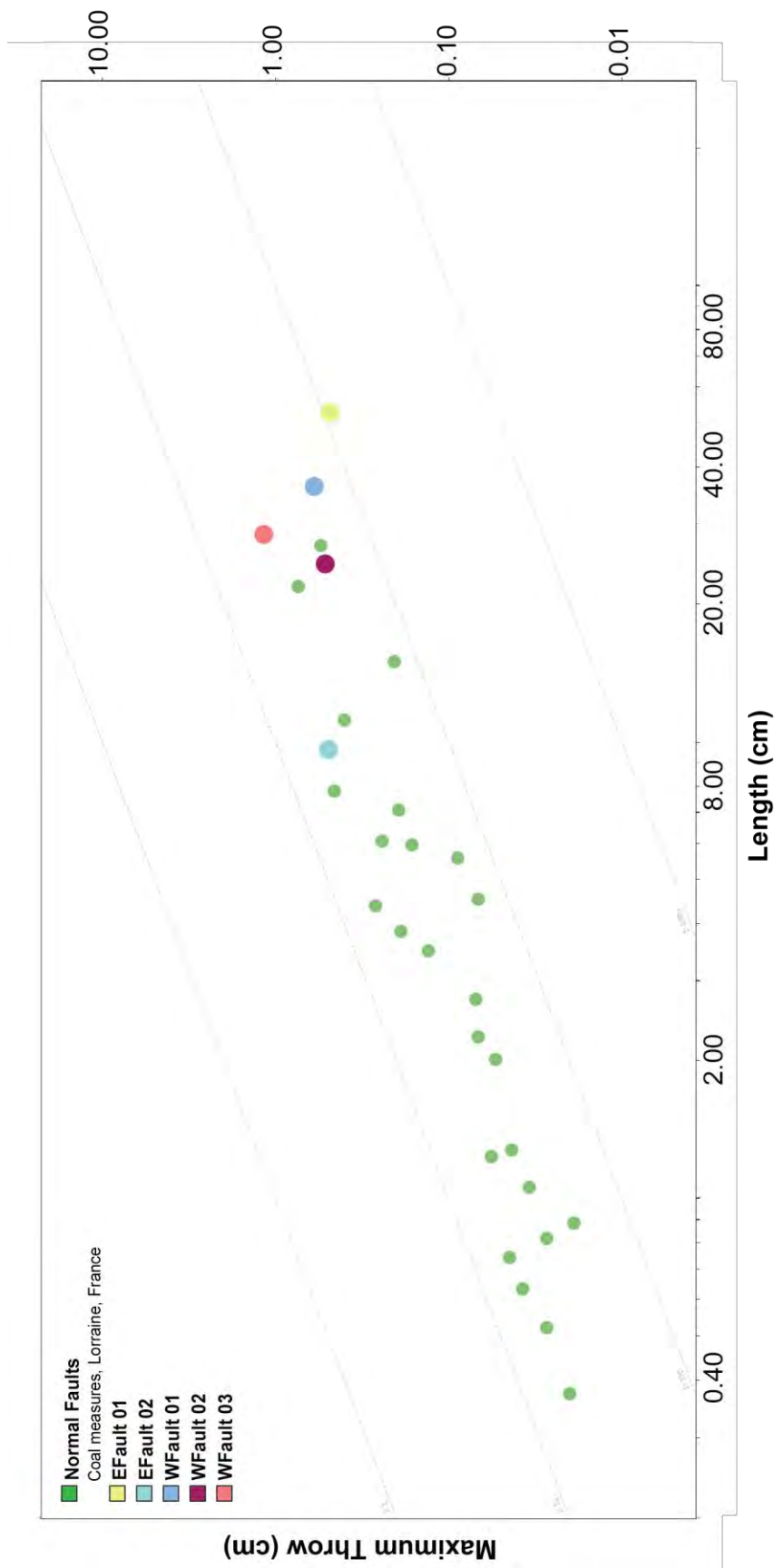


Figure 4.15 The fault scaling that are plotted by the ratio of maximum throw (m) to fault length (m) for faults (EFault 01, EFault 02, WFault 01, WFault 02 and WFault 03) in the orthogonal rift model (1 cm: 1000 m) compared to plots for normal faults in Lorraine coal basin, France

4.3 Oblique rift model (NRS005-60)

4.3.1 Fault systems

Another model is the three dimension of oblique rift model is characterized by shorter normal faults, segmented rift-border faults and intra-rift faults. The rift-border faults formed en echelon arrays have NNW-SSE striking that are parallel to the underlying zone of the pre-existing structure beneath the basin, whereas the orientation of intra-rift faults have N-S striking that are perpendicular to the extension direction around the center of rift zone (Fig 4.16). These intra-rift faults may develop to be parallel with the border rift zone due to the architecture of the pre-existing structure beneath the basins in the scaled physical models controlled them. No strike-slip or oblique-slip transfer faults were found in this model.

The dip directions of intra-rift faults can be divided into two sets which are the same direction and the opposite direction with the extension direction, and the dip directions of rift-border faults are perpendicular to the pre-existing structure beneath the basins. The dip angles of faults occurring in the intra-rift zone are lower than the border-rift zone, as shown in figure 4.17, whereas the dip angles of faults in this model are a high angle in upper zones and continuously decrease the dip angle in lower zones. Moreover, the mean directions of fault orientation analyzed from rose diagrams from the west dipping faults and the east dipping faults are 164 degrees and 336 degrees respectively (Fig 4.18).

The fault linkages in this model having both lateral fault linkages and vertical fault linkages occurring during extension and the can be observed from both map views and oblique views of the 3D orthogonal rift model and cross-section views of model section images respectively. The rift-border faults and the intra-rift faults in this model are segmented along-strike with relay ramp structures formed between overlapping fault tips. Moreover, along the strike of intra-rift faults in the oblique rift model that have the half-graben structure located in north and south around intra-rift zone. The offsets of depocenters are accomplished by accommodation zones formed by interlocking conjugate fault arrays. Besides, the elevation map shown in figure 4.16 can be observed the location of accommodation zones located in the intra-rift zone.

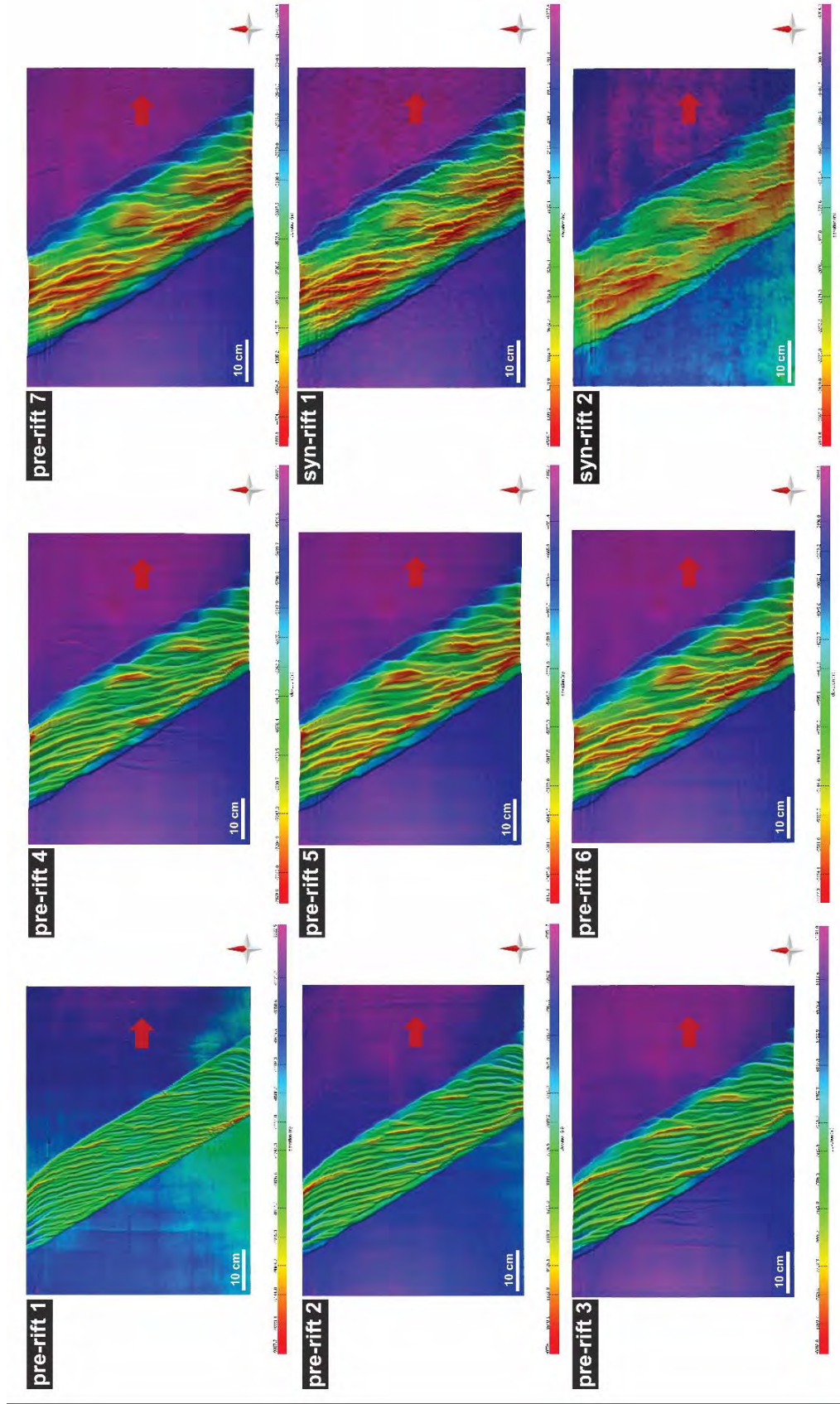


Figure 4.16 The map visualization of elevation maps from oblique rift model that consists of pre-rift 1 to pre-rift 7 and syn-rift 1 to syn-rift 2. These elevation map present pattern of fault system and other structures occurring in the rift basin.

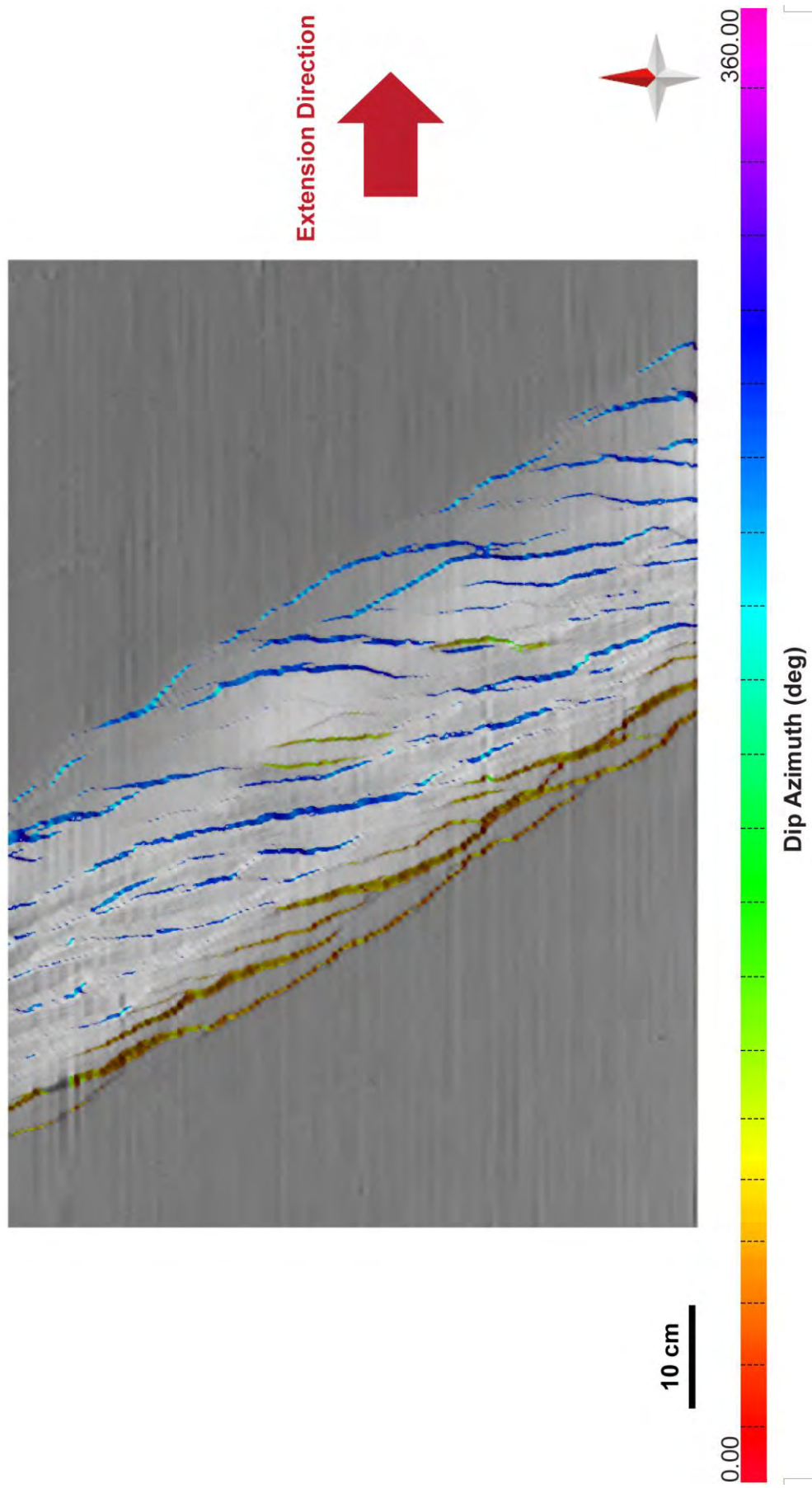


Figure 4.2 The dip azimuth map of pre-rift 7 from oblique rift model that present the west dipping faults (blue) and the east dipping faults (green) occurring in the rift basin.

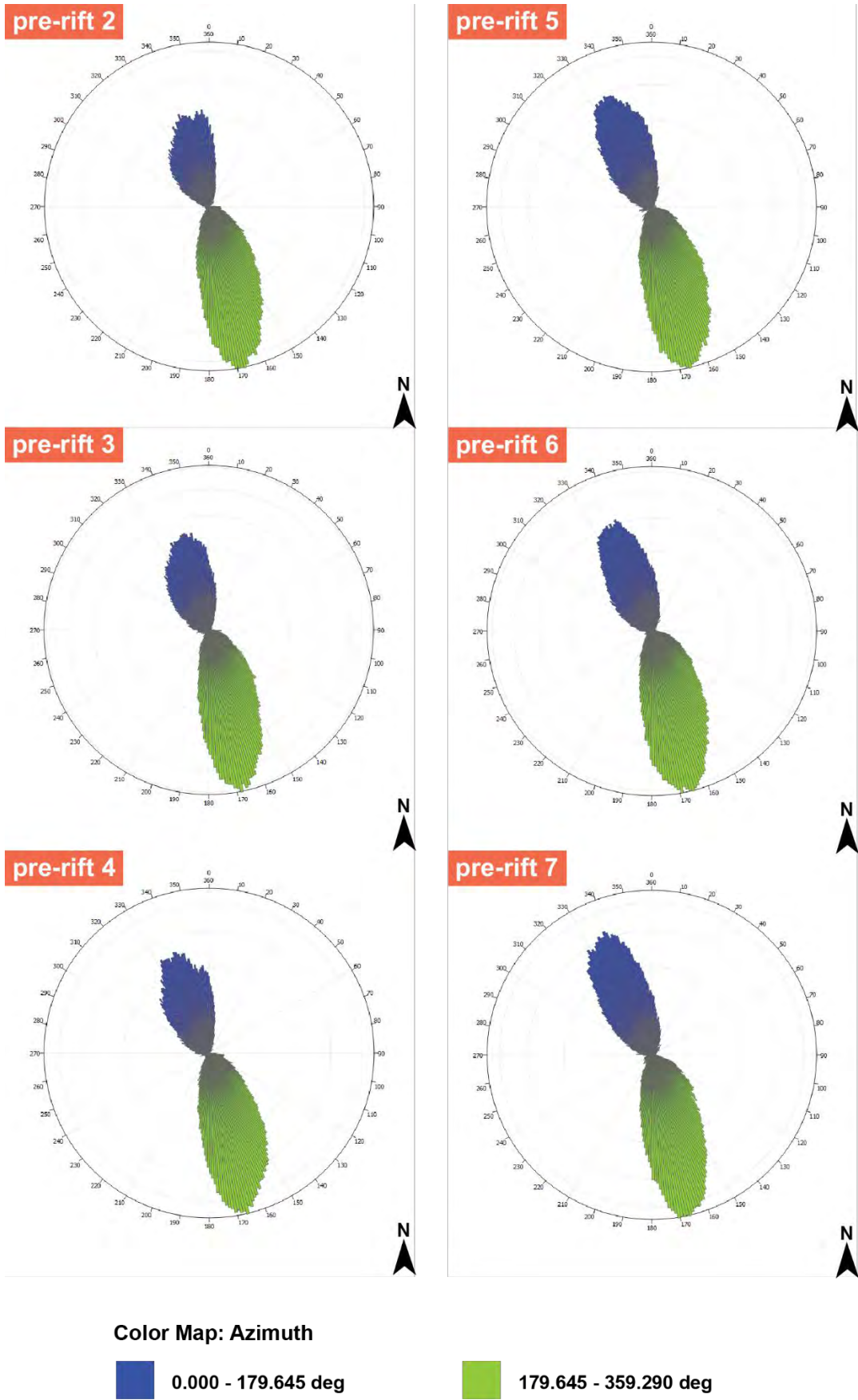


Figure 4.18 The rose diagrams of pre-rift 2 to pre-rift 7 from oblique rift model that present the N-S striking of faults pattern in the rift basin. These rose diagrams also show the intensity of mesh files of east dipping faults and west dipping faults that were separated by the green color and the blue color respectively.

4.3.2 Fault analysis

Figure 4.19 shows a map and an oblique 3D visualization of Pre-rift 6 horizon surface mapped in the oblique rift model that consists of west dipping faults (WFault 01 and WFault 02) and east dipping faults (EFault 01 and EFault 02). Essential examples of displacement profiles on the west dipping faults and the east dipping faults are shown and described as follows.

4.3.2.1 East dipping fault displacement profiles

- **EFault 01**

The dip angle of EFault 01 surface are 50 to 65 degrees, as shown in figure 4.20a. In addition to, the dip azimuth is oblique (50 to 65 degrees) to the extension direction (Fig 4.20b).

The example of 3D EFault 01 (Fig 4.21a) shows an offset profile having NNW-SSE striking rift-border fault segmented. The graph in figure 4.21b shows a fault throw calculated from the horizon surfaces of pre-rift 3 to pre-rift 7. This graph shows the largest amounts of offset at the pre-rift 3 (Peak- A), the pre-rift 6 (Peak B) and the pre-rift 5 (Peak C), with each maximum displacement up to 0.498 centimeters, 0.465 centimeters and 0.479 centimeters respectively. Both Peak B and Peak C are downward-fault development located in the center of fault, whereas the Peak A is upward-fault development located in a lower center of this fault. Besides, this graph shows a lateral fault linkage between zones of Peak B and Peak C that can be observed from dropping of linkage zone shown in the graph. Furthermore, a vertical fault linkage between zones of Peak A and Peak B that can be observed by changing the uncommon throw distance of pre-rifts in the zones of Peak A and Peak B having decreasing the throw distance of pre-rift 6 but the pre-rift 7 has more throw distance.

In the fault scaling of EFault 01 (Fig 4.28), the length of this fault is 14.9158 centimeters, whereas the maximum throw is 0.4981 centimeters. The ratio of maximum throw to fault length shown in the graph presents the location of a similarly natural normal fault, which are coal measures located in Lorraine, France.

- **EFault 02**

The dip angle of EFault 02 surface has high angle (55-65 degrees) in an upper surface and a low angle in lower surface (41-54 degrees), as shown in figure 4.22a. In addition to, the dip azimuth is sub-parallel to parallel to the extension direction (Fig 4.22b).

The example of 3D EFault 02 (Fig 4.23a) shows an offset profile having N-S striking intra-rift fault segmented. The graph in figure 4.23b shows a fault throw calculated from the horizon surfaces of pre-rift 3 to pre-rift 6. This graph shows the largest amounts of offset at the pre-rift 6 (Peak- A) and the pre-rift 3 (Peak B), with each maximum displacement up to 0.647 centimeters and 0.741 centimeters respectively. The Peak A is located in the upper center of fault, whereas the Peak B is located in lower center of fault. Furthermore, this graph shows a vertical fault linkage between zones of Peak A and Peak B that can be observed by changing the uncommon throw distance of the pre-rifts in the zones of Peak A and Peak B having decreasing the throw distance of pre-rift 5 but the pre-rift 6 has more throw distance.

In the fault scaling of EFault 02 (Fig 4.28), the length of this fault is 13.1652 centimeters, whereas the maximum throw is 0.7412 centimeters. The ratio of maximum throw to fault length shown in the graph presents the location of a similarly natural normal fault, which are coal measures located in Lorraine, France.

4.3.2.2 West dipping fault displacement profiles

- ***WFault 01***

The dip angle of WFault 01 surface has a high angle (55-64 degrees) in northward and a low angle in southward (41-55 degrees), as shown in figure 4.24a. In addition to, the dip azimuth is sub-parallel to parallel to the extension direction in the southward and oblique to the extension direction in the northward (Fig 4.24b).

The example of 3D WFault 01 (Fig 4.25a) shows an offset profile having NNW-SSE striking rift-border fault segmented. The graph in figure 4.25b shows a fault throw calculated from the horizon surfaces of pre-rift 2 to pre-rift 6. This graph shows the largest amount of offset at the pre-rift 6 (Peak), with the maximum displacement up to 0.964 centimeters, which is downward-fault development located in the upper-northward of the fault. Furthermore, this graph shows abrupt changing in the pre-rift 5 and the pre-rift 6 that present the location of earlier fault linkages occurring in this fault.

In the fault scaling of WFault 01 (Fig 4.28), the length of this fault is 14.6998 centimeters, whereas the maximum throw is 0.6944 centimeters. The ratio of maximum throw to fault length shown in the graph presents the location of a similarly natural normal fault, which are coal measures located in Lorraine, France.

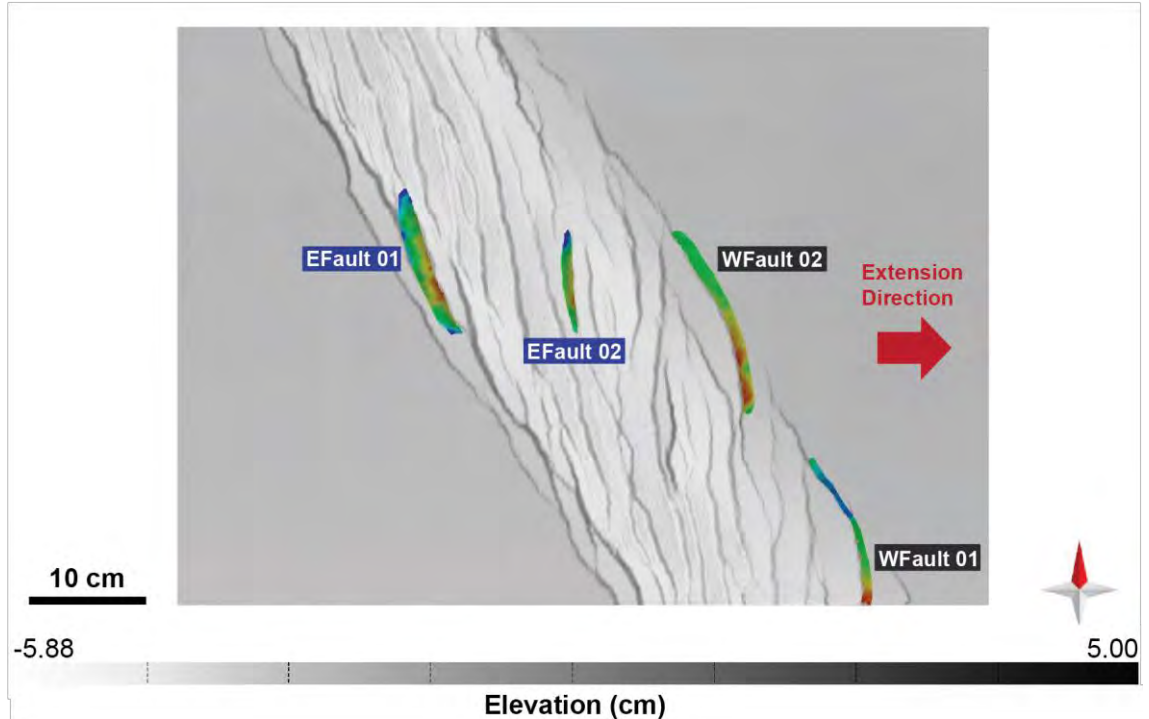
- **WFault 02**

The dip angle of this fault surface has a high angle (55-62 degrees) in southward and a low angle in northward (48-55 degrees), as shown in figure 4.26a. In addition to, the dip azimuth is sub-parallel (250-270 degrees) to the extension direction in the southward and oblique to the extension direction in the northward (226-245 degrees) (Fig 4.26b).

The example of 3D WFault 02 (Fig 4.27a) shows an offset profile having NNW-SSE striking rift-border fault segmented. The graph in figure 4.27b shows a fault throw calculated from the horizon surfaces of pre-rift 3 to pre-rift 6. This graph shows the largest amount of offset at the pre-rift 6 (Peak), with the maximum displacement up to 0.959 centimeters located in the southward of fault. Furthermore, this graph shows fault propagation from the southward to the northward and shows a good development of fault linkage occurring simultaneously.

In the fault scaling of WFault 02 (Fig 4.28), the length of this fault is 18.2409 centimeters, whereas the maximum throw is 0.9598 centimeters. The ratio of maximum throw to fault length shown in the graph presents the location of a similarly natural normal fault, which are coal measures located in Lorraine, France.

a) Map View of Oblique Rift Model (NRS005-60)



b) Oblique View of Oblique Rift Model (NRS005-60)

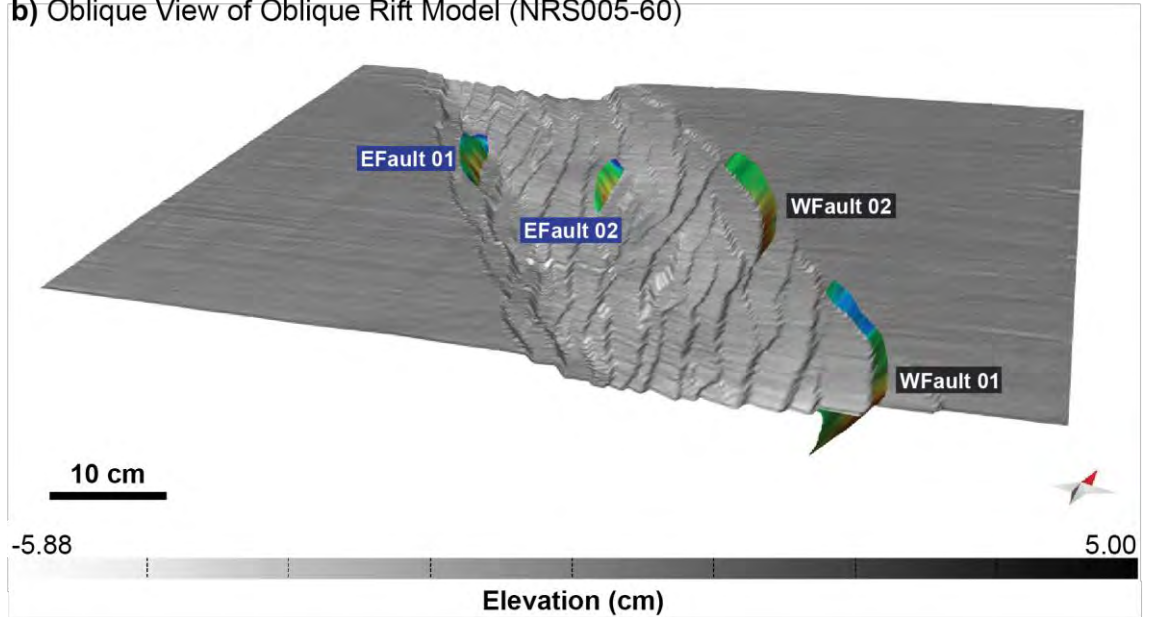
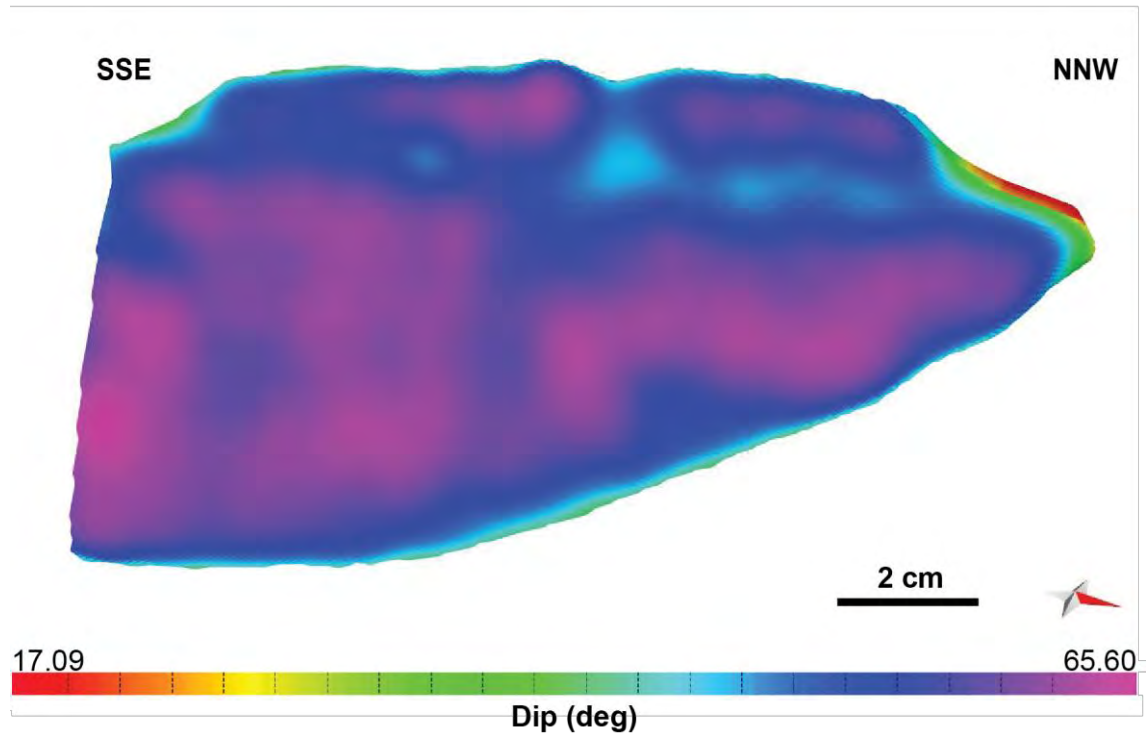


Figure 4.19 (a) The map visualization and (b) the 3D oblique visualization (looking NNW) of pre-rift 6 surface from oblique rift model that show the elevation map having west dipping fault surfaces (WFault 01 and WFault 02) and east dipping fault surfaces (EFault 01 and EFault 02) in the rift basin.

a) Dipping Fault Profile of NRS005-60 EFault 01



b) Dip Azimuth Fault Profile of NRS005-60 EFault 01

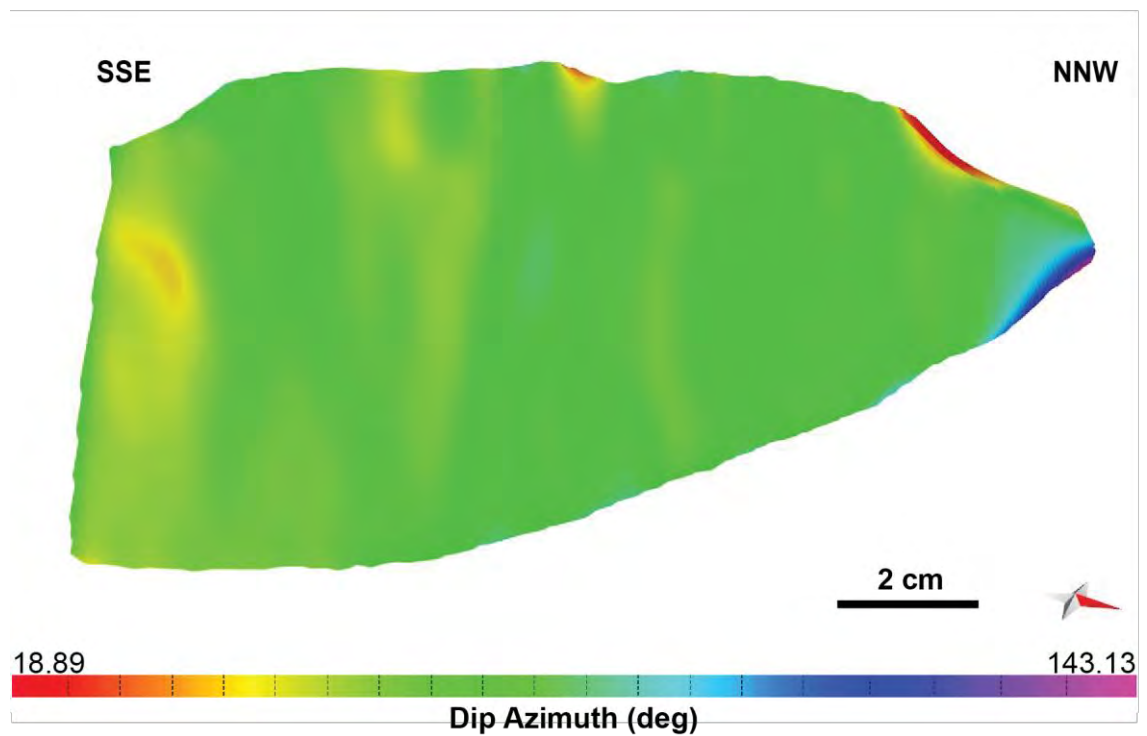


Figure 4.20 (a) The dipping fault profile of NRS005-60 EFault 01 (looking perpendicular to the strike) that shows the dip angle on fault surface of EFault 01. (b) The dip azimuth fault profile of NRS005-60 EFault 01 that shows the direction of dip azimuth on this fault surface.

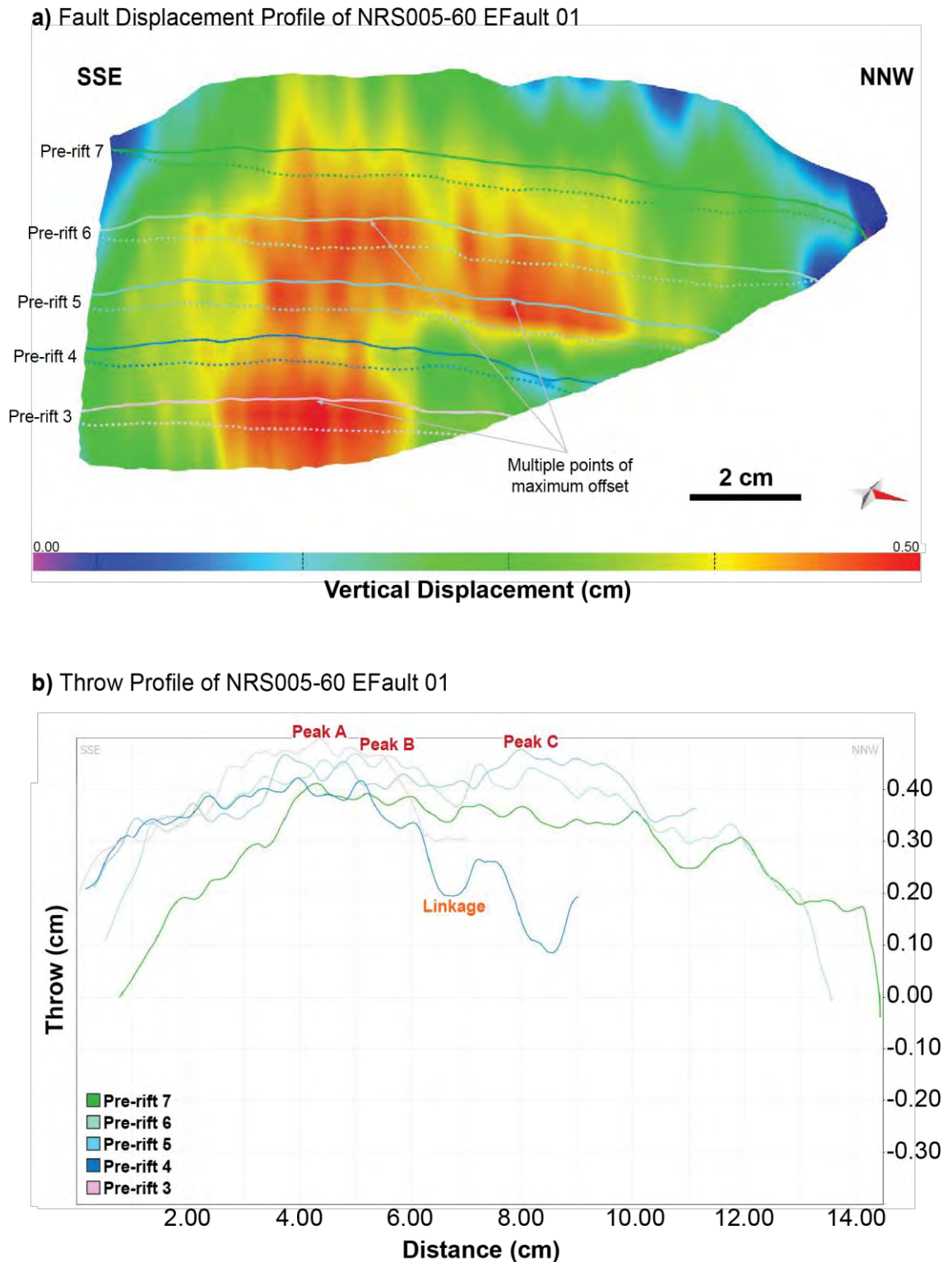
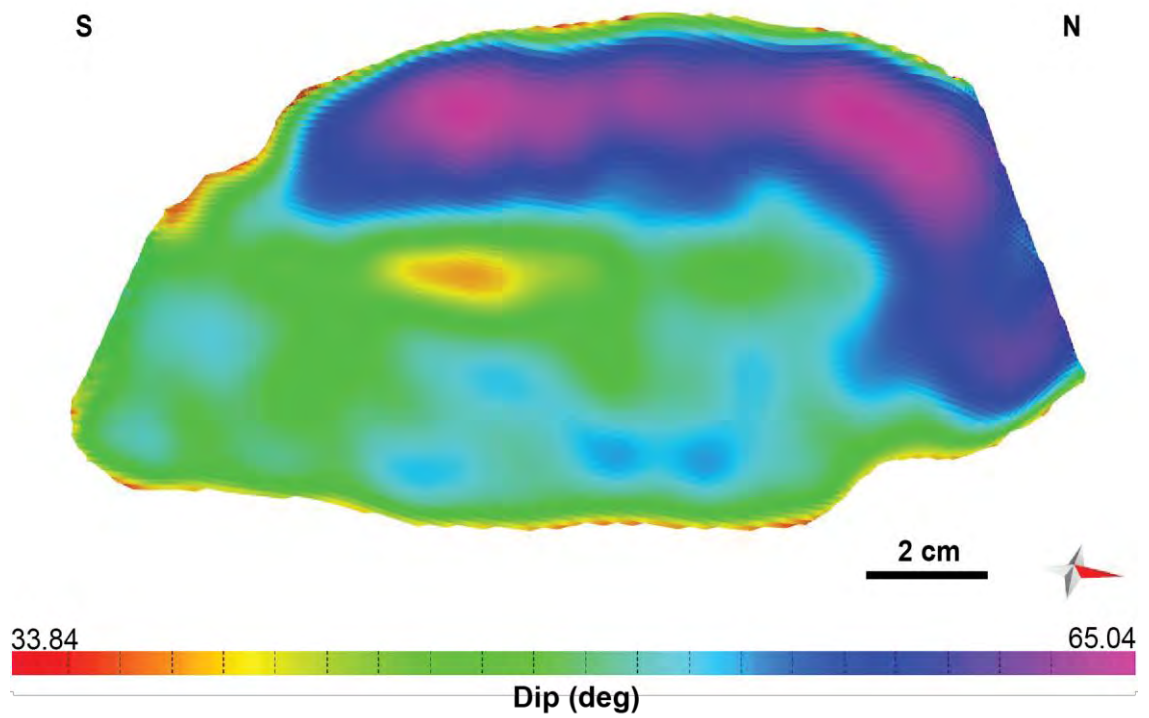


Figure 4.21 (a) Displacement profile of NRS005-60 EFault 01 (looking perpendicular to the strike). Line across the fault surface are hangingwall (dashed line) and footwall (solid lines) cutoffs from interpreted horizons. (b) Fault offset showing fault throw measured perpendicular to strike orientation along the fault. Fault location is shown in figure 4.19.

a) Dipping Fault Profile of NRS005-60 EFault 02



b) Dip Azimuth Fault Profile of NRS005-60 EFault 02

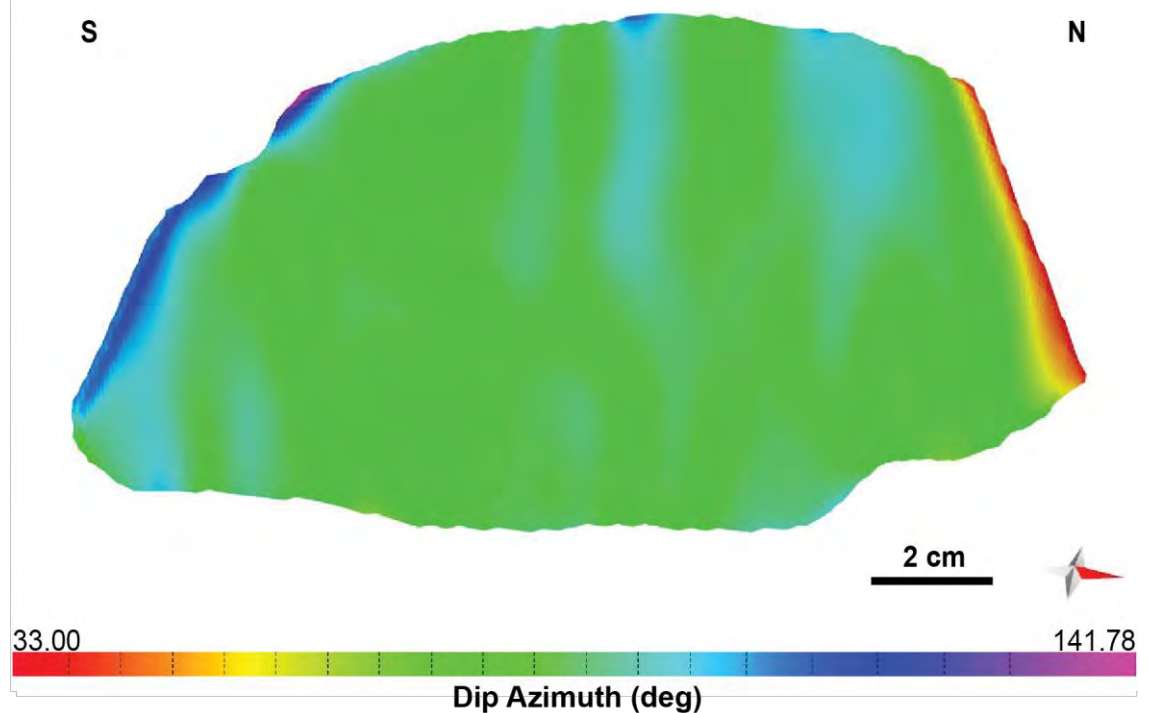
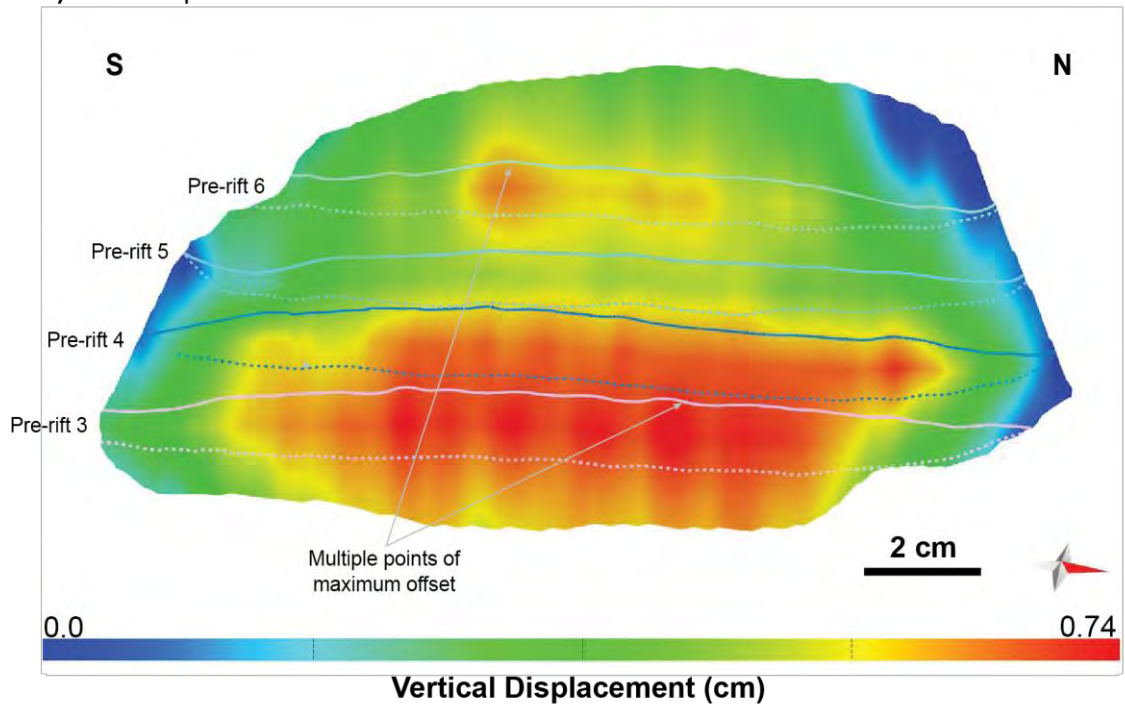


Figure 4.22 (a) The dipping fault profile of NRS005-60 EFault 02 (looking perpendicular to the strike) that shows the dip angle on fault surface of EFault 02. (b) The dip azimuth fault profile of NRS005-60 EFault 02 that shows the direction of dip azimuth on this fault surface.

a) Fault Displacement Profile of NRS005-60 EFault 02



b) Throw Profile of NRS005-60 EFault 02

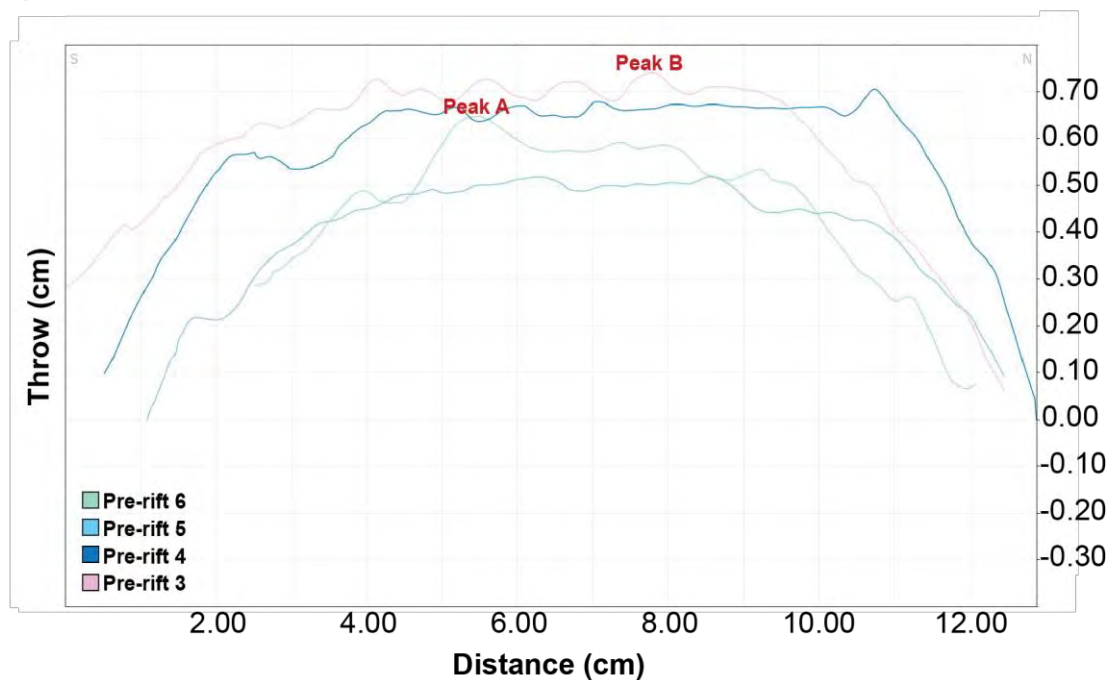
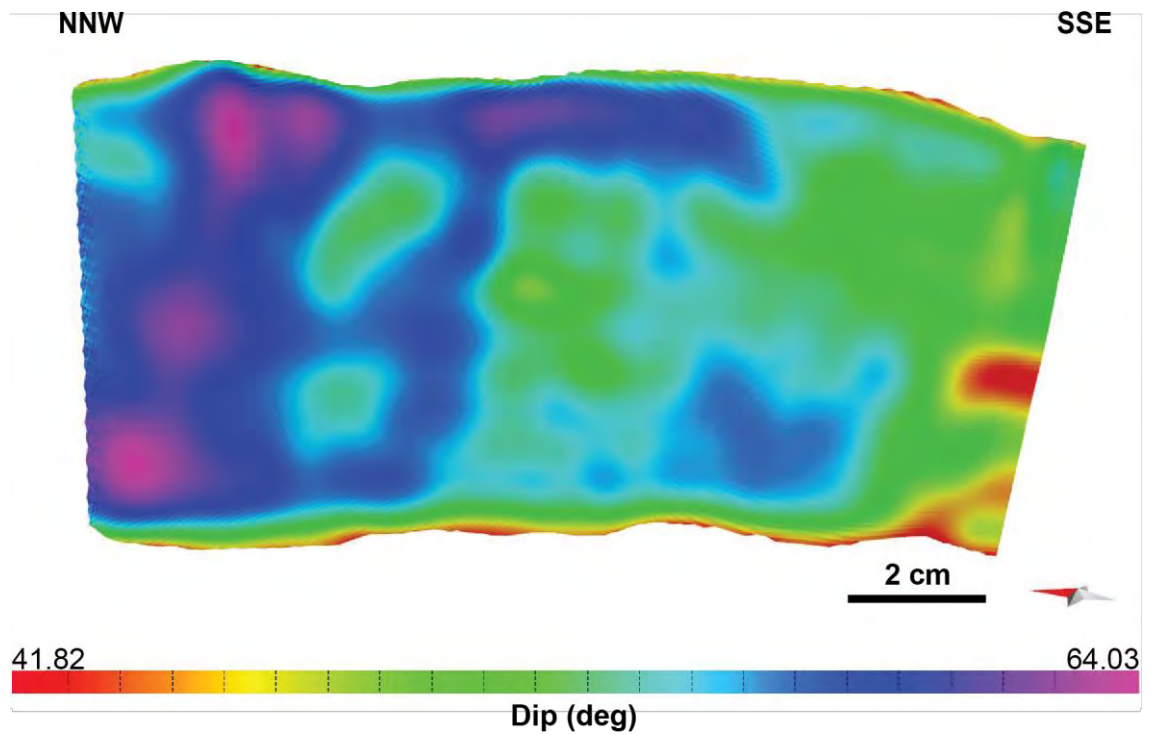


Figure 4.23 (a) Displacement profile of NRS005-60 EFault 02 (looking perpendicular to the strike). Line across the fault surface are hangingwall (dashed line) and footwall (solid lines) cutoffs from interpreted horizons. (b) Fault offset showing fault throw measured perpendicular to strike orientation along the fault. Fault location is shown in figure 4.19.

a) Dipping Fault Profile of NRS005-60 WFault 01



b) Dip Azimuth Fault Profile of NRS005-60 WFault 01

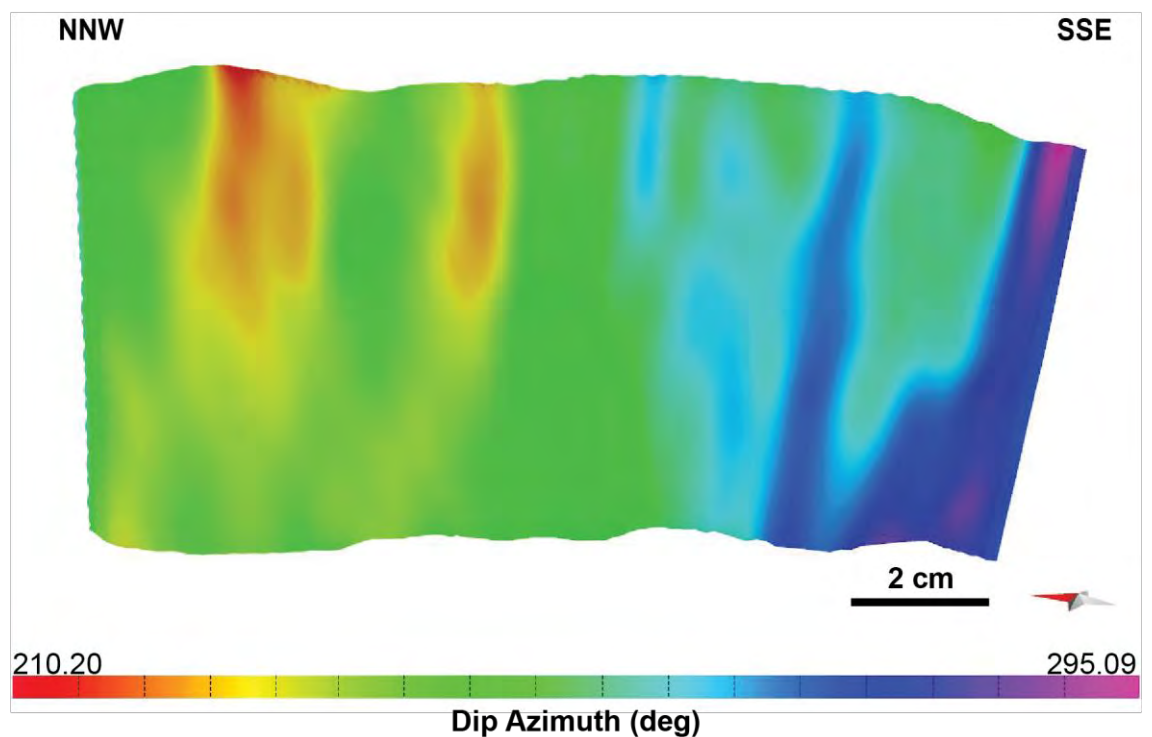
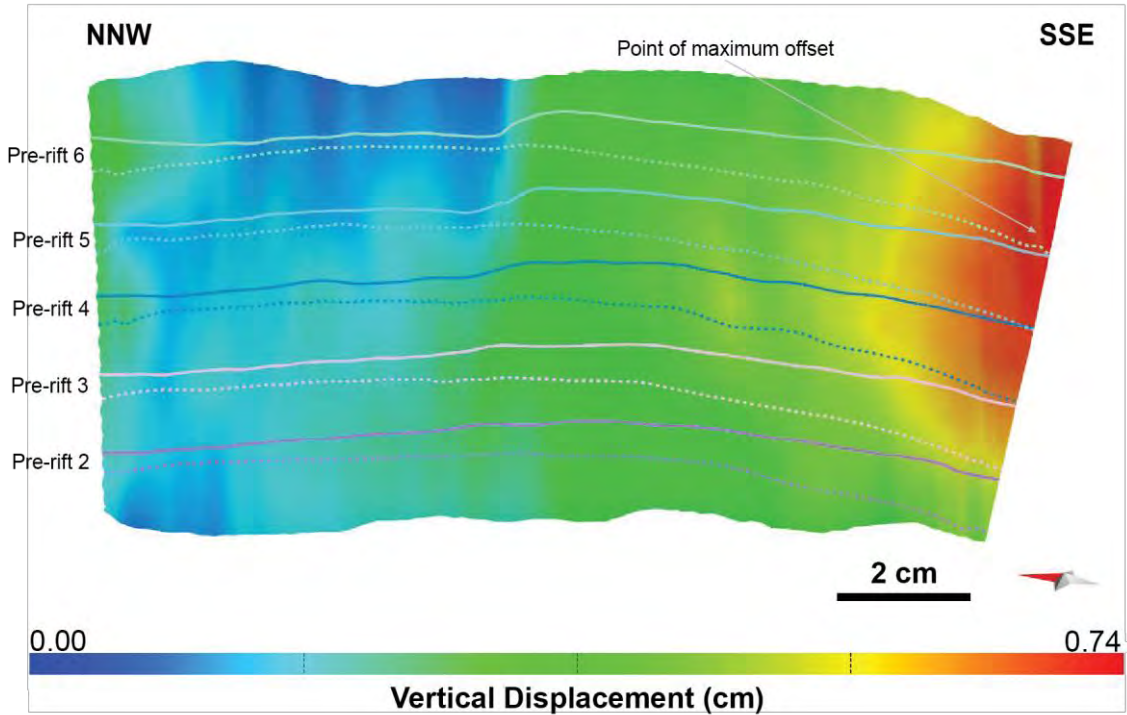


Figure 4.24 (a) The dipping fault profile of NRS005-60 WFault 01 (looking perpendicular to the strike) that shows the dip angle on fault surface of WFault 01. (b) The dip azimuth fault profile of NRS005-60 WFault 01 that shows the direction of dip azimuth on this fault surface.

a) Fault Displacement Profile of NRS005-60 WFault 01



b) Throw Profile of NRS005-60 WFault 01

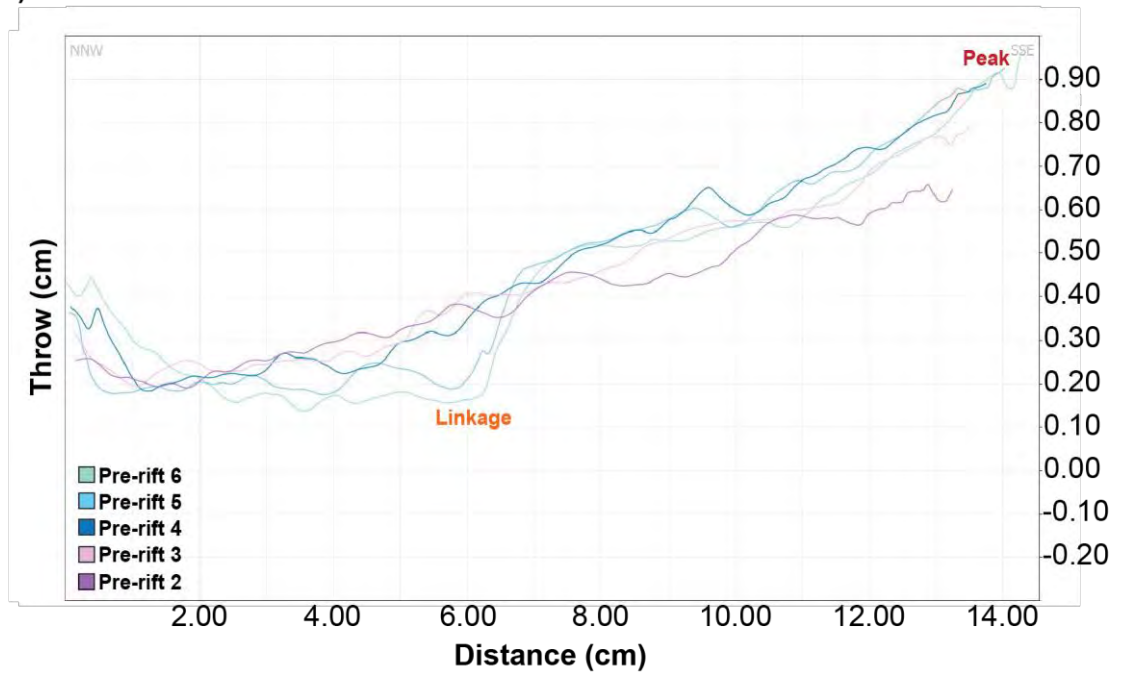
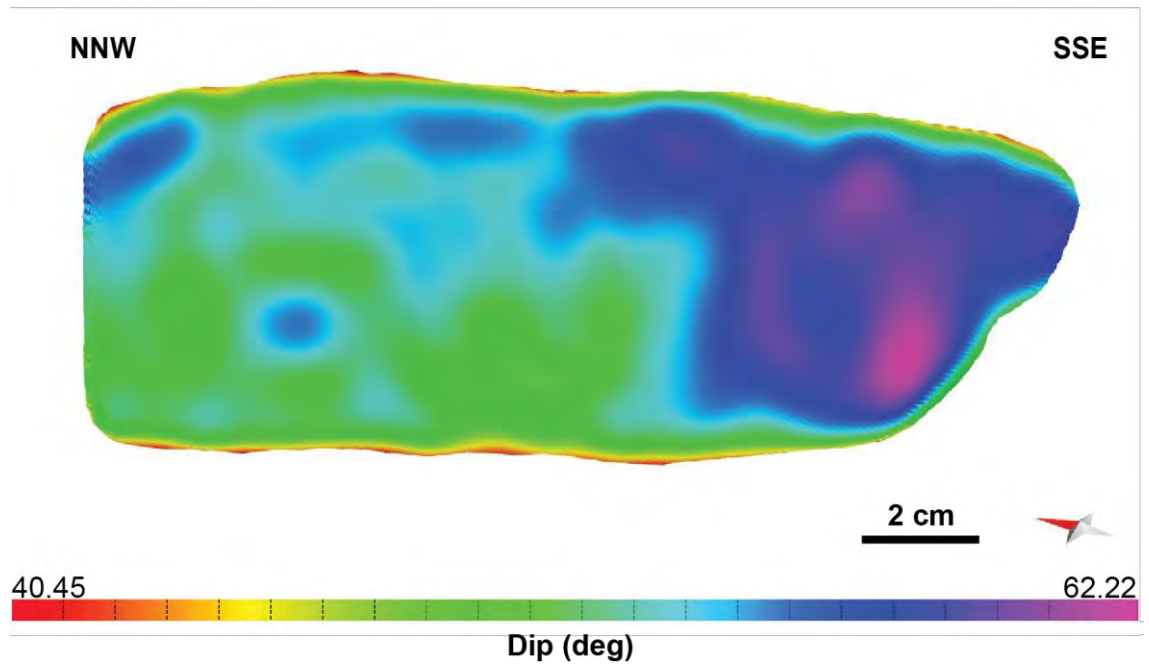


Figure 4.25 (a) Displacement profile of NRS005-60 WFault 01 (looking perpendicular to the strike). Line across the fault surface are hangingwall (dashed line) and footwall (solid lines) cutoffs from interpreted horizons. (b) Fault offset showing fault throw measured perpendicular to strike orientation along the fault. Fault location is shown in figure 4.19.

a) Dipping Fault Profile of NRS005-60 WFault 02



b) Dip Azimuth Fault Profile of NRS005-60 WFault 02

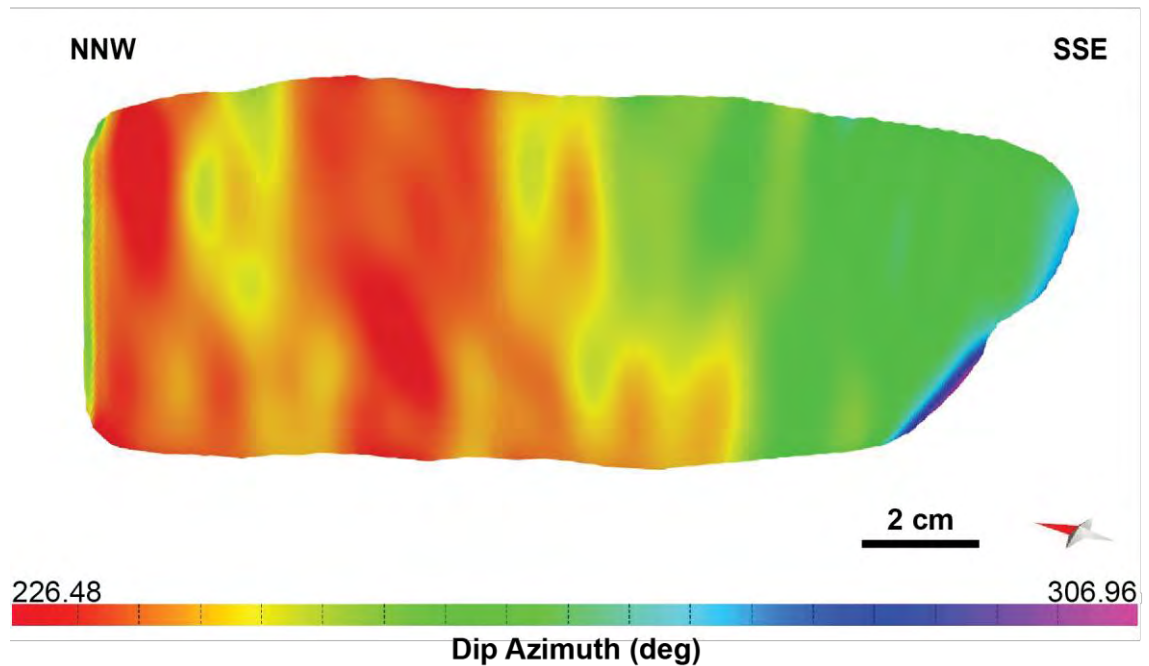
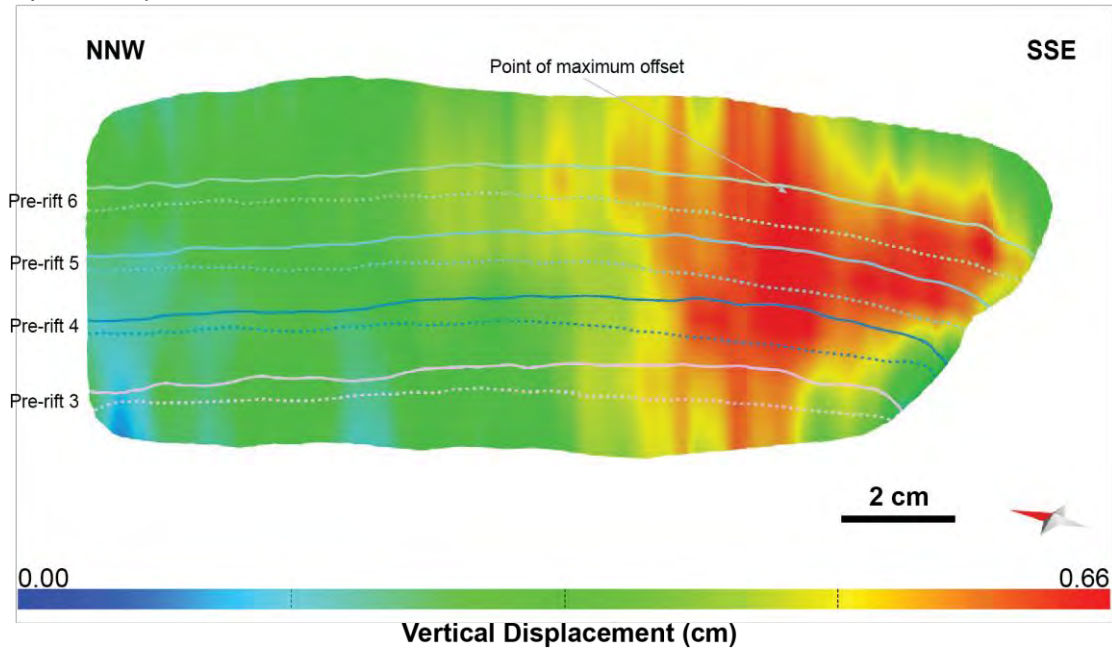


Figure 4.26 (a) The dipping fault profile of NRS005-60 WFault 02 (looking perpendicular to the strike) that shows the dip angle on fault surface of WFault 02. (b) The dip azimuth fault profile of NRS005-60 WFault 02 that shows the direction of dip azimuth on this fault surface.

a) Fault Displacement Profile of NRS005-60 WFault 02



b) Throw Profile of NRS005-60 WFault 02

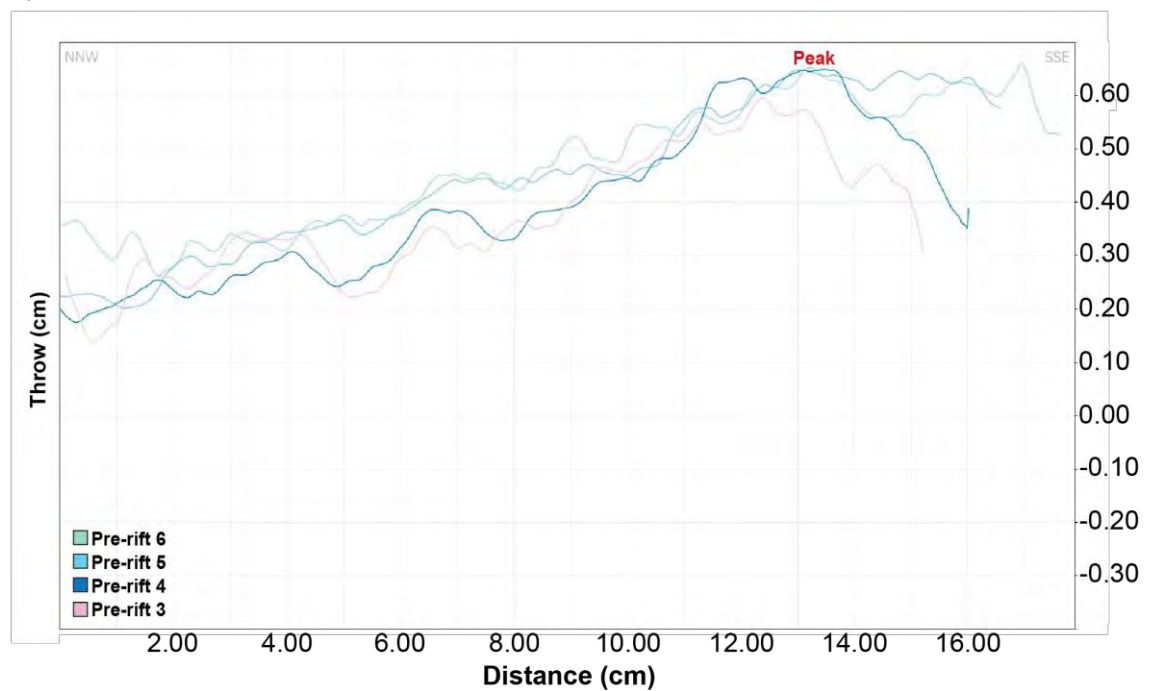


Figure 4.27 (a) Displacement profile of NRS005-60 WFault 02 (looking perpendicular to the strike). Line across the fault surface are hangingwall (dashed line) and footwall (solid lines) cutoffs from interpreted horizons. (b) Fault offset showing fault throw measured perpendicular to strike orientation along the fault. Fault location is shown in figure 4.19.

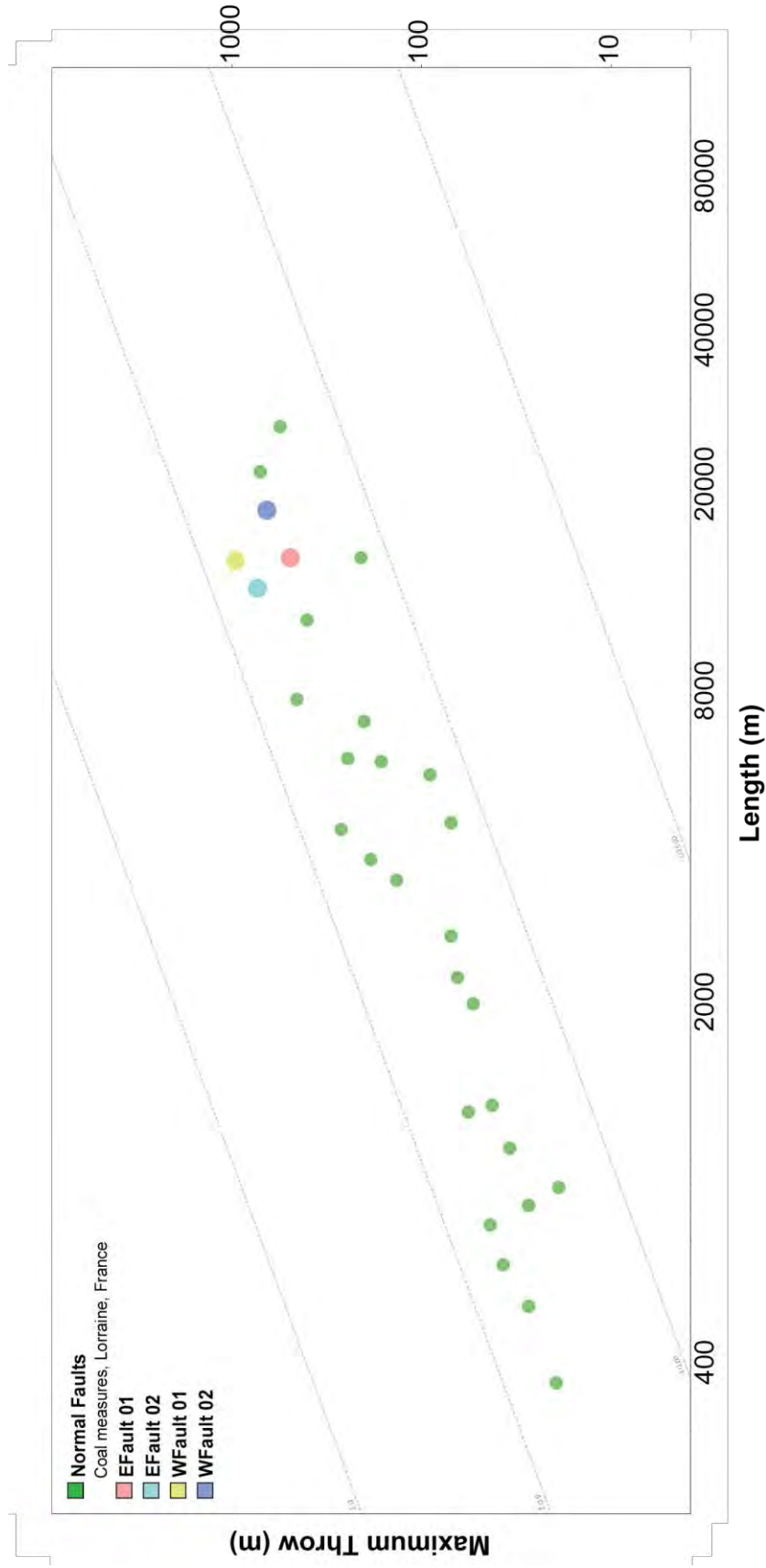


Figure 4.28 The fault scaling that are plotted by the ratio of maximum throw (m) to fault length (m) for faults (EFault 01, EFault 02, WFault 01 and WFault 02) in the oblique rift model (1 cm: 1000 m) compared to plots for normal faults in Lorraine coal basin, France

Chapter 5

Discussions

5.1 Comparison between orthogonal and oblique rift model

5.1.1 Fault systems

The study about 3D internal structures of the orthogonal rift model are characterized by long, straight segmented normal faults in north-south striking of both intra-rift faults and rift-border faults that are perpendicular to the extension direction and parallel to the pre-existing structure beneath the basin in the scaled physical models. But, on the other hand, the oblique rift model is characterized by shorter normal faults, segmented rift-border faults and intra-rift faults. The rift-border faults are NNW-SSE striking that parallel to the underlying zone of the pre-existing structure beneath the basin, whereas the orientation of intra-rift faults have N-S trend that are perpendicular to sub-perpendicular to the extension direction. These intra-rift faults may develop to be parallel with the border rift zone due to the pre-existing structure beneath the basins in the scaled physical models controlled them. However, no strike-slip or oblique-slip transfer faults were found in both models.

5.1.2 Dip angle of faults

The comparison with the dip angles of both models, the orthogonal rift model has a high dip angle in the upper fault surfaces that approximately are 60-70 degrees, whereas the lower fault surfaces have a low dip angle that approximately are 30-60 degrees. Besides, the oblique rift model has the high dip angle in the upper fault surfaces that approximately are 55-65 degrees, whereas the lower fault surfaces have the low dip angle that approximately are 40-55 degrees. thus, both models almost are higher dip angles in the upper fault surfaces than lower fault surfaces.

5.1.3 Dip azimuth of faults

The dip azimuth of the orthogonal rift model is sub-parallel to parallel to the extension direction both intra-rift faults and rift-border faults, but on the other hand the dip azimuths of the oblique rift model are sub-parallel to parallel to the extension direction in the intra-rift faults, whereas the rift-border faults are oblique to the direction extension (parallel to the pre-existing structure beneath the basin).

5.1.4 Fault analysis

The results from studying and interpretation about faults analysis of the orthogonal rift model and the oblique rift model can be described as follow:

- ***The location of maximum displacement*** that can be observed from the result of fault displacement profile shown by color shades of vertical displacement and graphs of throw profile that shows the peak of maximum displacement.
- ***The stages of fault linkage*** can be divided into two stages that are early fault linkage and late fault linkage observed from changing the graph of throw profile.
- ***The evolution direction of fault movement*** that can be observed from positions spacing of fault linkages in throw profile. They can be divided into two types: the first one is downward fault development that can be observed by linkage position of older pre-rift is closer the Peak than younger pre-rifts. The another one is upward fault development shown by the peak zone that has the linkage position of the younger pre-rifts to be closer than the older pre-rifts.
- ***Types of fault linkages*** that can be divided into two types: the vertical fault linkage that can be observed from changing the uncommon throw distance of the pre-rifts in the peak zone, whereas the lateral fault linkage that can be observed from dropping the linkage position from the graph of throw profile.

The comparison between the orthogonal rift model and the oblique rift model, the displacement of the faults in the oblique rift model almost are more displacement than the faults in the orthogonal rift model. In both models, the typical fault displacements of the intra-rift faults are commonly more displacement than the rift-border faults because these intra-rift faults may well develop than the rift-border faults.

Furthermore, the stages of fault linkages and the evolution direction of fault movement can be found in both models, whereas the types of fault linkages that are the vertical linkages can be observed in the oblique rift model to be easier than the orthogonal rift model.

5.2 Comparisons with natural examples of rift systems

5.2.1 Orthogonal rift

The Gregory rift in East Africa shows excellent example of segmented rift border fault systems, as well as long, relatively straight, intra rift faults in syn-rift Miocene volcanic unit (Figs 5.1a and 5.1b). Both the rift-border and intra-rift faults are dominantly N-S striking and have long overlap regions between adjacent faults. Along-strike displacement transfer is by soft-linked relay-ramp structures, and no strike-slip or oblique-slip transfer faults are found (cf. Bosworth et al., 1986). This pattern is similar to the pattern of 3D internal structures in the orthogonal rift model and also indicate that the extension direction was perpendicular to the pre-existing beneath the rift model.

Thus, the results of faults analysis that came from the orthogonal rift model can be used to predict the fault displacement and the fault linkages in the Gregory rift that have similar characteristics to this model.

5.2.2 Oblique rifts

The natural example of oblique rift basin is the extended volcanic tablelands in Owens Valley, north of Bishop, California, shows the 700 ka Bishop tuff downthrown in a NNW trending extensional structure. The margins of this zone of extension are oblique to the E-W oriented extension (e.g., Dawers et al., 1993; Dawers and Anders, 1995) (Figs 5.2a and 5.2b). These structures occurring in this basin almost are similar the pattern of structures in the oblique rift model.

Accordingly, the extended volcanic tablelands can be used the faults analysis of the oblique rift model to study and predict some fault displacement and fault linkages that may be similar to this basin.

Moreover, the significant natural example of oblique rift basin in the southern Thailand is Mergui basin. The main period of structural development in this basin was an extension phase in the Oligocene (WNW-ESE extension direction)-Early Miocene (NW-SE extension direction) (Curry, 2005). In Oligocene (Fig 5.3), the intra-rift faults had strike to be perpendicular to the extension direction but the rift-border faults had strike to be oblique to the extension direction since these faults were controlled by the pre-existing structures occurred from Ranong and Khlong Marui fault beneath the Mergui basin. In Early Miocene (Fig 5.4), the extension direction occurring in the Mergui basin was changed from WNW-ESE to NW-SE extension direction and was

developed in the northward of the basin. In this period, both intra-rift faults and border-rift faults had strike to be perpendicular to the extension direction because the northern area of this basin has the pre-existing structures beneath the basin which have the architecture to be perpendicular to the extension direction.

5.3 Apply to petroleum system

In the petroleum system, the structural trap is a type of geological trap that forms as a result of changes in the structure of the subsurface due to tectonic setting. Another kind of structural trap is a fault trap, so the study about the fault displacement can be used to indicate the capability of occurring the fault trap that faults bring an impermeable stratum in contact with a layer of permeable reservoir rock and forms a barrier to petroleum migration respectively. Besides, the location that has opposite dipping faults together can be occurred the horst structure that has a potential to be the structural trap.

Furthermore, the relay ramp structure occurred from a zone of fault linkage can be important for the petroleum system because this structure may be the migration pathways of hydrocarbon.



Figure 5.1a East African rift system, Kenya. Landsat thematic mapper (TM) image of the Gregory rift west of Nairobi, Kenya (modified after McClay et al., 2002). Continued.

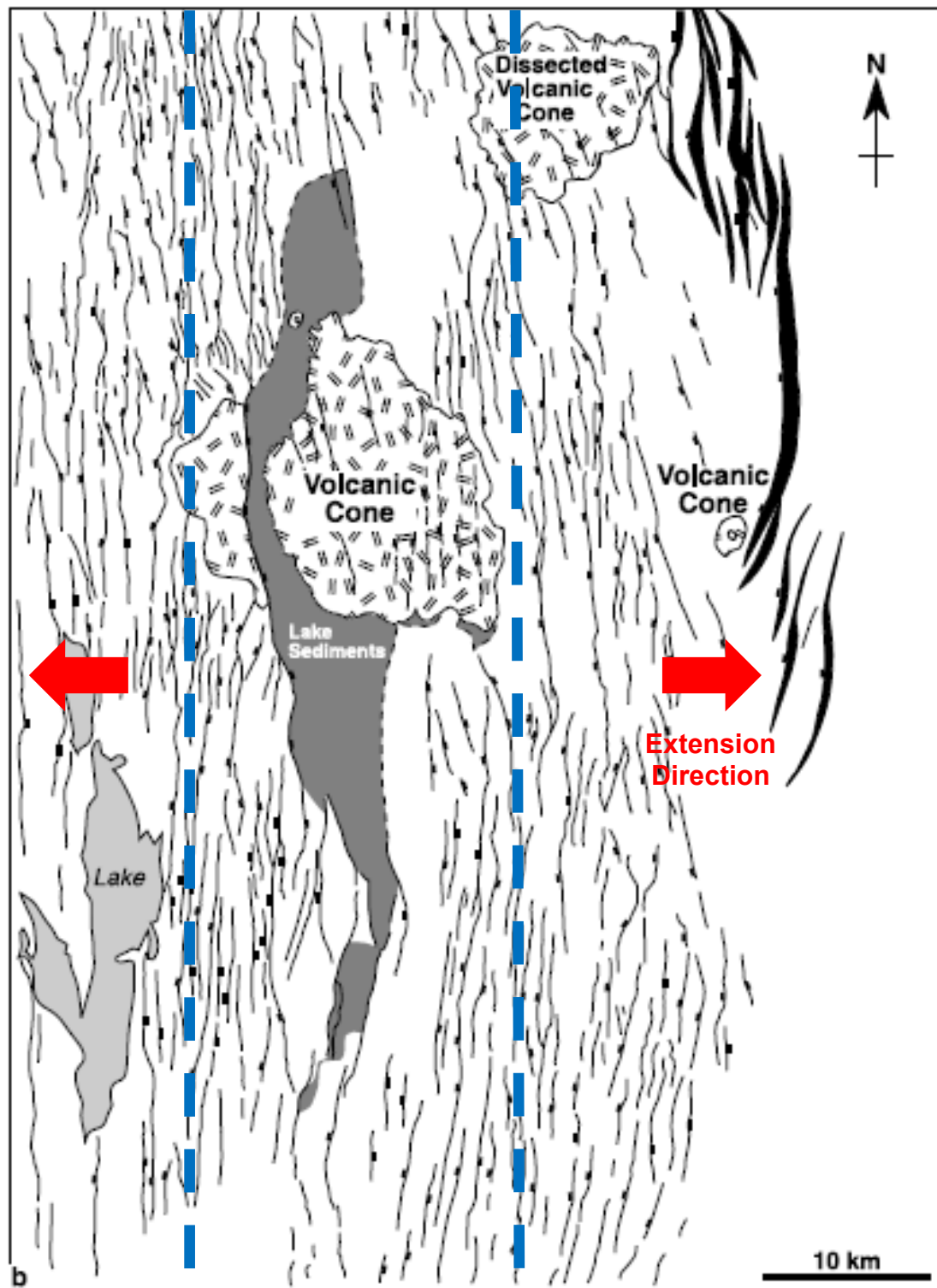


Figure 5.1b Continued. Line diagram interpretation of (a) showing the segmented and slightly offset rift-border system on the east and a high density of north-south-oriented intra-rift faults in the main part of the rift. This pattern is characteristic of orthogonal rift model with the extension direction to be perpendicular to the pre-existing beneath the basin (modified after McClay et al., 2002).



Figure 5.2a Radar image of the volcanic tablelands, Bishop, California. The image shows a series of en echelon marginal faults in the Bishop running obliquely across the image with north-south-oriented interior faults in the center left of the image (modified after McClay et al., 2002). Continued.

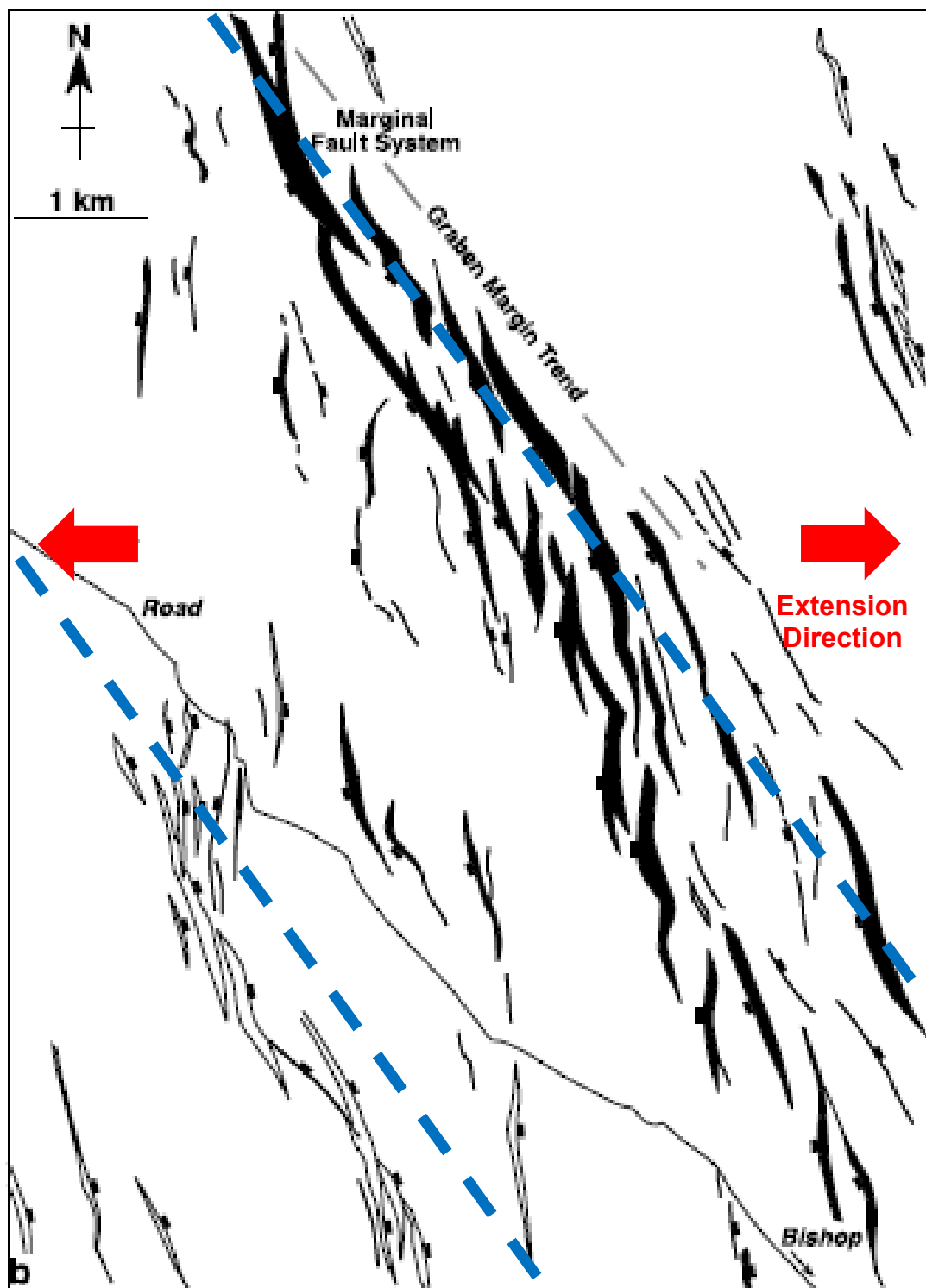


Figure 5.2b Continued. Line diagram interpretation of (a). This image is an example of oblique rift model (modified after McClay et al., 2002).

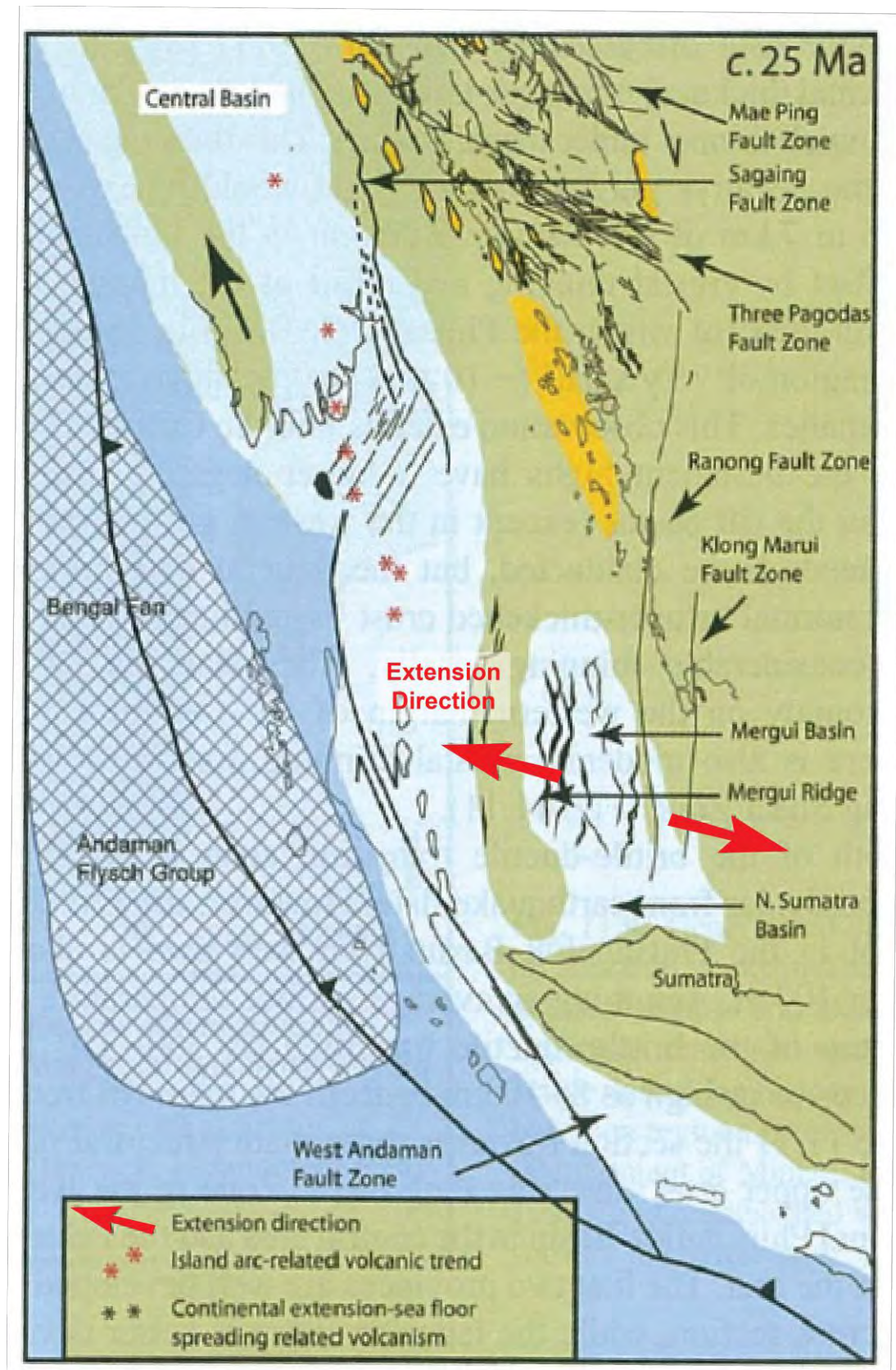


Figure 5.3 Oligocene structural and tectonic evolution of mergui basin located in southern Thailand, Andaman sea (modified after Curray, 2005).

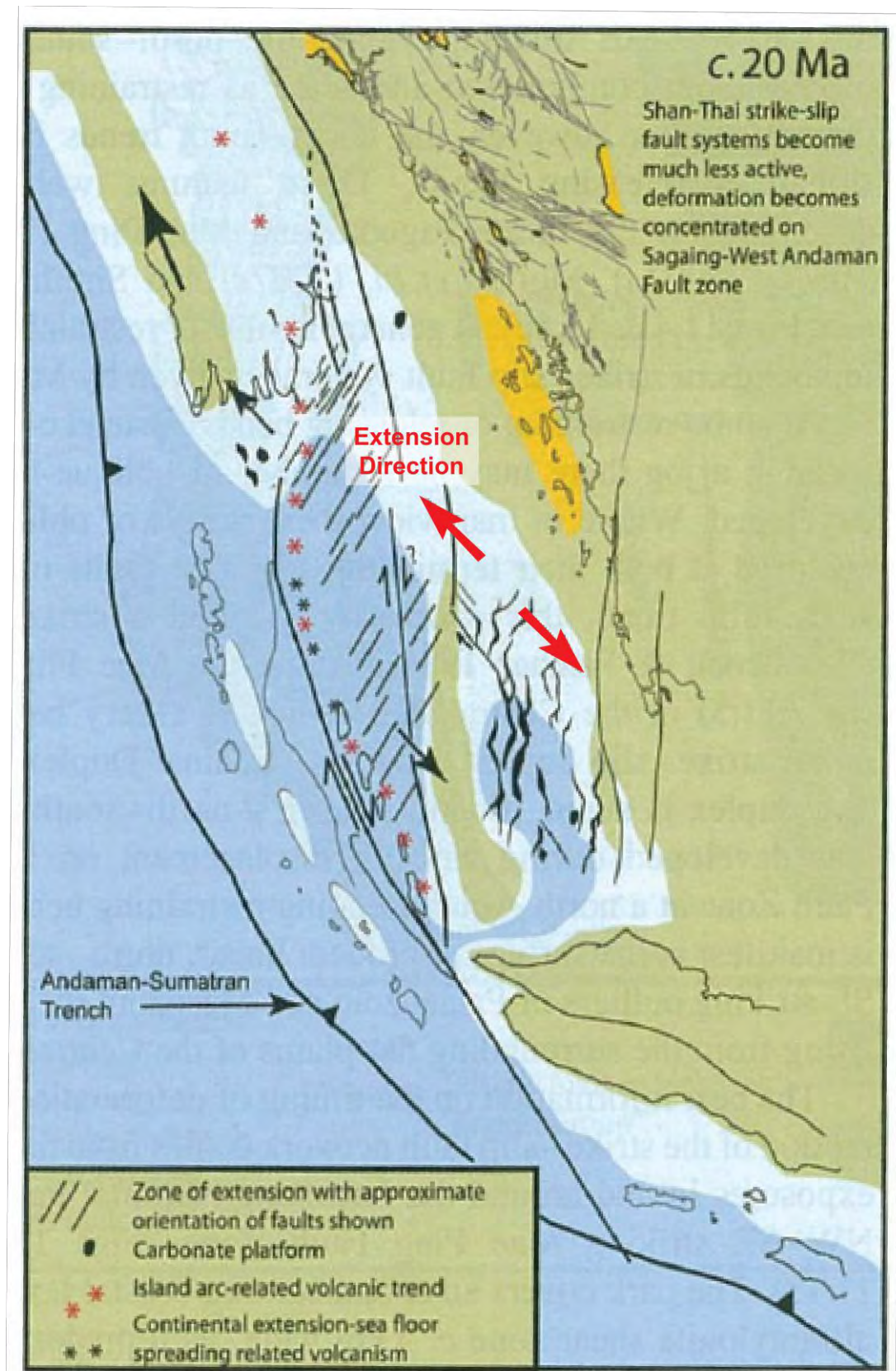


Figure 5.4 Early-Miocene structural and tectonic evolution of Mergui basin located in southern Thailand, Andaman sea (modified after Curray, 2005).

Chapter 6

Conclusions

The 3D internal structures of both orthogonal rift model (NRS006-60) and oblique rift model (NRS005-60) that were created by the new methodology using geological software: Kogeo®, OpendTect®, Petrel 2014 and Move™ to analyst and compare the differences from characteristics of horizon surfaces and fault surfaces generated from both model section images of each scaled physical model, they can be conclude following in a table below;

	Orthogonal Rift Model	Oblique Rift Model
Fault Orientation	<i>Mean of west dipping faults is 178 degrees</i>	<i>Mean of west dipping faults is 164 degrees</i>
	<i>Mean of east dipping faults is 358 degrees</i>	<i>Mean of east dipping faults is 336 degrees</i>
Fault Throw Profile	<i>Maximum displacements are located at fault center</i>	<i>Maximum displacements are located at fault edges</i>
	<i>Vertical linkages are hardly observed</i>	<i>Vertical linkages are easily observed</i>
Fault Scaling	<i>Normal faults, Coal Measures, Lorraine, France</i>	
Natural Example	<i>The Gregory rift in East Africa</i>	<ul style="list-style-type: none"> - <i>Extend Volcanic Tablelands in Owens Valley, California</i> - <i>Mergui basin in Andaman sea, Thailand</i>

Moreover, this study about the 3D internal structures of rift basin from both scaled physical models can be used to study about natural rift basins and apply to petroleum system about fault trap and migration pathways of hydrocarbon.

References

- Abers, G. A., 2001. Evidence for seismogenic normal faults at shallow dips in continental rifts. In: Wilson, R. C. L., Whitmarsh, R. B., Taylor, B., Froitzheim, N. (Eds.) Non-volcanic rifting of continental margins: A comparison of evidence from land and sea. Geological Society of London, Special Publication, 187, 305-318.
- AGSO NORTH WEST SHELF STUDY GROUP, 1994. Deep reflections on the North West Shelf: changing perceptions of basin formation. In: Purcell, P.G. and Purcell, R.R. (Eds.) The Sedimentary Basins of Western Australia: Proceedings of West Australian Basins Symposium, 63-76.
- Bassi, G., 1995. Relative importance of strain rate and rheology for the mode of continental extension, *Geophysical Journal International*, 122, 195-210.
- Bosworth, W., 1985. Geometry of propagating continental rifts. *Nature*, 316, 625-627.
- Bosworth, W., Crevello, P., Winn Jr, R. D. and Steinmetz, J., 1986. A new look at Gregory's rift: the structural style of continental rifting: *EOS*, 67, 582-583.
- Brun, J. P. and Tron, V., 1993. Development of the North Viking Graben - Inferences from laboratory modelling. *Sedimentary Geology*, 86, 31-51.
- Buck, W. R., 2004. Consequences of asthenospheric variability on continental rifting. In: Karner, G. D., Taylor, B., Driscoll, N. A., Kohlstedt, D. L. (Eds.) Rheology and deformation of the lithosphere at continental margins. Columbia University Press, New York, 1-30.

- Carbotte, S. M. and Macdonald, K. C., 1994. Comparison of seafloor tectonic fabric at intermediate, fast, and super-fast spreading ridges: Influence of spreading rate, plate motions, and ridge segmentation on fault patterns, *Journal of Geophysical Research* 99, 13609-13631.
- Chenin, P. and Beaumont, C., 2013. Influence of offset weak zones on the development of rift basins: Activation and abandonment during continental extension and breakup, *Journal of Geophysical Research Solid Earth*, 118, 1698-1720.
- Corti, G., 2008. Control of rift obliquity on the evolution and segmentation of the main Ethiopia rift, *Nature Geoscience*, 1, 258-262.
- Corti, G., 2009. Continental rift evolution: from rift initiation to incipient break-up in the Main Ethiopian Rift, East Africa. *Earth Science Reviews*, 96, 1-53.
- Corti, G., 2012. Evolution and characteristics of continental rifting: Analogue modeling-inspired view and comparison with examples from the East African Rift System: *Tectonophysics*, 522-523, 1-33.
- Clifton, A. E., Schlische, R. W., Withjack, M. O. and Ackermann, R. V., 2000. Influence of rift obliquity on fault-population systematics: results of experimental clay models. *Journal of Structural Geology*, 22, 1491-1509.
- Clifton, A. E. and Schlische, E. W., 2001. Nucleation, growth, and linkage of faults in oblique rift zone: results from experiment clay models and implications for maximum fault size. *Geology*, 29, 455-458.
- Curry, J. R., 2005. Tectonics and history of the Andaman Sea region. *Journal of Asian Earth Sciences*, 25, 187-232.

- d'Acremont, E., Leroy, S., Beslier, M.O., Bellahsen, N., Fournier, M., Robin, C., Maia, M. and Gente, P., 2005. Structure and evolution of the eastern Gulf of Aden conjugate margins from seismic reflection data. *Geophysical Journal International*, 160, 869-890.
- Daly, M. C., Chorowicz, J. and Fairhead, J. D., 1989. Rift basin evolution in Africa; the influence of reactivated steep basement shear zones. In: Cooper, M. A., Williams, G. D. (Eds.). *Inversion Tectonics*. Geological Society of London, Special Publication, 44, 309-334.
- Dawers, N. H., and Anders, M. A., 1995. Displacement-length scaling and fault linkages: *Journal of Structural Geology*, 17, 607-614.
- Dawer, N. H., Anders, M. H. and Scholtz, C. H., 1993. Growth of normal faults and accommodation zones, Kivu-Rusizi rift, Africa: *Tectonics*, 8, 117-137.
- Ebinger, C. J., 1989. Geometric and kinematic development of border faults and accommodation zones, Kivu-Rusizi rift (Africa). *Tectonics*, 8, 117-133.
- Ebinger, C. J. and Casey, M., 2001. Continental breakup in magmatic provinces: An Ethiopia example. *Geology*, 29, 527-530.
- Faereth, R. B., Knudsen, B. E., Liljedahl, T., Midboe, P. S. and Soderstrom, B., 1997. Oblique rifting and sequential faulting in the Jurassic development of the northern North Sea. *Journal of Structural Geology*, 19, 1285-1302.
- Faulds, J. E. and Varga, R. J., 1998. The role of accommodation zones and transfer zones in the regional segmentation of extended terranes. In: Faulds, J. E., Stewart, J. H. (Eds.). *Accommodation zones and transfer zones; the regional segmentation of the Basin and Range Province*. The Geological Society of America, Boulder, Colorado. 1-45.

- Gawthorpe, R. L., Jackson, C. A. L., Young, M. J., Sharp, I. R., Moustafa, A. R. I. and Leppard, C. W., 2003. Normal fault growth, displacement localization and the evolution of normal fault population: the Hamman Faraun fault block, Suez Rift, Egypt. *Journal of Structural Geology*, 25, 1347-1348.
- Gawthorpe, R. L. and Leeder, M. R., 2000. Tectono-sedimentary evolution of active extensional basins. *Basin Research*, 12, 195-218.
- Goldsworthy, M. and Jackson, J., 2001. Migration of activity within normal fault systems: examples from the Quaternary of mainland Greece. *Journal of Structural Geology*, 23, 489-506.
- Gupta, A. and Scholz, C. H., 2000a. A model of normal fault interaction based on observations and theory. *Journal of Structural Geology*, 22, 865-879.
- Gupta, A. and Scholz, C. H., 2000b. Brittle strain regime transition in the Afar depression: Implications for fault growth and seafloor spreading. *Geology*, 28, 1087-1090.
- Gupta, A., Cowie, P. A., Dawers, N. H. and Underhill, J. R., 1998. A mechanism to explain rift-basin subsidence and stratigraphic patterns through fault-array evolution. *Geology*, 26, 595-598.
- Hayward, N. J. and Ebinger, C. J., 1996. Variations in the along-axis segmentation of the Afar Rift system. *Tectonics*, 15, 244.
- Huerta, A. D. and Harry, D. L., 2007. The transition from diffuse to focused extension: modeled evolution of the West Antarctic Rift system. *Earth and Planetary Science Letters*, 225, 133-147.

- Jitmahantakul, S., 2014. Tectono-stratigraphic evolution of the Exmouth sub-basin, North West shelf of Australia. Unpublished PhD Thesis. Royal Holloway University of London.
- Keir, D., Ebinger, C. J., Stuart, G. W., Daly, E. and Ayele, A., 2006. Strain accommodation by magmatism and faulting as rifting proceeds to breakup: Seismicity of the northern Ethiopian rift. *Journal of Geophysical Research-Solid Earth*, 111,17.
- Khalil, S. and McClay, K., 2001. Tectonic evolution of the northwestern Red Sea-Gulf of Suez Rift System. In: Wilson, R. C. L., Whitemarsh, R. B., Taylor, B. and Frotzheim, N. (Eds.). *Nonvolcanic Rifting of Continental Margins: a Comparison of Evidence from Land and Sea*. Geological Society, London, Special Publications, 187, 453-473.
- Kusznir, N. J. and Park, R. G., 1987. The extensional strength of the continental lithosphere; its dependence on geothermal gradient, and crustal composition and thickness. In: Coward, M. P., Dewy, J. F., Hancock, P. L. (Eds.). *Continental Extensional Tectonics*. Geological Society of London, Special Publication, 28, 35-52.
- Macdonald, K., 1998. Linkages between faulting, volcanism, hydrothermal activity and segmentation of fast spreading centers, In: Buck, W. R., Delaney, P. T., Karson, J. A., Lagabriele, Y. (Eds.), *Faulting and magmatism at mid-ocean ridges*. Vol. 106 of *Geophysical Monograph*. AGU, 27-58.
- McClay, K. R., 1990. Extensional fault systems in sedimentary basins - A review of analogue model studies. *Marine and Petroleum Geology*. 7, 206-238.

- McClay, K. R., Dooley, T., Whitehouse, P., Fullerton, L., Chantraprasert, S. 2004. 3D analogue models of rift systems: templates for 3D seismic interpretation. In: Davies, R. J., Cartwright, J. A., Stewart, S. A., Lappin, M., Underhill, J. R. (Eds.). 3D seismic technology; application to the exploration of sedimentary basins. Geological Society Memoirs 29, London. 101-115.
- McClay, K. R., Dooley, T., Whitehouse, P. and Mills, M., 2002. 4-D Evolution of Rift Systems: Insights from Scaled Physical Models. AAPG Bulletin, 86, 935-959.
- McClay, K. R. and White, M. J., 1995. Analogue modelling of orthogonal and oblique rifting. Marine and Petroleum Geology, 12, 137-151.
- McKenzie, D., 1978. Some remarks on the development of sedimentary basins. Earth and Planetary Science Letters, 40, 25-32.
- McLeod, A. E., Dawers, N. H. and Underhill, J. R., 2000. The propagation and linkage of normal faults; insights from the Strathspey - Brent - Statfjord fault array. Basin Research, 12, 263-284.
- Meyer, V., Nicol, A., Childs, C., Walsh, J. J., Watterson, J., 2002. Progressive localization of strain during the evolution of a normal fault population. Journal of Structural Geology, 24, 1215-1231.
- Morley, C. K., Haranya, C., Phoosongsee, W., Pongwapee, S., Kornsawan, A. and Wonganan, N., 2004. Activation of Rift Oblique and Rift Parallel Pre-existing Fabrics During Extension and their effect on Deformation Style: Examples from Rifts of Thailand. Journal of Structural Geology, 26, 1803-1829.
- Olsen, K. H., Morgan, P., 1995. Introduction: progress in understanding continental rifts. In: K. H. Olsen (Ed.). Continental Rifts: Evolution, Structure, Tectonics. Elsevier, Developments in Geotectonics, 25, 3-26.

- Serra, S., Nelson, R. A., 1988. Clay modelling of rift asymmetry and associated structures. *Tectonophysics*, 153, 307-312.
- Tron, V. and Brun, J. P., 1991. Experiments on oblique rifting in brittle-ductile systems. *Tectonophysics*, 188, 71-84.
- Whitehouse, P. S., 2005. Fault and fracture development in extensionally reactivated fault systems. Unpublished PhD Thesis. Royal Holloway University of London.
- Withjack, M. O. and Jamison, W. R., 1986. Deformation produced by oblique rifting. *Tectonophysics*, 126, 99-124.
- Withjack, M. O. and Schlische, R. W., 2005. A review of tectonic events on the passive margin of eastern North America, in Post, P., ed., *Petroleum Systems of Divergent Continental Margin Basins: 25th Bob S. Perkins Research Conference*, Gulf Coast Section of SEPM, 203-235.
- Ziegler, P. A. and Cloetingh, S., 2004. Dynamic processes controlling evolution of rifted basins. *Earth-Science Reviews*, 64, 1-50.

Appendix

Appendix 1 The dip azimuth database of faults in orthogonal and oblique rift model which were recorded by rose diagrams created from Move™.

Rift Models	Horizon Surfaces	Mean Direction		Number of Point Data	
		East dipping faults	West dipping faults	East dipping faults	West dipping faults
Orthogonal Rift Model	Pre-rift 1	none	None	none	none
	Pre-rift 2	358.79°	179.1°	32456	64544
	Pre-rift 3	358.81°	178.77°	32863	62507
	Pre-rift 4	358.53°	178.88°	35012	57591
	Pre-rift 5	358.52°	177.87°	38435	57999
	Pre-rift 6	358.3°	178.35°	43830	65531
	Pre-rift 7	358.19°	178.58°	43624	65192
	Syn-rift 1	358.36°	178.8°	41191	60119
	Syn-rift 2	358.73°	178.42°	22784	30871
Oblique Rift Model	Pre-rift 1	None	None	none	none
	Pre-rift 2	340.89°	165.09°	22237	51652
	Pre-rift 3	337.9°	164.7°	29342	61340
	Pre-rift 4	336.22°	163.67°	29007	56565
	Pre-rift 5	335.68°	163.87°	34068	58032
	Pre-rift 6	336.14°	164.12°	31810	70403
	Pre-rift 7	335.11°	164.15°	37689	54714
	Syn-rift 1	335.66°	164.76°	44422	72579
	Syn-rift 2	336.5°	165.89°	11043	11972

